THE STRESS FIELD SURROUNDING THE TIP OF A CRACK PROPAGATING IN A FINITE BODY

by

Ravinder Chona

Dissertation submitted to the Faculty of the Graduate School
of the University of Maryland in partial fulfillment
of the requirements for the degree of
Doctor of Philosophy
1987

APPROVAL SHEET

Title of Dissertation: The Stress Field Surrounding the Tip of a Crack Propagating in a Finite Body

Name of Candidate: Ravinder Chona
Doctor of Philosophy, 1987

Dissertation and Abstract Approved: George R. Irwin

George R. Irwin, Visiting Professor
Department of Mechanical Engineering
University of Maryland
College Park, Maryland 20742

Date Approved: April 24, 1987

ABSTRACT

Title of Dissertation: The Stress Field Surrounding the Tip of a Crack Propagating in a Finite Body

Name of Candidate: Ravinder Chona
Doctor of Philosophy, 1987

Dissertation directed by: Professor George R. Irwin
Department of Mechanical Engineering
University of Maryland, College Park, MD.

The goal of this dissertation was to establish the relationship between a parameter descriptive of the trajectory of a smoothly curving crack, such as the curvature of the crack path, and the local stress state in the close vicinity of the crack tip. The behavior of fast-running cracks propagating along straight and smoothly curving paths in fracture specimens of various geometries was examined using dynamic photoelasticity and representations of the running crack stress field were developed in terms of the coefficients of a set of infinite series, for both opening and shear mode loading conditions. Analysis of the isochromatic patterns, using local collocation methods based on this stress field representation, allowed the stress state in the neighborhood of the propagating crack-tip to be modelled with a high degree of accuracy and results were obtained for the variations with crack tip position of both the singular and leading non-singular stress field coefficients of interest.

The results obtained for quasi-static and rapid crack propagation under opening mode conditions in a ring segment revealed the

importance of retaining terms of order (at a minimum) $r^{1/2}$ even when only the singular term was to be determined accurately. Furthermore, it was found that the non-singular stress field coefficients varied similarly in both static and dynamic situations, with some variations in magnitude that could be attributed to crack speed.

The results from the curved crack experiments also showed systematic variation of the non-singular terms, but more importantly, it was found that the instantaneous curvature of the crack path was related to the magnitude of the lowest order non-singular stress component (the coefficient of the $r^{1/2}$-term) associated with the local shear mode of deformation in the vicinity of the tip of the running crack. Furthermore, the results established that the only singularity associated with a crack propagating along a smoothly curving path in a brittle, isotropic material was that associated with the opening mode stress intensity factor, K_I, and that the shear mode singularity, K_{II}, was identically equal to zero.

To my wife and my parents

ACKNOWLEDGEMENTS

I would like to express my sincere appreciation of the unfailing patience, encouragement, and guidance that I have always received from my advisor, Professor George Irwin, and from Professor R. Joseph Sanford, both before and after he joined the University of Maryland faculty. I am also grateful to Drs. Barker, Dally, and Fourney, for their advice, comments and consistent support over the years of my association with them. My special thanks are due to Dr. Arun Shukla of the University of Rhode Island for his help in obtaining the experimental data that made this dissertation possible, and for his many helpful suggestions and comments during the course of this work.

The support received from Oak Ridge National Laboratory through their subcontract with the University of Maryland and the computational support provided by the Computer Science Center of the University of Maryland are both gratefully acknowledged.

TABLE OF CONTENTS

TABLE OF CONTENTS (CONTINUED)

TABLE OF CONTENTS (CONTINUED)

CHAPTER 1

INTRODUCTION

Trajectory problems in mechanics, such as the problem of determining the path followed by a particle in a potential field such that it traverses the distance between two points in the shortest time (the brachistochrone problem first considered by Bernoulli), have long been recognised as being complex [1.1]. The problem of prediction of the crack path in fracture mechanics is no less so, even when attention is restricted to a two-dimensional planar crack that is propagating at a constant speed [1.2].

The solution to the general crack trajectory problem requires: (a) the computation of the stress intensity factors and other related stress field parameters for a given crack in an arbitrary body at any instant in time; and (b) a means of defining the next increment of crack growth in terms of geometrical parameters that are related to the previously computed information about the crack tip stress field. The solution to this problem has been attempted by a number of researchers for certain special cases, using either closed-form, quasi-static, analytical solutions, or numerical techniques to compute the small change of direction for each forward increment of crack extension based on the maximization of the normal tensile stress ahead of the crack tip [1.3]. However, little or no attention has been given to the trajectory curvature, which is a point function of position along any smoothly curving path.

The aim of the present work is to establish the relationship between the curvature of the crack path and the stress field in the local region surrounding the tip of a smoothly curving, propagating crack. This will be done by first carefully evaluating the magnitude of the leading non-singular stress terms in the crack-tip stress field for cracks propagating along smoothly curving paths in a brittle, isotropic material, and then examining the curvature of the crack path relative to the magnitude of both the singular and non-singular stress field parameters.

The need for considering non-singular stress field parameters in addition to the stress intensity factor when modelling the stress and strain distribution around the tip of a stationary crack in a finite-sized body is well established [1.4]. Several procedures for reliably evaluating the parameters of interest from full-field experimental data have been developed in recent years, and it has been demonstrated that the influence of non-singular stress terms must be considered even when attention is restricted to accurate determinations of the singular term alone [1.5, 1.6].

It has also been shown in a previous study, that the leading non-singular stress field coefficients vary systematically as a function of crack length for cracks subjected to opening mode loading and that the magnitude and variation of these parameters depends on the shape and in-plane dimensions of the particular geometry being considered. The results obtained have proved useful in formulating criteria that can be utilized to establish, in a quantitative manner, the size and shape of the singularity-dominated zone around the crack tip, which was found to be a small fraction of the distance from the crack tip to the nearest specimen boundary [1.7, 1.8].

As stated previously, the objective of the present work is to examine the existence of possible relationships between the magnitude of the non-singular stress effects local to the crack tip and the path which the crack tip follows, for cases where the crack is propagating along a smoothly curving path in a brittle, isotropic material. That such a relationship may exist is suggested by the following. For a general curve in space, any infinitesmal segment of the curve can always be considered as a straight line without loss of generality. However, successful analytical modelling of a finite, non-zero curvature requires a non-zero second derivative for any function used to describe the curve and the resulting radius of curvature is a point function of position along the curve. Thus, a rationale for studying higher order effects when studying crack propagation along a curved path is apparent from a geometric viewpoint.

The approach adopted here has been to use dynamic photoelasticity and a high speed camera system of the Cranz-Schardin type to obtain full-field information about the stress state surrounding the tip of a crack propagating in a plate specimen fabricated from a brittle, birefringent polymer [1.9]. The resulting information was in the form of isochromatic fringe patterns, or contours of constant maximum in-plane shear stress, which provided the data base for further analyses. Local collocation procedures were then employed, in which the appropriate stress field representations for running cracks were combined with a multiple data point, overdeterministic, non-linear algorithm to obtain the stress field parameters of interest in a least-squares sense [1.10 - 1.12].

Initial work in this study focussed on opening mode cracking, in which the crack propagated along an axis of symmetry of the specimen geometry. This provided a comparison of quasi-static and running crack propagation behaviors in the same specimen configuration and allowed higher order term influences to be examined in a dynamic setting. The ability to obtain accurate values for the higher order terms of interest was also established. Further studies were then undertaken in which a rapidly propagating crack was initiated from a starter notch in such a manner that the crack followed a smoothly curving path as a consequence of non-symmetric loading conditions remote from the crack tip.

The results from the straight crack experiments showed that the non-singular stress field coefficients varied in a manner similar to that obtained for static situations in the same geometry, with some variations in magnitude that could be attributed to crack speed. The results from the curved crack experiments also showed systematic variation of the non-singular terms, but more importantly, it was found that the instantaneous curvature of the crack path was related to the magnitude of the lowest order non-singular stress terms associated with the local shear mode of deformation in the vicinity of the tip of the running crack. Furthermore, the results suggested that the only singularity associated with a crack propagating along a smoothly curving path in a brittle, isotropic material was that associated with the opening mode stress intensity factor, K_I.

REFERENCES

1.1 Goldstein, H., **Classical Mechanics**, Addison-Wesley Publishing Company, Reading, Massachusetts (1959).

1.2 Freund, L.B., "Dynamic Crack Propagation in Solids," in **Computational Methods in the Mechanics of Fracture**, S.N. Atluri, editor, North-Holland Publishing Company, New York, pp. 85-120 (1986).

1.3 Swenson, D. and A.R. Ingraffea, "A Finite Element Model of Dynamic Crack Propagation with an Application to Intersecting Cracks," **Proceedings of the Fourth International Conference on Numerical Methods in Fracture Mechanics**, A.R. Luxmoore, et al., editors, Pineridge Press, Swansea, U.K., pp. 191-204 (1987).

1.4 Sanford, R.J., "A Critical Re-examination of the Westergaard Method for Solving Opening-Mode Crack Problems," **Mechanics Research Communications**, 6, pp. 289-294 (1979).

1.5 Chona, R., W.L. Fourney, R.J. Sanford and A. Shukla, "Determining Stress Intensity Factors for Running Cracks," **Modeling Problems in Crack Tip Mechanics**, J.T. Pindera, editor, Martinus Nijhoff Publishers, pp. 207-215 (1984).

1.6 Barker, D.B., R.J. Sanford and R. Chona, "Determining K and Related Stress Field Parameters From Displacement Fields," **Experimental Mechanics**, Vol. 25, No. 4, pp. 399-407 (1985).

1.7 Chona, R., G.R. Irwin and R.J. Sanford, "Influence of Specimen Size and Shape on the Singularity Dominated Zone," **Fracture Mechanics: Fourteenth Symposium - Volume I: Theory and Analysis,** G.R. Sines and J.C. Lewis, editors, ASTM STP 791, pp. I-3 - I-23 (1983).

1.8 Chona, R., **Non-Singular Stress Effects in Fracture Test Specimens -- A Photoelastic Study,** M.S. Thesis, University of Maryland (1985).

1.9 Riley, W.F. and J.W. Dally, "Recording Dynamic Fringe Patterns with a Cranz-Schardin Camera," **Experimental Mechanics,** 9, pp. 27N-33N (1969).

1.10 Sanford, R.J. and J.W. Dally, "A General Method for Determining Mixed Mode Stress Intensity Factors from Isochromatic Fringe Patterns," **Engineering Fracture Mechanics,** 11, pp. 621-633 (1979).

1.11 Sanford, R.J., "Application of the Least-Squares Method to Photoelastic Analysis," **Experimental Mechanics,** 20, pp. 192-197 (1980).

1.12 Sanford, R.J. and R.E. Link, "Local Collocation - A Hybrid Technique in Fracture Mechanics", **Proceedings of the Twelfth Southeastern Conference on Theoretical and Applied Mechanics (SECTAM XII),** pp. 183-187 (1984).

CHAPTER 2

REVIEW OF PREVIOUS WORK

The behavior of cracks under mixed-mode, i.e., combined tension and forward shear, loading conditions has been studied over more than two decades by different investigators. Most of these studies have assumed infinite bodies under quasi-static conditions and confined attention to the singular stress fields in the immediate vicinity of the crack tip. For a running crack, the need for incorporating the effects of inertia is generally acknowledged. The major hesitation in using dynamic analysis methods to address this problem has been the increased complexity of the analysis and the difficulties encountered in determining the crack tip stress field parameters of interest when considering running cracks propagating in finite geometries. Despite the lack of attention to the problem of interest, i.e., non-singular stress field influences on a smoothly curving crack propagating in the plane of a finite body, some useful information can generally be obtained from quasi-static considerations and a brief review of previous work on the topic is presented below.

2.1 Studies Based on a Maximum Stress Approach

Early work by Erdogan and Sih [2.1] used a maximum circumferential stress criterion to predict the direction of crack extension of an angled segment emanating from the tip of an originally straight crack. Each segment of crack extension was assumed to occur normal to the maximum hoop stress associated with the original crack tip and attention was given only to the stress field contribution due to the mode I and mode II stress intensity factors.

A first attempt at incorporating possible influences of non-singular stresses was the work of Williams and Ewing [2.2], who considered the influence of the constant stress parallel to the original crack direction, σ_{ox}, on the direction of crack extension of the angled segment. Later work by Finnie and Saith [2.3] and Streit and Finnie [2.4] corrected some errors in [2.2] and suggested that an additional parameter that needed consideration was the distance from the crack tip at which the maximum circumferential stress occurred relative to some critical distance, r_c. The concept of crack path stability being governed by σ_{ox} was also examined by Cotterell and Rice [2.5], who considered quasi-static crack growth of a slightly curved crack and used perturbation theory for their analysis.

2.2 Studies Based on an Energy Approach

The principle of maximization of the rate of loss of stress field energy is a concept that generally governs macroscopic deformation behaviors, and as such is often encountered in mechanics. Its usefulness for studying crack extension behaviors would therefore be expected and investigations of crack kinking or crack extension along non-straight crack paths based on energy arguments have also been pursued. These generally fall into two broad categories. One is prediction of the direction of crack extension based upon maximization of the strain energy release rate [2.6 - 2.10]. The other approach is to use the concept of minimization of the strain energy density [2.11, 2.12].

Some attention has also been given to considering the direction along which the in-plane shear mode singularity, K_{II}, vanishes [2.13 - 2.16] for an infinitesmally small segment of crack extension. However, it has been shown in [2.10, 2.16] that a $K_{II} = 0$ condition is equivalent to maximization of the strain energy release rate for small kink angles.

2.3 Studies on Dynamic Crack Curving

Some very early work by Yoffe [2.17] and later by Sih [2.18] attempted to bring into the picture the effects of inertia and crack speed. More recently, a much more detailed study of the dynamic crack curving problem was performed by Ramulu and his co-workers [2.19 - 2.25].

The result of this work was a set of criteria that were proposed for dynamic crack curving based on a maximum circumferential stress theory and a critical distance concept, similar to that previously suggested by Streit and Finnie [2.4] for the static case. The proposed criteria were evaluated using dynamic photoelastic data and reasonable agreement between predictions and experimental observations was reported.

Though the work by Ramulu, et al., used dynamic stress field expressions, the influence of terms of order $r^{1/2}$ and beyond was neglected in this study also. Attention was paid only to the opening and shear mode stress intensity factors, K_I and K_{II}, and the constant stress term, σ_{ox}. One immediate consequence of using such a stress field model, that utilized only a very limited number of terms, was to presuppose that all of the asymmetry in both the local and far-field regions around the crack tip was due only to the shear mode singularity.

In addition, since these investigators recognised that their stress field representation was valid only in a region of very limited size around the crack tip, they proceeded to very carefully perform the evaluation of their proposed criteria using experimental data taken very close to the crack tip. In some cases, this meant that the thickness of the specimens used to obtain experimental data greatly exceeded the size of the region of data acquisition, resulting in significant three-dimensional effects that were not considered and which have been shown recently to result in erroneous evaluations of the stress intensity factors using other optical methods [2.26].

Consequently, while the work of Ramulu, et al., represents the first systematic attempt to use full-field information about the crack-tip stress field and to develop a crack curving criterion that incorporated the influences of crack speed, the problem was approached from a very restricted viewpoint and could be considered to suffer from certain drawbacks that render the conclusions questionable. The differences between that work and the results of the present study will be discussed in more detail in subsequent parts of this dissertation.

REFERENCES

2.1 Erdogan, F. and G.C. Sih, "On the Crack Extension in Plates Under Plane Loading and Transverse Shear," **Journal of Basic Engineering**, 85, pp. 519-527 (1963).

2.2 Williams, J.G. and P.D. Ewing, "Fracture Under Complex Stress - The Angled Crack Problem," **International Journal of Fracture Mechanics**, 8, pp. 441-446 (1972).

2.3 Finnie, I. and A. Saith, "A Note on the Angled Crack Problem and the Directional Stability of Cracks," **International Journal of Fracture**, 9, pp. 484-486 (1973).

2.4 Streit, R. and I. Finnie, "An Experimental Investigation of Crack-Path Directional Stability," **Experimental Mechanics**, 20, pp. 17-23 (1980).

2.5 Cotterell, B. and J.R. Rice, "Slightly Curved or Kinked Cracks," **International Journal of Fracture**, 16, pp. 155-169 (1980).

2.6 Palaniswamy, K. and W.G. Knauss, "Propagation of a Crack Under General In-plane Tension," **International Journal of Fracture Mechanics**, 8, pp. 114-117 (1972).

2.7 Hussain, M.A., Pu, S.L. and Underwood, J.H., "Strain Energy Release Rate for a Crack Under Combined Mode I and Mode II," **Fracture Analysis**, G.R. Irwin, editor, **ASTM STP 560**, pp. 2-28 (1974).

2.8 Wu, C.H., "Fracture Under Combined Loads by Maximum-Energy-Release-Rate Criterion, **Journal of Applied Mechanics**, 45, pp. 553-558 (1978).

2.9 Karihaloo, B.L., L.M. Keer and S. Nemat-Nasser, "Crack Kinking Under Non-Symmetric Loading," **Engineering Fracture Mechanics**, 13, pp. 879-888 (1980).

2.10 Hayashi, K. and S. Nemat-Nasser, "Energy Release Rate and Crack Kinking," **International Journal of Solids and Structures**, 17, pp. 107-114 (1981).

2.11 Sih, G.C., "A Special Theory of Crack Propagation," in **Methods of Analysis and Solutions of Crack Problems (Mechanics of Fracture Volume I)**, G.C. Sih, editor, Noordhoff International, Leyden, The Netherlands, pp. 21-45 (1973).

2.12 Theocaris, P.S. and N.P. Andrianopoulos, "A Modified Strain Energy Density Criterion Applied to Crack Propagation," **Journal of Applied Mechanics**, 49, pp. 81-86 (1982).

2.13 Goldstein, R.V. and R.L. Salganik, "Brittle Fracture of Solids With Arbitrary Cracks," **International Journal of Fracture**, 10, pp. 507-523 (1974).

2.14 Karihaloo, B.L., L.M. Keer, S. Nemat-Nasser and A. Oranratnachai, "Approximate Description of Crack Kinking and Curving," **Journal of Applied Mechanics**, 48, pp. 515-519 (1981).

2.15 Sumi, Y., S. Nemat-Nasser and L.M. Keer, "On Crack Branching and Curving in a Finite Body," **International Journal of Fracture**, 21, pp. 67-79 (1983); Erratum: **International Journal of Fracture**, 24, p. 159 (1984).

2.16 Amestoy, M. and J.B. Leblond, "Curvilinear Cracks in Planar Situations," **Fracture Control of Engineering Structures (Proceedings of the Sixth European Conference on Fracture, ECF6)**, (1986).

2.17 Yoffe, E.H., "The Moving Griffith Crack," **Philosophical Magazine**, 42, pp. 739-750 (1951).

2.18 Sih, G.C., "Dynamic Crack Problems: Strain Energy Density Fracture Theory," in **Elastodynamic Crack Problems (Mechanics of Fracture Volume 4)**, G.C. Sih, editor, Noordhoff International, Leyden, The Netherlands, pp. 17-37 (1977).

2.19 Kobayashi, A.S. and M. Ramulu, "Dynamic Stress-Intensity Factors for Unsymmetric Dynamic Isochromatics," **Experimental Mechanics**, 21, pp. 41-48 (1981).

2.20 Ramulu, M., **Dynamic Crack Curving and Branching**, PhD Dissertation, University of Washington (1982).

2.21 Ramulu, M. and A.S. Kobayashi, "Dynamic Crack Curving -- A Photoelastic Evaluation," **Experimental Mechanics**, 23, pp. 1-9 (1983).

2.22 Ramulu, M., A.S. Kobayashi, B.S.-J. Kang and D.B. Barker, "Further Studies on Dynamic Crack Branching," **Experimental Mechanics**, 23, pp. 431-437 (1983).

2.23 Ramulu, M., A.S. Kobayashi and B.S.-J. Kang, "Dynamic Crack Branching -- A Photoelastic Evaluation," **Fracture Mechanics: Fifteenth Symposium**, R.J. Sanford, editor, **ASTM STP 833**, pp. 130-148 (1984).

2.24 Hawang, J.S., A.S. Kobayashi, M.S. Dadkhah, B.S.-J. Kang, and Ramulu, M., "Dynamic Crack Curving and Crack Branching Under Biaxial Loading," **Proceedings of the 1985 SEM Spring Conference on Experimental Mechanics**, Las Vegas, Nevada, pp. 127-133 (June 1985).

2.25 Ramulu, M., A.S. Kobayashi and D.B. Barker, "Analysis of Dynamic Mixed-Mode Isochromatics," **Experimental Mechanics**, 25, pp. 344-353 (1985).

2.26 Rosakis, A.J. and K. Ravi-Chandar, **On Crack Tip Stress State: An Experimental Evaluation of Three-Dimensional Effects**, Report No. SM-84-2, Graduate Aeronautical Laboratories, California Institute of Technology, Pasadena, California (March 1984).

CHAPTER 3

FULL-FIELD REPRESENTATIONS OF THE CRACK-TIP STRESS FIELD

The work discussed here pertains to the analysis of stress fields associated with two-dimensional cracks under both static and dynamic, opening and shear mode loading conditions. It is therefore necessary as a first step, to develop appropriate expressions for the in-plane stresses for each case, such that these expressions can be used to describe the stress field over a reasonable sized region around the tip of a crack in a finite geometry. The analysis approach that will be employed will provide a representation of far-field influences on the local crack-tip stress field in terms of powers of distance from the crack tip.

3.1 Opening Mode; Static

It has been shown [3.1, 3.2], that in order to completely describe the stress state associated with two-dimensional cracks under static opening mode loading, a generalized form of the Westergaard equations [3.3] is necessary. This generalization follows from an Airy stress function of the form

$$F_I = \mathrm{Re}\,\bar{\bar{Z}}(z) + y\,\mathrm{Im}\,\bar{Z}(z) + y\,\mathrm{Im}\,\bar{Y}(z) \qquad (3.1)$$

from which,

$$\sigma_{x_I} = \mathrm{Re}\, Z - y\, \mathrm{Im}\, Z' - y\, \mathrm{Im}\, Y' + 2\, \mathrm{Re}\, Y \tag{3.2}$$

$$\sigma_{y_I} = \mathrm{Re}\, Z + y\, \mathrm{Im}\, Z' + y\, \mathrm{Im}\, Y' \tag{3.3}$$

and
$$\tau_{xy_I} = - y\, \mathrm{Re}\, Z' - y\, \mathrm{Re}\, Y' - \mathrm{Im}\, Y \tag{3.4}$$

where $\bar{Z}(z) = \frac{d}{dz}\bar{\bar{Z}}(z), \quad Z(z) = \frac{d}{dz}\bar{Z}(z), \quad Z'(z) = \frac{d}{dz}Z(z)$

and $\bar{Y}(z) = \frac{d}{dz}\bar{\bar{Y}}(z), \quad Y(z) = \frac{d}{dz}\bar{Y}(z), \quad Y'(z) = \frac{d}{dz}Y(z)$

are functions of the complex variable, $z = x + iy$, and the symbols 'Re' and 'Im' have their usual meaning, i.e., the Real and Imaginary parts of a complex function, respectively.

For opening mode problems, these functions are subject to the constraints that $\mathrm{Re}\, Z(z) = 0$ on the crack faces and $\mathrm{Im}\, Y(z) = 0$ along the crack line. Thus, for a single-ended, stress-free crack, with the origin of coordinates at the crack tip and the negative x-axis coinciding with the crack faces, as shown in Figure 3.1, the functions $Z(z)$ and $Y(z)$ can be represented as

$$Z(z) = \sum_{n=0}^{\infty} A_n\, z^{n-1/2} \tag{3.5}$$

and
$$Y(z) = \sum_{m=0}^{\infty} B_m\, z^{m} \tag{3.6}$$

where the A_n and B_m are real constants, and the opening mode stress intensity factor, K_I, is related to A_0, i.e., $K_I = A_0\sqrt{2\pi}$.

3.2 Shear Mode; Static

The shear mode counterpart for the static problem can be obtained by following a procedure similar to that described in References [3.1] and [3.2], and results in an Airy stress function of the form

$$F_{II} = \text{Re}\ \bar{\bar{Y}}^*(z) + y\ \text{Im}\ \bar{Y}^*(z) + y\ \text{Im}\ \bar{Z}^*(z) \tag{3.7}$$

where the symbols have the same meaning as before and the asterisk has been used (consistently both here and in subsequent sections) to distinguish the Westergaard type stress functions for shear mode loading from those used for the opening mode case.

The resulting expressions for the in-plane Cartesian stress components can then be obtained as

$$\sigma_{x_{II}} = \text{Re}\ Y^* - y\ \text{Im}\ Y^{*\prime} - y\ \text{Im}\ Z^{*\prime} + 2\ \text{Re}\ Z^* \tag{3.8}$$

$$\sigma_{y_{II}} = \text{Re}\ Y^* + y\ \text{Im}\ Y^{*\prime} + y\ \text{Im}\ Z^{*\prime} \tag{3.9}$$

and

$$\tau_{xy_{II}} = -\ y\ \text{Re}\ Y^{*\prime} - y\ \text{Re}\ Z^{*\prime} - \text{Im}\ Z^* \tag{3.10}$$

For the shear mode problem, the functions $Z^*(z)$ and $Y^*(z)$ are subject to the constraints that $\text{Im}\ Z^*(z) = 0$ on the crack faces and $\text{Re}\ Y^*(z) = 0$ along the crack line. Appropriate choices for $Z^*(z)$ and $Y^*(z)$ for the single-ended, stress-free crack problem, using the coordinate system of Figure 3.1, are then

$$Z^*(z) = \sum_{n=0}^{\infty} -i\, C_n\, z^{n-1/2} \qquad (3.11)$$

and
$$Y^*(z) = \sum_{m=0}^{\infty} -i\, D_m\, z^{m} \qquad (3.12)$$

The functions $Z^*(z)$ and $Y^*(z)$ are similar to the functions $Z(z)$ and $Y(z)$ introduced previously for the opening mode problem. The desired antisymmetry for shear mode loading is obtained through use of the multiplication factor of $i = \sqrt{-1}$ and the minus sign has been introduced solely for computational convenience. The C_n and D_m are real constants and the shear mode stress intensity factor, K_{II}, is related to C_0, i.e., $K_{II} = C_0\sqrt{2\pi}$.

3.3 Opening Mode; Dynamic

The problem of a semi-infinite crack translating at a fixed speed, c, in the positive x-direction under plane-strain conditions was first considered by Irwin [3.4]. He showed, that the dilatation, Δ, and rotation, ω, can be expressed, without loss of generality, in the form

$$\Delta = \frac{\partial u}{\partial x} + \frac{\partial v}{\partial y} = \alpha\,(1 - \lambda_1^{\,2})\ \mathrm{Re}\ \Gamma_1(z_1) \qquad (3.13)$$

and

$$\omega = \frac{\partial v}{\partial x} - \frac{\partial u}{\partial y} = \beta\,(1 - \lambda_2^{\,2})\ \mathrm{Im}\ \Gamma_2(z_2) \qquad (3.14)$$

where λ_1 and λ_2 are functions of the crack speed, c, relative to the longitudinal wave speed, c_1, and the shear wave speed, c_2, in the material, and z_1 and z_2 are velocity-transformed coordinates defined in Figure 3.2. The terms, Γ_1 and Γ_2, denote a pair of velocity-coupled, complex stress functions of the variables, z_1 and z_2, respectively, and are used to separate the dilatational and rotational components of the stress field. The exact form of these functions for a particular problem depends on the crack problem of interest, and the constants, α and β, have to be evaluated after making a choice for the pair, Γ_1 and Γ_2, so as to satisfy the specific boundary conditions on the problem being considered.

Constructing expressions for the strains, and using Hooke's Law, it can then be shown that the Cartesian in-plane stress components for the general elastodynamic problem are

$$\sigma_{xx} = \mu [\alpha (1 + 2\lambda_1{}^2 - \lambda_2{}^2) \, \text{Re } \Gamma_1 - 2\beta \lambda_2 \, \text{Re } \Gamma_2] \qquad (3.15)$$

$$\sigma_{yy} = \mu [-\alpha (1 + \lambda_2{}^2) \, \text{Re } \Gamma_1 + 2\beta \lambda_2 \, \text{Re } \Gamma_2] \qquad (3.16)$$

and $$\tau_{xy} = \mu [-2\alpha \lambda_1 \, \text{Im } \Gamma_1 + \beta (1 + \lambda_2{}^2) \, \text{Im } \Gamma_2] \qquad (3.17)$$

where μ is the shear modulus, and the other terms are as previously defined.

For the static opening mode problem, it has been demonstrated [3.2, 3.5] that two independent series stress functions are required to completely describe the stress field in specimens with finite boundaries, one beginning with an inverse-square-root singularity and the other with a constant term. These were denoted Z and Y, respectively, and choices that are appropriate for single-ended, stress-free, stationary cracks under opening-mode loading were presented in equations (3.5) and (3.6). A similar approach can be followed to obtain stress functions suitable for the dynamic opening-mode problem.

A logical first choice, similar to equation (3.5), is to define a pair of functions, Γ_1 and Γ_2, such that

$$\Gamma_1 = Z_1 = \sum_{n=0}^{\infty} A_n z_1^{n-1/2} \quad ; \quad \Gamma_2 = Z_2 = \sum_{n=0}^{\infty} A_n z_2^{n-1/2} \qquad (3.18)$$

with the notation Z_1 and Z_2 being introduced for ease of comparison with the static analog. The leading coefficient, A_0, is once again related to the opening mode stress intensity factor, $K_I = A_0\sqrt{2\pi}$, and the leading term is the familiar inverse-square-root stress singularity. For this choice of Γ_1 and Γ_2, $\sigma_{yy} = 0$ on the crack faces, and the symmetry condition ($\tau_{xy} = 0$) along the crack line requires that $\beta = 2\lambda_1\alpha/(1+\lambda_2^{\,2})$.

A second choice, which follows from the above, and which is analogous to equation (3.6), is to define

$$\Gamma_1 = Y_1 = \sum_{m=0}^{\infty} B_m z_1^m \quad ; \quad \Gamma_2 = Y_2 = \sum_{m=0}^{\infty} B_m z_2^m \tag{3.19}$$

where the introduction of the symbols Y_1 and Y_2 is again for convenience of comparison with the static counterpart. In this case, the requirement of traction-free crack faces results in $\beta = \alpha(1+\lambda_2^2)/2\lambda_2$, with the symmetry condition being automatically satisfied by the form of the expressions in equation (3.19).

The remaining constant, α, can be determined from the definition of the opening mode stress intensity factor

$$K_I = \lim_{r \to 0} \sqrt{2\pi r}\, \sigma_{yy}\big|_{\theta=0} \tag{3.20}$$

as $\alpha\mu = (1+\lambda_2^2) \;/\; [4\lambda_1\lambda_2 - (1+\lambda_2^2)^2]$.

Superposition of the two solutions given by equations (3.18) and (3.19) yields a general solution to the constant speed, opening mode elastodynamic crack problem as

$$\sigma_{xx_I} = \frac{(1+\lambda_2{}^2)}{4\lambda_1\lambda_2 - (1+\lambda_2{}^2)^2} \{ (1+2\lambda_1{}^2-\lambda_2{}^2) \text{ Re } Z_1 - \frac{4\lambda_1\lambda_2}{1+\lambda_2{}^2} \text{ Re } Z_2$$

$$+ (1+2\lambda_1{}^2-\lambda_2{}^2) \text{ Re } Y_1 - (1+\lambda_2{}^2) \text{ Re } Y_2 \} \qquad (3.21)$$

$$\sigma_{yy_I} = \frac{(1+\lambda_2{}^2)}{4\lambda_1\lambda_2 - (1+\lambda_2{}^2)^2} \{ - (1+\lambda_2{}^2) \text{ Re } Z_1 + \frac{4\lambda_1\lambda_2}{1+\lambda_2{}^2} \text{ Re } Z_2$$

$$- (1+\lambda_2{}^2) \text{ Re } Y_1 + (1+\lambda_2{}^2) \text{ Re } Y_2 \} \qquad (3.22)$$

$$\tau_{xy_I} = \frac{(1+\lambda_2{}^2)}{4\lambda_1\lambda_2 - (1+\lambda_2{}^2)^2} \{ - 2\lambda_1 \text{ Im } Z_1 + 2\lambda_1 \text{ Im } Z_2$$

$$- 2\lambda_1 \text{ Im } Y_1 + \frac{(1+\lambda_2{}^2)^2}{2\lambda_2} \text{ Im } Y_2 \} \qquad (3.23)$$

These expressions reduce to their static counterpart, equations (3.2)-(3.4), in the limit as the crack speed tends to zero. The limit as $c \to 0$ must, however, be taken with some care, since terms inside and outside the braces both go to zero and $z_1 \to z_2 \to z$. The static equivalent cannot thus be obtained by simply substituting $c = 0$ in equations (3.21)-(3.23).

3.4 Shear Mode; Dynamic

The shear mode counterpart to equations (3.21)-(3.23) can be obtained from the following considerations. First, equations (3.13)-(3.17) are general solutions that are not restricted to the opening mode crack problem. Second, the major difference between mode I and mode II stress fields is the antisymmetric nature of the stress field resulting from shear mode loading.

Analogous to equation (3.11), and a logical first step, is to select the stress functions, Γ_1 and Γ_2, as

$$\Gamma_1 = Z_1{}^* = \sum_{n=0}^{\infty} -i\ C_n\ z_1{}^{n-1/2}\ ;\ \Gamma_2 = Z_2{}^* = \sum_{n=0}^{\infty} -i\ C_n\ z_2{}^{n-1/2} \qquad (3.24)$$

The boundary conditions for the mode II problem require that, for this choice of Γ_1 and Γ_2, $\beta = \alpha(1+\lambda_2{}^2)/2\lambda_2$, to make $\sigma_{yy} = 0$ along the crack line. (The other boundary condition, namely that $\tau_{xy} = 0$ on the crack faces is automatically satisfied by the particular choices for Γ_1 and Γ_2.) In this case, the leading coefficient, C_0, is related to the shear mode stress intensity factor, $K_{II} = C_0\sqrt{2\pi}$.

The second pair of choices for Γ_1 and Γ_2, which follows from equation (3.12), and is analogous to equation (3.19) is

$$\Gamma_1 = Y_1{}^* = \sum_{m=0}^{\infty} -i\ D_m\ z_1{}^{m}\ ;\ \Gamma_2 = Y_2{}^* = \sum_{m=0}^{\infty} -i\ D_m\ z_2{}^{m} \qquad (3.25)$$

In this case $\sigma_{yy} = 0$ along $y = 0$ and to make $\tau_{xy} = 0$ on the crack faces requires that $\beta = 2\lambda_1 \alpha/(1+\lambda_2^2)$. The definition of the mode II stress intensity factor

$$K_{II} = \lim_{r \to 0} \sqrt{2\pi r}\ \tau_{xy}\big|_{\theta=0} \tag{3.26}$$

yields $\alpha\mu = 2\lambda_2 / [4\lambda_1\lambda_2 - (1+\lambda_2^2)^2]$.

The shear mode counterpart to equations (3.21)-(3.23) can then be written as

$$\sigma_{xx_{II}} = \frac{2\lambda_2}{4\lambda_1\lambda_2 - (1+\lambda_2^2)^2} \{ (1+2\lambda_1^2-\lambda_2^2) \text{ Re } Y_1^* - \frac{4\lambda_1\lambda_2}{1+\lambda_2^2} \text{ Re } Y_2^*$$

$$+ (1+2\lambda_1^2-\lambda_2^2) \text{ Re } Z_1^* - (1+\lambda_2^2) \text{ Re } Z_2^* \} \tag{3.27}$$

$$\sigma_{yy_{II}} = \frac{2\lambda_2}{4\lambda_1\lambda_2 - (1+\lambda_2^2)^2} \{ - (1+\lambda_2^2) \text{ Re } Y_1^* + \frac{4\lambda_1\lambda_2}{1+\lambda_2^2} \text{ Re } Y_2^*$$

$$- (1+\lambda_2^2) \text{ Re } Z_1^* + (1+\lambda_2^2) \text{ Re } Z_2^* \} \tag{3.28}$$

$$\tau_{xy_{II}} = \frac{2\lambda_2}{4\lambda_1\lambda_2 - (1+\lambda_2^2)^2} \{ - 2\lambda_1 \text{ Im } Y_1^* + 2\lambda_1 \text{ Im } Y_2^*$$

$$- 2\lambda_1 \text{ Im } Z_1^* + \frac{(1+\lambda_2^2)^2}{2\lambda_2} \text{ Im } Z_2^* \} \tag{3.29}$$

Once again, these expressions reduce to their static counterparts, equations (3.8)-(3.10), in the limit as $c \to 0$, if the limit is taken with some care, as discussed in the previous section.

3.5 Some General Observations

It has been pointed out in the preceding discussion that, in each case, the leading term in each of the series stress functions, Z and Z*, provides the inverse-square-root stress singularity generally associated with a crack-tip stress field and that the coefficient of the leading term is related to the opening (or shear mode) stress intensity factor.

The leading term of the second set of series stress functions, Y, gives rise to a constant stress in the direction of crack propagation for the opening mode case, equations (3.6) and (3.19). In this case the coefficient, B_0, is related to the familiar σ_{ox}-term in Irwin's near-field static equations [3.6], with $\sigma_{ox} = 2B_0$.

However, the leading term, D_0, of the similar set of series stress functions, Y*, that are used for the shear mode case, does not influence the stress components of equations (3.8)-(3.10) and (3.27)-(3.29). Hence, there is no counterpart to the σ_{ox}-term for either a stationary or a propagating crack under pure shear loading conditions. This in turn implies that the lowest-order non-singular term that influences the shear mode stress field is the $r^{1/2}$-term (the second term in the series stress function, Z*).

Since the problems being considered here are all linear elastic in nature, the general expressions for mixed-mode elastostatic or elastodynamic problems of cracks in finite geometries can be obtained by simple superposition of the appropriate expressions for opening and shear modes. A comparison of the results obtained here with those developed by other investigators for the static [3.7] and dynamic [3.8 - 3.11] cases, using complex potentials and eigen-function methods, reveals that these results are functionally equivalent to those given in the references cited, after suitable changes of variables. However, the results developed here are computationally efficient to implement, as will be seen in subsequent sections.

The results obtained for the series coefficients from specimens that are geometrically similar can often be correlated more easily if the series stress functions, Z and Y, are rewritten using non-dimensional coefficients. Equations (3.5) and (3.6), for example, can be rewritten as

$$Z(z) = \frac{A_0}{\sqrt{W}} (z/W)^{-1/2} \sum_{n=0}^{\infty} \frac{A_n}{A_0} W^n (z/W)^n$$

$$= \frac{K_I}{\sqrt{2\pi W}} (z/W)^{-1/2} \sum_{n=0}^{\infty} A_n' (z/W)^n \tag{3.30}$$

and

$$Y(z) = \frac{A_0}{\sqrt{W}} (z/W)^{-1/2} \sum_{m=0}^{\infty} \frac{B_m}{A_0} W^{m+1/2} (z/W)^{m+1/2}$$

$$= \frac{K_I}{\sqrt{2\pi W}} (z/W)^{-1/2} \sum_{m=0}^{\infty} B_m' (z/W)^{m+1/2} \tag{3.31}$$

where the A_n' and B_m' are now dimensionless real constants ($A_0' \equiv 1$) and W is some characteristic in-plane length dimension, such as the specimen width. Similar results can also be obtained for each of the other series stress functions of equations (3.11)-(3.12), (3.18)-(3.19), and (3.24)-(3.25), with the normalization being performed with reference to either A_0 or C_0, whichever is more appropriate for the particular problem being considered.

3.6 Application to Cracks Propagating Along Curved Paths

The stress field expressions that have been derived and discussed here all pertain to straight cracks, for which the origin of coordinates has been placed at the crack tip and the negative branch of the x-axis coincides with the crack faces. These expressions are also suitable for the representation of curving crack stress fields, if the x and y directions are taken as the instantaneous tangent and normal to the crack path, respectively. However, the region over which such a stress field representation would be considered reasonable is clearly a region whose size is small relative to the radius of curvature of the crack path at the point in question. Some care must therefore be exercised in selecting a region for data acquisition and analysis when using straight crack stress functions for the study of curving crack problems, to ensure that the radius of curvature of the crack path is large relative to the size of the region from which data is taken for analysis purposes. Further comments on this subject will be made later.

Some estimates of the possible errors introduced by using straight crack expressions for curved crack problems have been provided for cases where the curved crack stress field has a closed-form solution [3.12]. The conclusion drawn was that, for the cases of interest in the present study, namely gradually and smoothly curving cracks, any errors involved would be small provided that the guidelines given in the preceding discussion were kept in mind.

3.7 Application to Cracks Propagating at Non-Constant Speeds

It was pointed out that the general expressions, equations (3.13)-(3.14), followed from a constant crack speed assumption. Since the problems of interest may involve crack propagation at non-constant speeds, some discussion on this subject is in order.

The constant crack speed assumption and the consequences of removing this restriction have been studied by several investigators from an analytical viewpoint [3.13 - 3.17]. An excellent discussion on the subject has been provided recently by Freund, in which he argues that since the equation of motion for the crack is a first order differential equation in terms of crack speed, the crack velocity (and not the acceleration) changes in phase with the crack-tip driving force [3.18]. (In physical terms, this is equivalent to the statement that the crack-tip singularity field is massless and has zero inertia.) This allows variations in crack speed as a function of time, without violating the validity of the stress field expressions derived from a constant crack speed assumption, since these expressions depend only on the instantaneous crack velocity.

It should also be kept in mind that the crack propagation problems of interest here all involve continously propagating cracks under remote mechanical loading conditions. Any changes in crack speed that do occur thus take place in a gradual manner and not abruptly or discontinously, as would be the case in impact or explosive type loading conditions. If some care is exercised to ensure that the crack-tip stress pattern of interest for analysis purposes is one that is in fact changing gradually with time, it would appear from the above discussion that equations (3.21)-(3.23) and (3.27)-(3.29) can be used to describe the running crack stress field without error, even when the crack speed is not constant.

3.8 Application to Cracks Propagating in Plate Specimens

The general expressions for the stress field, equations (3.13)-(3.17), were obtained assuming plane-strain conditions. If the crack is propagating in a plate, the stress state of interest (removed from the immediate vicinity of the crack tip) becomes one of plane-stress. In this instance, the longitudinal wave speed, c_1, should be replaced by the plate wave speed, c_p, when carrying out the velocity-dependent coordinate transformations defined in Figure 3.2.

When experimental data is obtained using either surface measurements or through-thickness averaging techniques, it is also necessary to exercise some degree of care in selecting a region for data acquisition, to ensure that all data pertain to generalized plane-stress conditions. This imposes a restriction that data be taken no closer to the crack tip than one-half the thickness of the plate [3.19].

REFERENCES

3.1 Irwin, G.R., W.L. Fourney, D.B. Barker, R.J. Sanford, J.T. Metcalf, A. Shukla and R. Chona, **Photoelastic Studies of Damping, Crack Propagation, and Crack Arrest in Polymers and 4340 Steel, NUREG/CR-1455,** University of Maryland (May 1980).

3.2 Sanford, R.J., "A Critical Re-examination of the Westergaard Method for Solving Opening-Mode Crack Problems," **Mechanics Research Communications,** 6, pp. 289-294 (1979).

3.3 Westergaard, H.M., "Bearing Pressures and Cracks," **Transactions ASME,** 61, A49-A53 (1939).

3.4 Irwin, G.R., **Constant Speed Semi-Infinite Tensile Crack Opened by a Line Force, P, at a Distance, b, from the Leading Edge,** Lehigh University Lecture Notes on Fracture Mechanics (1968).

3.5 Liebowitz, H., J.D. Lee and J. Eftis, "Biaxial Load Effects in Fracture Mechanics," **Engineering Fracture Mechanics,** 10, pp. 315-335 (1978).

3.6 Irwin, G.R., "Discussion of: The Dynamic Stress Distribution Surrounding a Running Crack - A Photoelastic Analysis", **Proceedings SESA,** XVI, pp. 93-96, (1958).

3.7 Williams, M.L., "On the Stress Distribution at the Base of a Stationary Crack," **Journal of Applied Mechanics,** 24, pp. 109-114, (1957)

3.8 Radok, J.R.M., "On the Solution of Problems of Dynamic Plane Elasticity," **Quarterly of Applied Mathematics,** 14, pp. 289-298 (1956).

3.9 Freund, L.B. and R.J. Clifton, "On the Uniqueness of Elastodynamic Solutions for Running Cracks," **Journal of Elasticity**, 4, pp. 293-299 (1974).

3.10 King, W.W., J.F. Malluck, J.A. Aberson, and J.M. Anderson, "Application of Running Crack Eigenfunction to Finite Element Simulation of Crack Propagation," **Mechanics Research Communications**, 3, pp. 197-202 (1976).

3.11 Nishioka, T. and Atluri, S.N., "Path Independent Integrals, Energy Release Rates and General Solutions of Near-Tip Fields in Mixed Mode Dynamic Fracture Mechanics", **Engineering Fracture Mechanics**, 18, pp. 1-22 (1983).

3.12 Ramulu, M., **Dynamic Crack Curving and Branching**, PhD Dissertation, University of Washington (1982).

3.13 Kostrov, B.V., "On the Crack Propagation with Variable Velocity," **International Journal of Fracture**, 11, pp. 47-56 (1975).

3.14 Eshelby, J.D., "The Elastic Field of a Crack Extending Non-Uniformly Under General Anti-Plane Loading," **Journal of the Mechanics and Physics of Solids**, 17, pp. 177-199 (1969).

3.15 Nilsson, F., "Dynamic Stress Intensity Factors for Finite Strip Problems," **International Journal of Fracture Mechanics**, 8, pp. 403-411 (1972).

3.16 Nilsson, F., "A Note on the Stress Singularity at a Nonuniformly Moving Crack Tip," **Journal of Elasticity**, 4, pp. 73-75 (1974).

3.17 Achenbach, J.D. and Z.P. Bazant, "Elastodynamic Near-Tip Stress and Displacement Fields for Rapidly Propagating Cracks in Orthotropic Media," **Journal of Applied Mechanics**, 42, pp. 183-189 (1975).

3.18 Freund, L.B., "Dynamic Crack Propagation in Solids," in **Computational Methods in the Mechanics of Fracture**, S.N. Atluri, editor, North-Holland Publishing Company, New York, pp. 85-120 (1986).

3.19 Rosakis, A.J. and K. Ravi-Chandar, **On Crack Tip Stress State: An Experimental Evaluation of Three-Dimensional Effects, Report No. SM-84-2**, Graduate Aeronautical Laboratories, California Institute of Technology, Pasadena, California (March 1984).

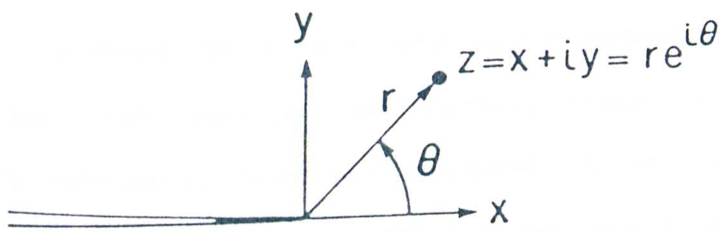

Figure 3.1 The crack-tip coordinate system for a single-ended, stress-free, stationary crack.

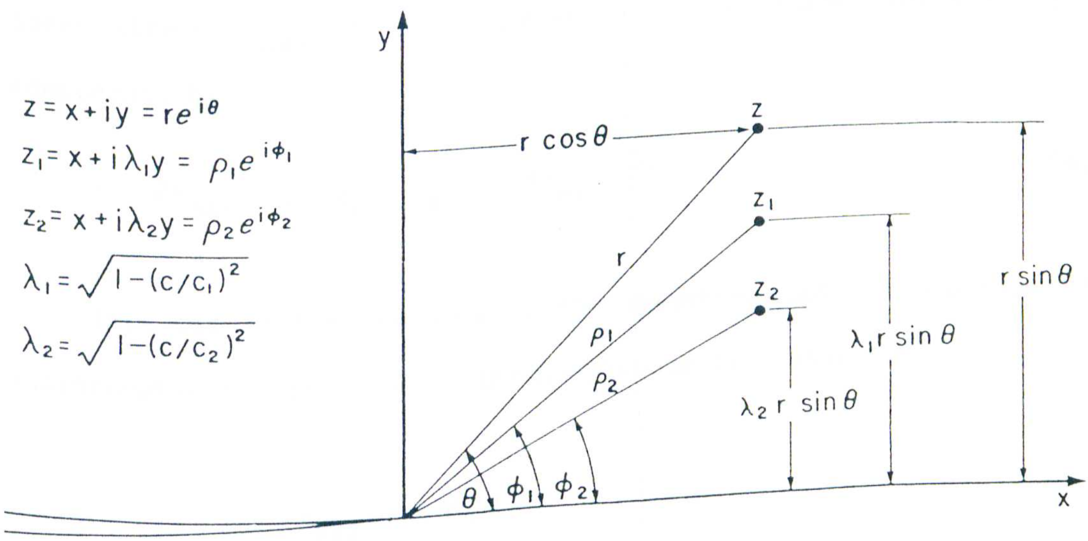

Figure 3.2 The crack-tip coordinate systems and the crack-speed dependent coordinate transformations employed in a constant crack speed stress field representation.

CHAPTER 4

DETERMINATION OF CRACK-TIP STRESS FIELD PARAMETERS FROM PHOTOELASTIC DATA

Dynamic photoelastic experiments provide full-field experimental data for the stress state in a large region around the tips of running cracks for both straight and curving crack situations. Plate specimens fabricated from a transparent, birefringent polymer were placed such that the plane of the specimen would be perpendicular to the optical axis of a high-speed, Cranz-Schardin camera system [**4.1, 4.2**], which provided a sequence of photographs of the stress field in the specimen during the course of the crack propagation event.

The stress field information was obtained in the form of isochromatic fringes, i.e., contours of constant maximum in-plane shear stress, τ_{max}, given in terms of the in-plane Cartesian stress components by

$$2\tau_{max} = [\ (\sigma_y - \sigma_x)^2 + 4\tau_{xy}{}^2\ ]^{1/2} \tag{4.1}$$

This was in turn related to the governing optical equations for isochromatic fringe patterns through the stress-optic law

$$2\tau_{max} = N f_\sigma / t \tag{4.2}$$

where N is the photoelastic fringe order at the point of interest, f_σ is the fringe sensitivity of the birefringent model material, and t is the model thickness.

The appropriate expressions for σ_x, σ_y, and τ_{xy}, developed in terms of the infinite series stress functions, Z, Y, Z*, and Y*, discussed in the previous chapter, were used with equations (4.1) and (4.2) to express the experimentally determined isochromatic fringe order at any point in the field in terms of the unknown coefficients, A_n, B_m, C_n, and D_m, the known crack speed, c, and the position coordinates (r,θ) of the point in question. (A detailed derivation of the expressions for the stress components has been provided in Appendix A.) The stress field parameters of interest were then determined using local collocation procedures as described below.

4.1 Parameter Determination Methodology

The first step in the application of the local collocation method to the analysis of a given isochromatic fringe pattern was to define a region around the crack tip for analysis purposes, extract a large number of individual data points distributed over the entire region, and determine the coordinates and fringe order at each data point. These data points were then used as inputs to an over-determined system of non-linear equations relating the fringe order and the series coefficients, and solved in a least-squares sense for the best-fit set of unknown coefficients, following the procedures outlined in [4.3 - 4.5]. The mathematical details of the procedure are given in Appendix B. Note that care was taken to exclude data points that would lie within one-half the plate thickness of the crack tip, for the reasons discussed in [4.6]. Otherwise, the only factor in data point selection was fringe clarity.

A given data set was analyzed using the computer programs listed in Appendix C. Sequential addition of terms to the truncated form of the power series representation of the stress field provided successively higher order stress field models, starting with a model of order 2, and increasing in steps of one until convergence of the results to stable values was obtained. The relationship between the order of the analysis model, J, and the highest power of radius, r^p, retained in the series stress field representation is given by $p = (J-2)/2$. A model of order 2 would therefore retain terms up to r^0, i.e., A_0, C_0, and B_0; a model of order 3 would retain terms up to $r^{1/2}$, i.e., A_0, C_0, B_0, A_1, and C_1; a model of order 4 would retain terms up to r^1, i.e., A_0, C_0, B_0, A_1, C_1, B_1, and D_1; and so on.

The highest order model which was needed for a particular data set depended upon the size of the data acquisition region and the distance from the crack tip to the boundaries of the specimen. Obviously, the coefficients of the two series Z^* and Y^* (C_n and D_m) entered into the analysis only when the crack was propagating along a non-straight path.

The average fringe order error, $|\Delta N|$, for a data set with a total of K points, has been defined in this study as the average difference between the specified (input) fringe order, N_i, at a given point and the fringe order (at the same point) computed from the best-fit set of coefficients, N_c. This quantity was computed for each analysis model from

$$|\Delta N| = \frac{1}{K} \sum_{k=0}^{k=K} | N_i - N_c |_k \tag{4.3}$$

and used as a measure of the quality of the fit between the experimental input data and the computed best-fit coefficient set. The behavior of $|\Delta N|$ as a function of the order of the analysis model was then examined and was typically found to stabilize to a value between 2% and 5% of the average input fringe order once the stress field had been modelled well over the region of data acquisition.

The behavior of the leading coefficients of each series was also examined and showed similar, stable behavior once a good fit had been achieved. Finally, each of the coefficient sets computed by the analysis algorithm was used to reconstruct the fringe pattern over the region of data acquisition so as to visually confirm that the stress state around the crack tip had in fact been properly modeled by the analysis model selected as being "correct". This eliminated the possibility of "false" solutions which can sometimes occur [4.7].

The techniques described above were used to analyze each of the crack-tip isochromatic fringe patterns that were obtained from the dynamic photoelastic experiments. Two illustrative examples, the first for a straight crack and the second for a curving crack, are discussed below in more detail.

4.2 Illustrative Example No. 1 -- Straight Crack

The methodology outlined above is illustrated here through the analysis of a crack propagation experiment performed using a 1/2-inch

(13 mm) thick ring segment fabricated from Homalite 100 [4.8], a brittle polymer that has been used extensively in dynamic photoelastic studies of fracture [4.2]. A total of 16 flash photographs of the isochromatic fringe patterns associated with the running crack were available over a range of crack lengths varying from a/W = 0.19 to a/W = 0.90 for the particular experiment selected for analysis from the data available in [4.8].

Figure 4.1 shows the isochromatic pattern 145 μs after crack initiation. The crack tip at this particular instant was located at an a/W of 0.52, and the crack speed, as determined from the slope of the crack position versus time record, was constant at 15,000 inches/sec (375 m/s; $c/c_2 = 0.31$). A total of 60 data points were taken for analysis purposes from within the circular region of radius 0.75 inches (19 mm; 0.15W) which has been marked on the fringe pattern in the figure. Note that no data were taken closer than 1/4-inch (6 mm) from the crack tip so as to ensure that all data points would lie within a region of generalized plane stress [4.6].

This data set was input to the least-squares algorithm and analyzed using successively higher order stress field representations as discussed earlier. Figure 4.2 shows the behavior of the error term defined in equation (4.3) and of the leading series coefficients, A_0, B_0, and A_1, as the order of the analysis model was increased from two (A_0, B_0) to six (A_0, B_0, A_1, B_1, A_2, B_2). The error term can be seen to decrease monotonically before stabilizing to a value of about 3% and stabilization with increasing order of analysis model is also readily apparent for the singular and leading non-singular coefficients also.

Figure 4.3 compares the experimental fringe pattern over the data acquisition region with the computer-generated fringe patterns corresponding to the best-fit coefficient set from each order model. It can be seen that a model of order six is required before the reconstructed pattern fully matches the salient features of the input experimental pattern. The same conclusion would also be reached from an examination of the error term in Figure 4.2.

Other noteworthy observations that can be made are as follows:

(a) The inner set of closed isochromatic fringes in Figure 4.3 show little change in size, shape, and orientation between models of order 4 through 6. This is to be expected since additional non-singular terms would have greater effects on the far-field features of the stress field.

(b) Examination of Figure 4.2, and the same data presented in tabular form in Table 4-1, shows that the singular term, A_0, changes by a significant amount when the $r^{1/2}$-term is retained in the analysis, but changes by less than 1% beyond a third-order model. This illustrates the importance of retaining terms of (at least) order $r^{1/2}$ when attempting to accurately determine even the singularity alone from photoelastic data and is in agreement with the conclusions arrived at previously from the study of stationary cracks for a variety of geometries and loading conditions [**4.7**] as well as optical methods other than photoelasticity [**4.9, 4.10**].

(c) Further examination of Figure 4.2 and Table 4-1 shows that the changes in the coefficients of r^0 and $r^{1/2}$ are small (of the order of 5% or less) once the analysis models are of order 4 and order 5, respectively. Reasonably accurate determination of a specific non-singular stress term is thus obtained once the analysis model retains at least one additional coefficient beyond the coefficient of interest in the particular series. This is not surprising, since it amounts simply to a restatement of a basic principle in numerical analysis, i.e., the coefficients of an infinite series which has been truncated at some point can be determined with reasonable accuracy only up to the term preceding the point of truncation; the last term absorbs a substantial portion of the error due to truncation.

4.3 Illustrative Example No. 2 -- Curving Crack

While the basic methodology for determining the crack-tip stress field coefficients does not change when analyzing photoelastic patterns for cracks that are propagating along curved paths, there are certain special considerations that need to be kept in mind, particularly with regard to selection of a region for data acquisition. A discussion similar to that of the previous example is therefore presented below for the case of a smoothly curving crack.

Figure 4.4 shows the crack-tip isochromatic fringe pattern for a crack propagating in a cross-shaped specimen under biaxial loading [4.11], and the particular pattern is Frame 12 from a set of 20 high speed photographs of the running crack stress patterns. The asymmetry of the pattern is readily apparent for this case. The crack was propagating at a constant speed in the specimen, which was fabricated in this instance from a 3/8-inch (10 mm) thick sheet of Homalite 100. The crack speed was determined to be 16,000 inches/sec (415 m/s; $c/c_2 = 0.33$).

The data acquisition region selected for analysis purposes had a radius of 1/2-inch (13 mm) and is marked on the fringe pattern of Figure 4.4. The size of the data acquisition region was selected so that it would provide adequate information about higher order term influences (based on previous experience) while simultaneously being of moderate size relative to the local radius of curvature of the crack path, which was of the order of 5 inches (127 mm) in this instance. The moderate size of the data acquisition region relative to the local radius of curvature of the crack path allowed the straight crack stress field expressions developed previously to be utilized without significant error. The crack-tip coordinate system was oriented so that the x-direction would correspond to the local tangent to the crack path, which was established from a post-mortem examination of the specimen.

A total of 60 data points distributed over the entire region were selected to form the data set for analysis purposes. However, care was taken to avoid (a) data closer to the crack tip than about one-half the specimen thickness (5 mm) as well as (b) data from the fringes that were very close to the curved crack boundaries, where the assumption of a locally straight crack would not be valid.

This data set was then analyzed sequentially with models whose order ranged from two (A_0, C_0, B_0) to six (A_0, C_0, B_0, A_1, C_1, B_1, D_1,

A_2, C_2, B_2, D_2). The changes in the fringe order error with an increase in the order of the analysis model were then examined and showed the behavior illustrated in Figure 4.5, which also shows the behavior of the leading coefficients of the series stress functions. The error term stabilized to an error of about 4% of the average input fringe order once the stress state had been modeled well over the region of data acquisition. The leading coefficients of each series were also found to stabilize once a good fit had been achieved and this is also shown in Figure 4.5.

Each of the coefficient sets obtained from the analysis was used to reconstruct the fringe pattern over the region of data acquisition and the results are shown in Figure 4.6. The model of order 5 can easily be seen to match the salient features of the stress field over the region of data acquisition; a conclusion similar to that available from an examination of the behavior of the error term in Figure 4.5.

Comments were made in the discussion of the straight crack example regarding the need for retaining terms of order $r^{1/2}$, even when trying to determine only the singular coefficients, as well as the need for retaining at least one term in each series beyond the point of immediate interest if reliable and accurate results were desired. Examination of the results for this particular example, shown graphically in Figures 4.5 and 4.6 and in tabular form in Table 4-2, shows that the same comments also apply to the parameter determination problem for curving cracks.

TABLE 4-1

PARAMETER VALUES COMPUTED FROM SUCCESSIVE ANALYSIS MODELS

FOR THE STRAIGHT CRACK EXAMPLE (FIGURE 4.2)

PARAMETER	ORDER OF MODEL (HIGHEST POWER OF r RETAINED)				
	2 (r^0)	3 ($r^{1/2}$)	4 (r^1)	5 ($r^{3/2}$)	6 (r^2)
A_0 (psi-in$^{1/2}$)	206.9	214.7	216.2	216.2	215.7
% of Final Value	95.9%	99.5%	100.2%	100.2%	100.0%
B_0 (psi-in^0)	61.5	82.4	97.7	96.7	94.4
% of Final Value	65.1%	87.3%	103.5%	102.4%	100.0%
A_1 (psi-in$^{-1/2}$)		-168.2	-308.9	-327.2	-320.5
% of Final Value		52.5%	96.4%	102.1%	100.0%
$\lvert \Delta N \rvert$	7.5%	5.1%	3.2%	2.7%	2.7%

TABLE 4-2

PARAMETER VALUES COMPUTED FROM SUCCESSIVE ANALYSIS MODELS

FOR THE CURVING CRACK EXAMPLE (FIGURE 4.5)

PARAMETER	ORDER OF MODEL (HIGHEST POWER OF r RETAINED)			
	2 (r^0)	3 ($r^{1/2}$)	4 (r^1)	5 ($r^{3/2}$)
A_0 (psi-in$^{1/2}$)	603.8	597.3	588.1	590.4
% of Final Value	102.3%	101.2%	99.6%	100.0%
C_0 (psi-in$^{1/2}$)	43.2	44.8	29.2	32.0
% of Final Value	135.0%	140.0%	91.3%	100.0%
B_0 (psi-in^0)	272.7	310.5	295.1	301.5
% of Final Value	90.5%	102.9%	97.9%	100.0%
A_1 (psi-in$^{-1/2}$)		-226.8	-53.9	-39.5
% of Final Value		574.2%	136.5%	100.0%
C_1 (psi-in$^{-1/2}$)		242.8	291.3	265.8
% of Final Value		91.3%	109.6%	100.0%
$\|\Delta N\|$	23.8%	6.1%	3.7%	3.5%

REFERENCES

4.1 Riley, W.F. and J.W. Dally, "Recording Dynamic Fringe Patterns with a Cranz-Schardin Camera," **Experimental Mechanics**, 9, pp. 27N-33N (1969).

4.2 Dally, J.W., "Dynamic Photoelastic Studies of Fracture," **Experimental Mechanics**, 19, pp. 349-367 (1979).

4.3 Sanford, R.J., "Application of the Least-Squares Method to Photoelastic Analysis," **Experimental Mechanics**, 20, pp. 192-197 (1980).

4.4 Irwin, G.R., W.L. Fourney, D.B. Barker, R.J. Sanford, J.T. Metcalf, A. Shukla and R. Chona, **Photoelastic Studies of Damping, Crack Propagation, and Crack Arrest in Polymers and 4340 Steel, NUREG/CR-1455**, University of Maryland (May 1980).

4.5 Sanford, R.J. and R.E. Link, "Local Collocation - A Hybrid Technique in Fracture Mechanics", **Proceedings of the Twelfth Southeastern Conference on Theoretical and Applied Mechanics (SECTAM XII)**, pp. 183-187 (1984).

4.6 Rosakis, A.J. and K. Ravi-Chandar, **On Crack Tip Stress State: An Experimental Evaluation of Three-Dimensional Effects**, Report No. **SM-84-2**, Graduate Aeronautical Laboratories, California Institute of Technology, Pasadena, California (March 1984).

4.7 Chona, R., **Non-Singular Stress Effects in Fracture Test Specimens -- A Photoelastic Study**, M.S. Thesis, University of Maryland (1985).

4.8 Shukla, A., **Study of Energy Loss During a Fracture Event**, PhD Dissertation, University of Maryland (1981).

4.9 Sanford, R.J., "The Influence of Nonsingular Stresses on Experimental Measurements of the Stress Intensity Factor," **Modeling Problems in Crack Tip Mechanics**, J.T. Pindera, editor, Martinus Nijhoff Publishers, pp. 317-324 (1984).

4.10 Barker, D.B., R.J. Sanford and R. Chona, "Determining K and Related Stress Field Parameters From Displacement Fields," **Experimental Mechanics**, 25, pp. 399-407 (1985).

4.11 Shukla, A. and S. Anand, "Dynamic Crack Propagation and Branching Under Biaxial Loading," **Fracture Mechanics: Seventeenth Symposium**, Underwood, J.H., et al., editors, **ASTM STP 905**, pp. 697-714 (1986).

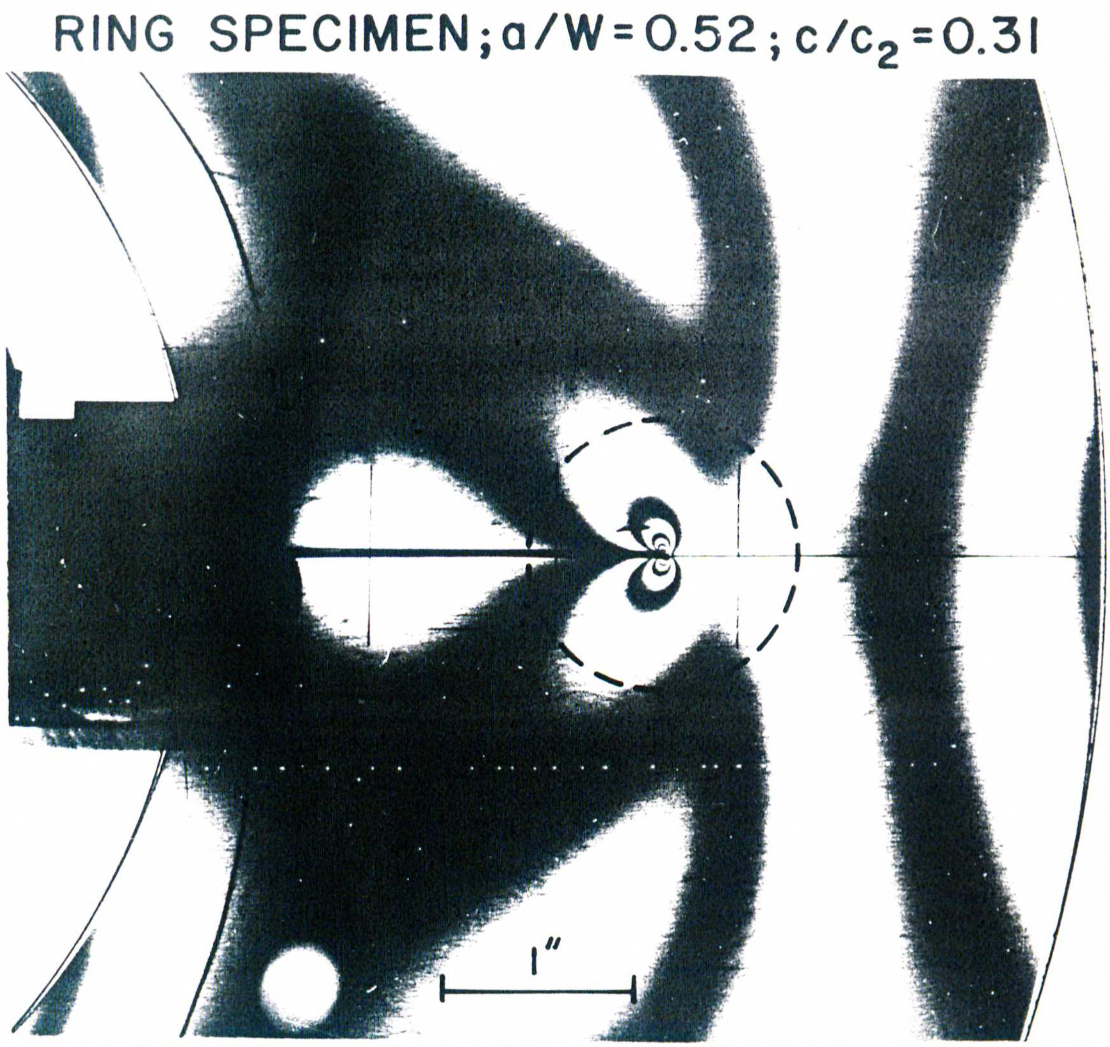

Figure 4.1 The crack-tip isochromatic fringe pattern recorded 145 μs after rapid crack initiation in a ring segment. The crack tip is located at $a/W=0.52$ and the crack is propagating at a speed of 15,000 inches/sec ($c/c_2=0.31$). The dashed circle indicates the region of data acquisition.

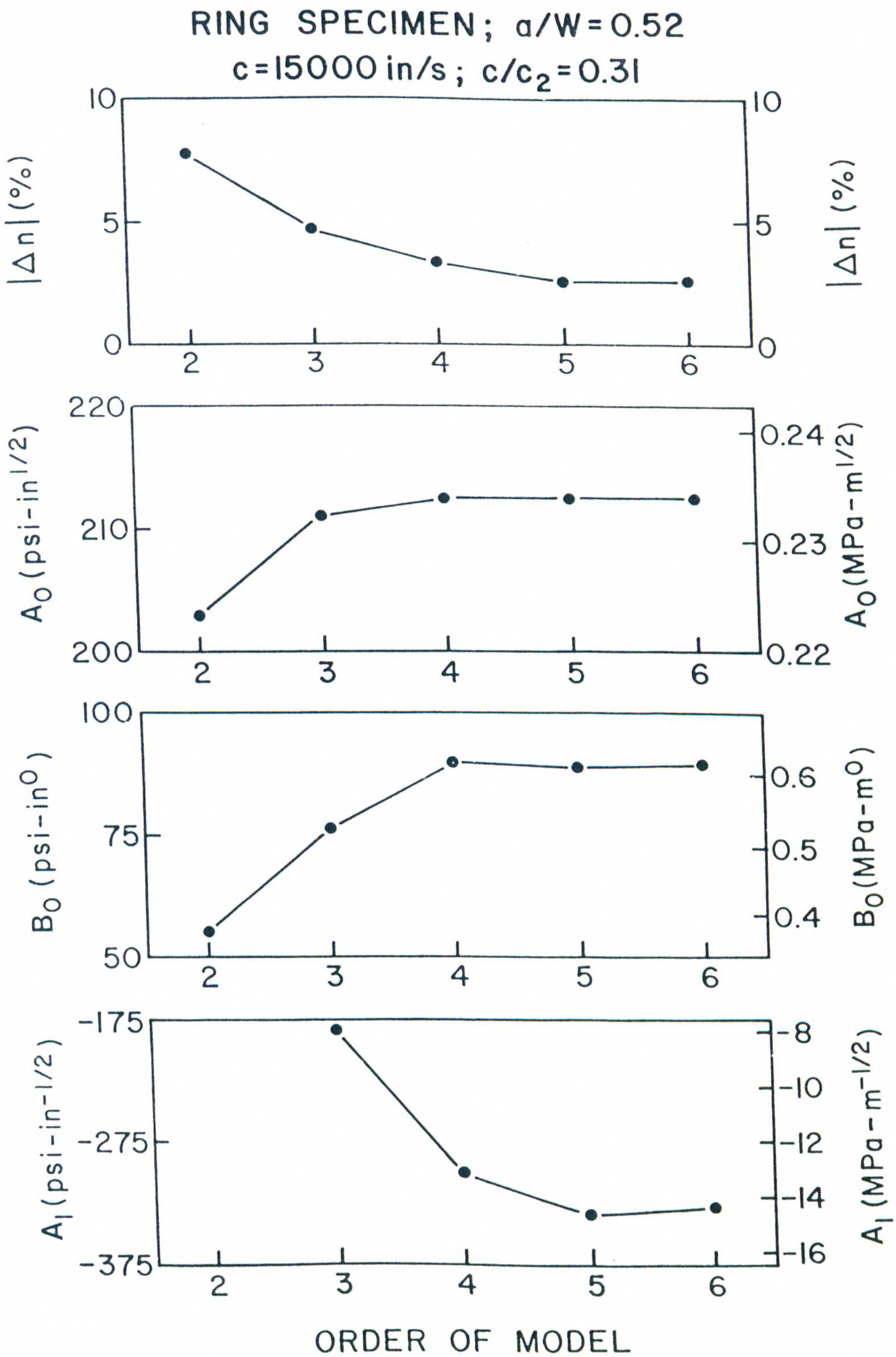

Figure 4.2 The changes with increasing order of analysis model in the error term and leading series coefficients from local collocation analyses of the fringe pattern of Figure 4.1.

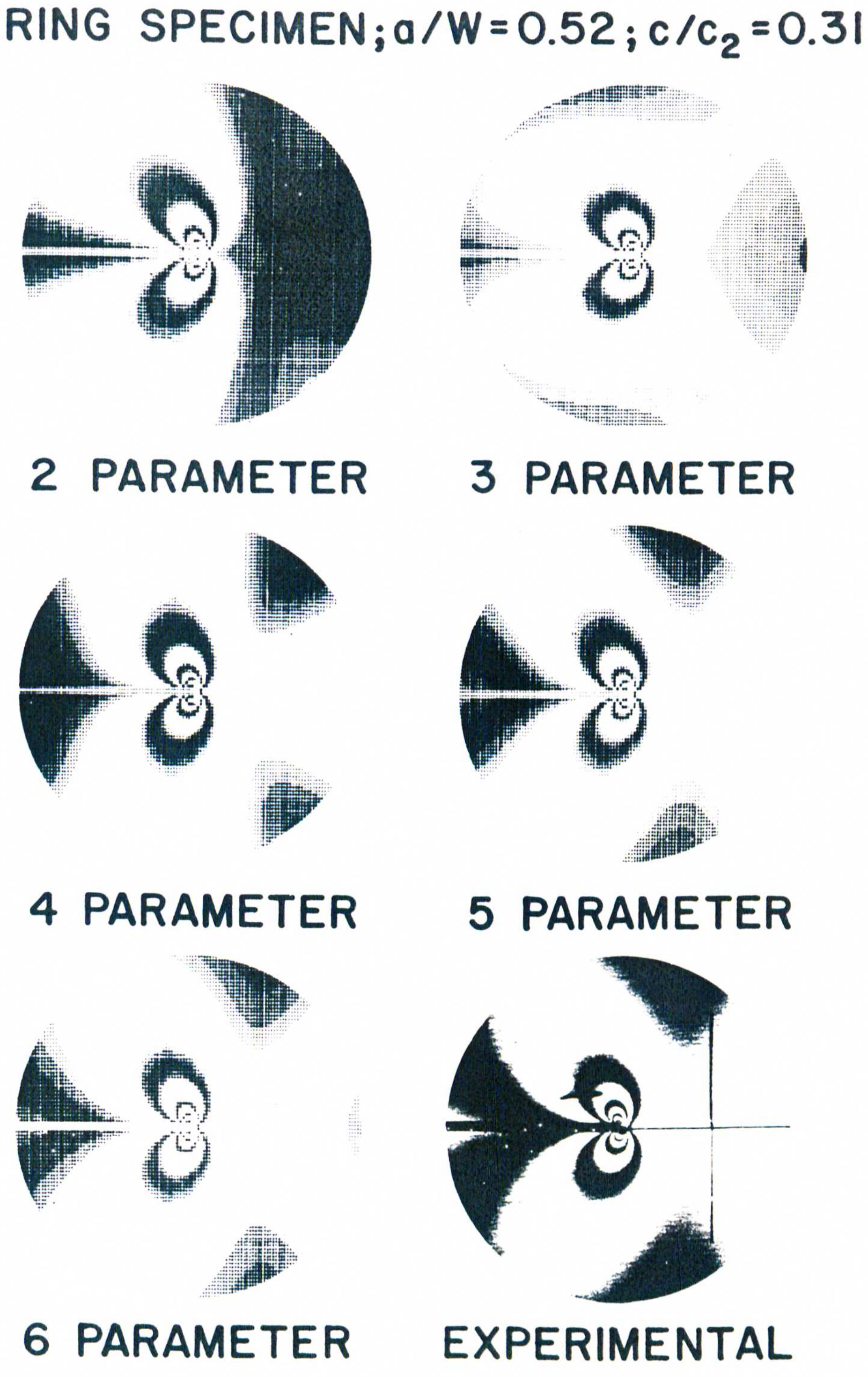

Figure 4.3 The experimental fringe pattern over the data acquisition region of radius equal to 0.75 inches and the reconstructed (computer generated) isochromatic patterns corresponding to successively higher order analysis models. The 2 Parameter (2nd Order) Model retains terms upto r^0, the 3 Parameter (3rd Order) Model retains terms upto $r^{1/2}$, and so on.

Figure 4.4 The crack-tip isochromatic fringe pattern recorded 154 μs after rapid crack initiation for a crack propagating along a curved path in a biaxially-loaded, cross-shaped specimen (Frame 12 from Experiment 11). The crack is propagating at a constant speed of 16,000 inches/sec (c/c_2=0.33) and the circle shows the region used for data acquisition purposes.

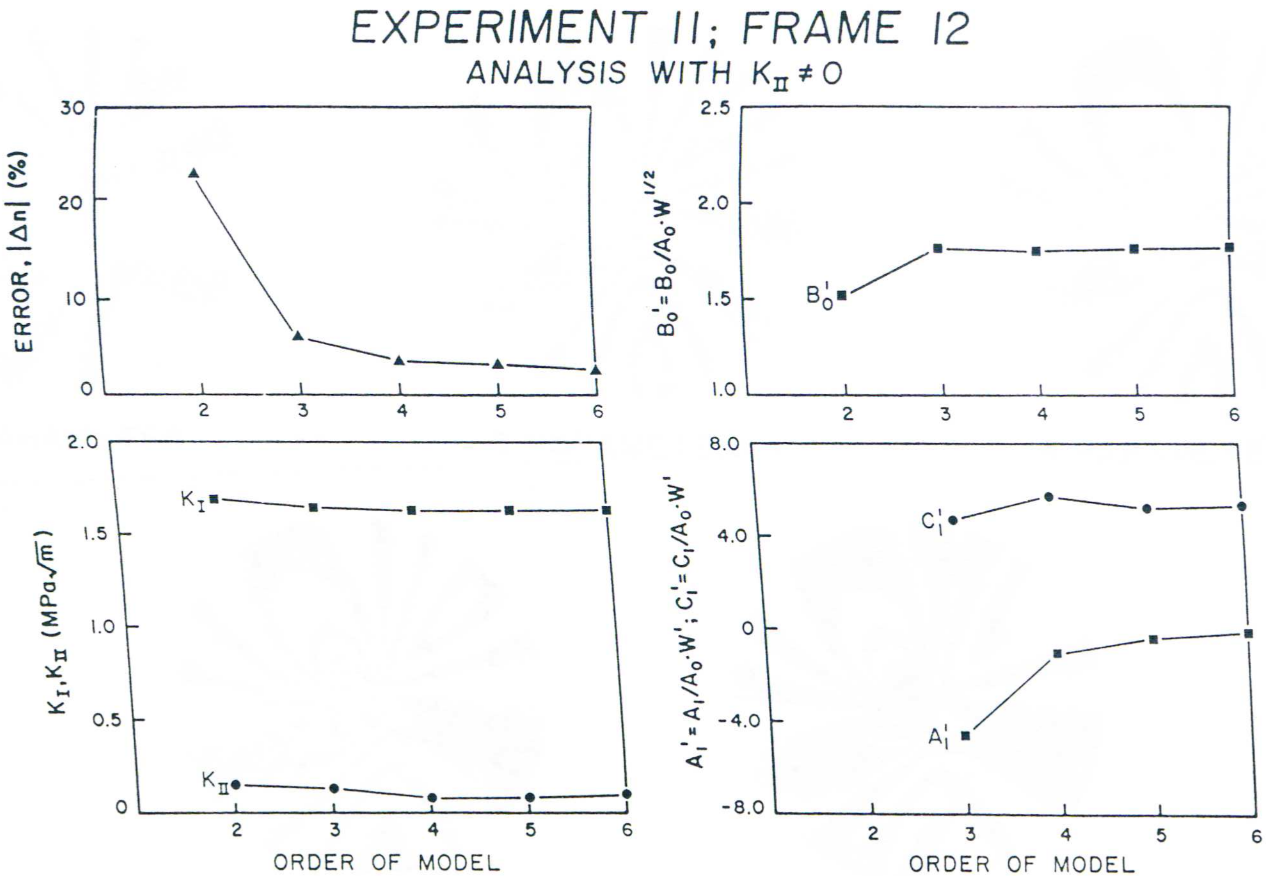

Figure 4.5 The changes with increasing order of analysis model in the error term and leading series coefficients from local collocation analyses of the fringe pattern of Figure 4.4.

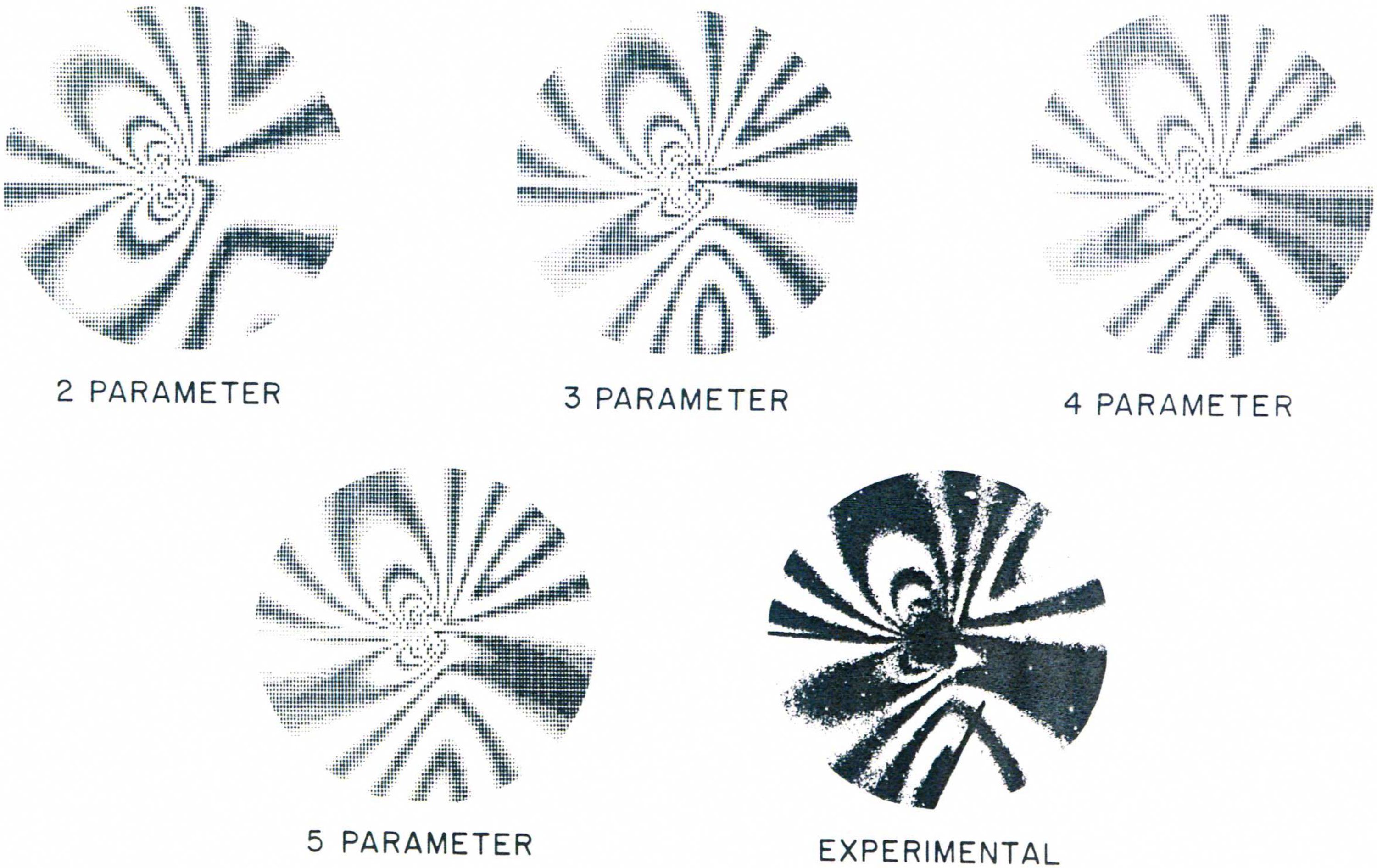

Figure 4.6 The experimental fringe pattern over the data acquisition region of radius equal to 0.50 inches and the reconstructed (computer generated) isochromatic patterns corresponding to successively higher order analysis models. The 2 Parameter (or 2nd Order) Model retains terms upto r^0, the 3 Parameter (or 3rd Order) Model retains terms upto $r^{1/2}$, and so on.

CHAPTER 5

RESULTS FOR CRACK PROPAGATION UNDER OPENING MODE AND COMBINED LOADING CONDITIONS

The techniques for determining the stress field parameters of interest from photoelastic fracture patterns that were described in the previous chapter were used to analyze experimental data pertaining to both straight and curving cracks. The results obtained from the analyses are described in the following sections.

5.1 Results for Crack Propagation Under Opening Mode Conditions

A crack propagation experiment performed using a ring segment with the geometry and loading shown in Figure 5.1 provided a total of 16 high speed photographs of the isochromatic fringe patterns associated with the running crack [5.1]. The specimen was fabricated from 1/2-inch (13 mm) thick Homalite 100 sheet and the fringe patterns were recorded using a Cranz-Schardin type camera system [5.2].

In the particular experiment selected from [5.1] for analysis purposes, the running crack was initiated from a blunt starter notch at a crack length to specimen width ratio of $a_0/W = 0.10$ and propagated continously across the specimen without arresting. The crack speed shortly after initiation was determined from the slope of the crack position versus time record as being 15,000 inches/sec (375 m/s; $c/c_2 = 0.31$). The crack propagated at this velocity for about 165 μsec until an a/W of 0.56, after which the crack speed gradually decreased in the last phases of crack propagation to about 4,000 inches/sec (100 m/s; $c/c_2 = 0.08$). Experimental data was thus obtained from a single experiment over a wide range of crack lengths ($a/W = 0.19$ to $a/W = 0.90$) and crack speeds ($c/c_2 = 0.31$ to $c/c_2 = 0.08$).

The analysis procedure followed for one frame from this experiment was discussed at some length in the previous chapter (Section 4.2). The same techniques were applied to each of the sixteen frames in the set and results obtained for the stress intensity factor, K_I, and for the leading non-singular stress terms, B_0, and A_1, as functions of the crack tip position in the specimen. The analyses required retention of terms ranging from r^1 to $r^{5/2}$, depending on the size of the region used for data acquisition purposes and the distance from the crack tip to the specimen boundaries. The number of data points for each fringe pattern varied between 40 and 60. As discussed previously, stability of the fringe order error and the leading stress field coefficients (K_I and B_0) was the primary measure used to decide when the stress state was being adequately modelled over the region of data acquisition. The quality of the match was confirmed for each case by reconstructing the fringe pattern corresponding to the computed set of coefficients and comparing it with the experimental data.

Figure 5.2 shows the results for the instantaneous crack-tip stress intensity factor as a function of a/W. A decreasing K-field is typical of this particular geometry and loading combination [5.3], and K_I is seen to decrease monotonically from an initially high value to essentially a constant as the crack propagated across the specimen and the crack speed decreased from its initial high value to the rather low speeds recorded during the last few frames.

The variation with crack position of the two leading non-singular terms (expressed in dimensionless form), B_0' and A_1', is shown in Figures 5.3 and 5.4, respectively. In both cases, the parameters in question are seen to vary in a systematic fashion as the crack length increases and their general trends are similar to previous results for stationary cracks in other specimen geometries [5.4, 5.5]. The influence of the approaching specimen boundary is readily apparent from the rather rapid changes in the non-singular terms that take place beyond an a/W of about 0.8 and the changes in sign and trends for both B_0' and A_1' at short crack lengths (a/W $\approx$ 0.3 or less) are consistent with previous observations also [5.6, 5.7].

5.2 Results for Cracks Propagating Along Curved Paths

A cross-shaped fracture specimen with the geometry shown in Figure 5.5 had been designed previously for the purpose of studying crack propagation behaviors under biaxial loading conditions [5.8]. Any eccentricity in the load, Q, applied parallel to the axis of symmetry of the specimen, would naturally result in a combined tension and forward shear loading condition, and cause a rapidly propagating crack to follow a non-straight path. Arrangements were therefore made with Dr. A. Shukla of the University of Rhode Island to test a series of such specimens under eccentric biaxial loading, to obtain the dynamic photoelastic data needed for detailed analysis.

The results from two such experiments, designated Experiments 11 and 12, respectively, were selected for analysis and discussion in the present study. The specimens in both cases were fabricated from 3/8-inch (10 mm) thick sheets of Homalite 100 and a Cranz-Schardin camera was once again used to obtain high speed photographs of the isochromatic fringe patterns around the tip of the propagating crack.

A sequence of frames showing the changes with crack propagation in the crack tip fringe patterns from each experiment is shown in Figures 5.6 and 5.7 for Experiments 11 and 12, respectively. In both cases the fringe patterns show considerable far-field asymmetry, indicating the presence of a substantial shear mode influence. The major difference between the two experiments was the magnitude of the tensile load, Q, applied parallel to the original crack line, with the load, P, applied normal to the initial crack direction being essentially the same in both experiments. Experiment 11 had a large, biaxial tension (about 50% of P), while Experiment 12 had only a small tensile load (about 10% of P) applied parallel to the initial crack direction. The fringe patterns recorded in each case confirm this observation, with the fringes of Experiment 11 (Figure 5.6) showing the strong backward-lean characteristic of this type of loading [5.9].

In both experiments, rapidly propagating cracks were initiated at load levels that were high enough to produce crack propagation at an essentially constant speed of 16,000 inches/sec (400 m/s; $c/c_2 = 0.33$) over the period of observation. This was one factor in selecting these two experiments for analysis purposes, since it was considered desirable to be able to study the non-singular effects on the local crack-tip stress field and the path followed by the propagating crack without introducing possible additional complexities due to variations in the crack speed.

The path followed by the propagating crack in each experiment is shown in Figure 5.8 for the portion of the crack propagation that was within the window of observation of the camera system. The position along each crack trajectory has been defined in terms of normalized coordinates, X/W and Y/W, oriented along the axes of symmetry of the specimen, with the origin located at the starter crack tip, as shown in Figure 5.5.

Post-mortem examination of the fractured specimens showed that the crack propagation event occurred without the intervention of any attempts at branching. (This was consistent with the crack-tip K-values obtained from the subsequent analyses and the magnitudes of both the primary and biaxial loads, P and Q, applied in each case [5.8].) The resulting fracture surfaces were smooth and the crack plane remained perpendicular to the plane of the specimen.

The crack trajectory for each experiment was traced and this trace was then used to digitize the position coordinates of approximately 100 points along each crack path, starting at the tip of the starter notch, and continuing well beyond that portion of the crack path for which isochromatic fringe pattern data was available. This digitized description of each crack path was then used to fit a 4th order polynomial of the form, $Y = F(X) = a_0 + a_1X + a_2X^2 + a_3X^3 + a_4X^4$, to each crack trajectory using standard least-squares techniques. An expression was thus obtained, which was then available to compute the slope of the tangent to the crack path for purposes of orienting the crack-tip coordinate system used to perform subsequent analyses of the photoelastic data. Calculations of the curvature of the crack path as a function of position along the trajectory were also made using the polynomial expression, both to ensure that the size of the data acquisition region(s) used would be moderate relative to the instantaneous radius of curvature of the path, and to provide the curvature information that was desired for further studies.

The isochromatic fringe patterns recorded in each experiment were analyzed using the local collocation method for parameter determination that was presented and discussed in the previous chapter, in which Frame 12 from Experiment 11 was discussed in some detail as a representative example. Results were thus obtained with a high degree of confidence for the mode I and mode II stress intensity factors, K_I and K_{II}, associated with each fringe pattern, as well as for the leading non-singular stress terms, B_0, A_1, and C_1.

The data acquisition regions used varied in radius between 1/2 and 3/4 inches (13 to 19 mm) and care was taken to keep the size of the data acquisition region moderate relative to the radius of curvature of the crack path, which ranged from 4 to 10 inches (100 to 250 mm) for the two experiments. Data points were not taken very close to the curved crack boundaries and a region of radius equal to one-half the specimen thickness (3/16 inch or 5 mm) was excluded for data acquisition purposes, for the reasons discussed previously. The number of data points digitized ranged between 50 and 60 for each fringe pattern and terms of order $r^{3/2}$ were found to be required before a good match was achieved between computed and experimental stress states over the region of data acquisition.

Figure 5.9 shows the values of K_I and K_{II} determined from local collocation of the the dynamic isochromatic fringe data for the two experiments. The results have been shown as functions of the time after rapid crack initiation, since the cracks propagated at a constant velocity in both experiments, but followed different paths. The opening mode stress intensity factor, K_I, was found to increase monotonically as the crack propagated into the specimen, changing from about 1300 psi$\sqrt{in}$ to about 1600 psi$\sqrt{in}$ in a time span of about 175 μsec. This result is consistent with the results one would expect if the crack had propagated straight across a specimen of this geometry with an initial applied load, P, equal to that used in these two experiments [5.8].

The calculated values of the shear mode stress intensity factor, K_{II}, on the other hand remained constant and very close to zero throughout, with calculated values that ranged between 2% and 5% of the instantaneous K_I. Since the crack trajectories and changes in curvature of the crack paths were significantly different in the two experiments, this result was felt to be particularly interesting relative to the assumption that has been made by other investigators [5.10], namely that K_{II} is the sole factor determining crack propagation along a curved path and the major source of the strong asymmetry that is observed in fringe patterns such as those presented here. The possibility that K_{II} was in fact identically zero will be discussed in more detail in the next chapter.

The results for the normalized opening mode constant stress term, B_0', are presented in Figure 5.10. As expected, the results for Experiment 11 correspond to a large remote tension parallel to the original starter notch, though B_0' does decrease as the crack propagates. In Experiment 12, on the other hand, the remote tension applied prior to rapid crack initiation was small, and B_0' remains small, positive, and essentially constant over the period of observation. Note that no results are presented for the corresponding term, D_0, from the shear mode series stress field representation, since this term makes no contribution to the stress components.

The results for the normalized coefficient of $r^{1/2}$ in the opening mode series stress field representation, A_1', are shown in Figure 5.11. The results from both experiments follow the same trends, with A_1' starting out at small, positive values and changing steadily to larger, negative values as the crack propagates into the specimen.

The normalized shear mode stress field coefficient of $r^{1/2}$, C_1', behaves somewhat differently than its opening mode counterpart, as shown in Figure 5.12. The computed value for C_1' is seen to increase rather rapidly during the initial stages of crack propagation in Experiment 11, reaches a maximum and then decreases steadily in magnitude to a final value that is about the same as it had initially. In Experiment 12, this coefficient behaves somewhat differently, with the results showing that it only undergoes small changes as the crack propagates. The sign of the coefficient remains positive throughout in both cases and the coefficient magnitude is comparable with that of A_1'.

Note that the results for C_1' have been normalized with respect to the magnitude of the opening mode singularity term, A_0, rather than with respect to the corresponding shear mode term, C_0. This has been done partially so that the values can be more easily compared in magnitude to the results for A_1', and also because the instantaneous values of C_0 (or K_{II}) were found to be uniformly small compared to A_0 (or K_I). The choice of A_0 as a normalizing factor is not inappropriate, even though the coefficient being discussed is associated with the shear mode stress field, since the purpose of this part of the normalization procedure is simply to scale the stress state at two different instants in time (or two different crack tip locations) with respect to the overall magnitude of the stress field. A characteristic length dimension is also needed for normalization purposes (see Section 3.5) and this was taken to be the specimen width, W = 11.5 inches = 292 mm, for both opening and shear mode stress field coefficients.

In summary, the results for the leading non-singular coefficients of both the opening and shear mode stress fields for the curving crack cases that have been presented above showed a behavior similar to that obtained previously for opening mode crack propagation, in that these coefficients were once again found to be smoothly varying functions of time (or crack tip position). The results for the opening mode stress intensity factor were similar in the two cases considered, which is consistent with the geometry and loading that was employed in the two experiments. The results for the opening mode constant stress term, B_0', while they were different for the two experiments, were also consistent with the initial biaxial loading conditions. The $r^{1/2}$ component of the opening mode stress field, A_1', was found to have similar values for the two experiments. The shear mode counterpart, C_1', while it had a magnitude comparable to the opening mode term, showed a distinctly different behavior for the two cases presented.

REFERENCES

5.1 Shukla, A., **Study of Energy Loss During a Fracture Event**, PhD Dissertation, University of Maryland (1981).

5.2 Dally, J.W., "Dynamic Photoelastic Studies of Fracture," **Experimental Mechanics**, 19, pp. 349-367 (1979).

5.3 Irwin, G.R., W.L. Fourney, D.B. Barker, R.J. Sanford, J.T. Metcalf, A. Shukla and R. Chona, **Photoelastic Studies of Damping, Crack Propagation, and Crack Arrest in Polymers and 4340 Steel, NUREG/CR-1455**, University of Maryland (May 1980).

5.4 Chona, R., **Non-Singular Stress Effects in Fracture Test Specimens -- A Photoelastic Study**, M.S. Thesis, University of Maryland (1985).

5.5 Sanford, R.J. and R. Chona, "Photoelastic Calibration of the Short-Bar Chevron-Notched Specimen," **Chevron-Notched Specimens: Testing and Stress Analysis**, J. H. Underwood, et al., editors, **ASTM STP 855**, pp. 81-97 (1984).

5.6 Sanford, R.J. and R. Chona, "Characterizing Fracture Mechanics Specimens by Photoelastic Methods," (1987) -- Manuscript in Preparation.

5.7 Franke, J.A., **Non-Singular Stress Effects in a Single-Edge-Notched Specimen**, MS Paper, University of Maryland (1985).

5.8 Shukla, A. and S. Anand, "Dynamic Crack Propagation and Branching Under Biaxial Loading," **Fracture Mechanics: Seventeenth Symposium**, Underwood, J.H., et al., editors, **ASTM STP 905**, pp. 697-714 (1986).

5.9 Fourney, W.L. and T. Kobayashi, "Influence of Loading System on Crack Propagation and Arrest Behavior in a DCB Specimen," **Fracture Mechanics Applied to Brittle Materials, ASTM STP 678**, pp. 47-59 (1979).

5.10 Ramulu, M., **Dynamic Crack Curving and Branching**, PhD Dissertation, University of Washington (1982).

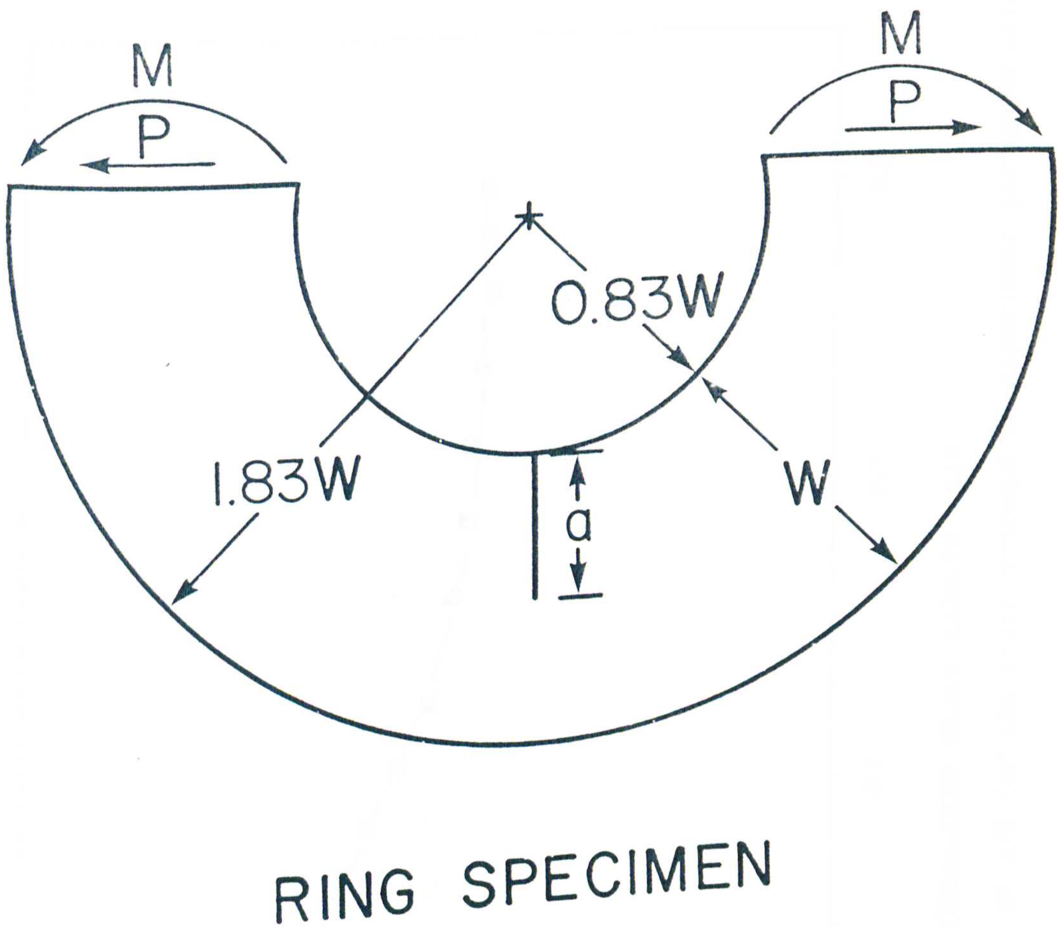

Figure 5.1 The geometry and loading of the ring segment used to study rapid crack propagation under opening mode conditions.

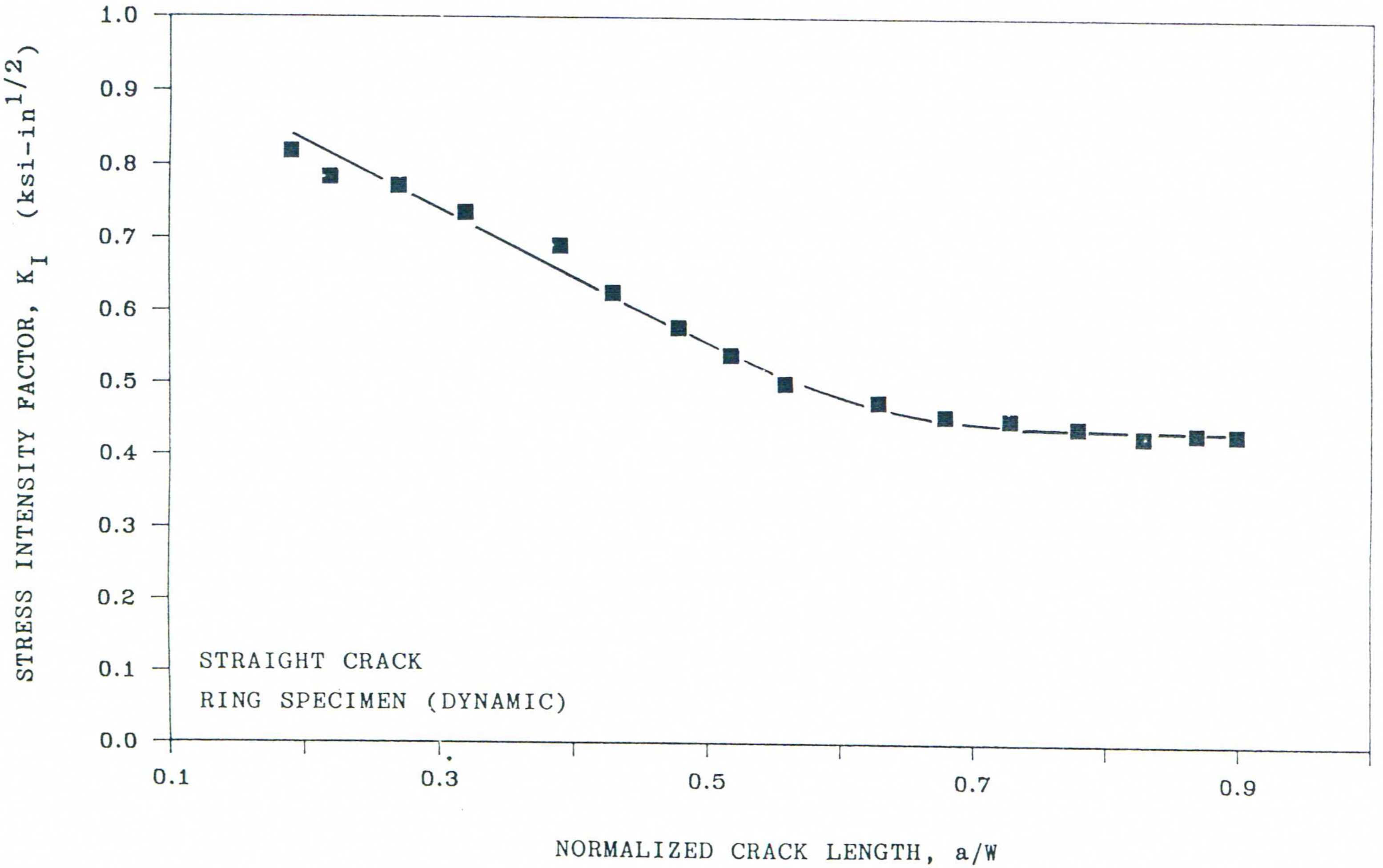

Figure 5.2 Results for K_I as a function of a/W for the crack propagation experiment performed using a ring segment.

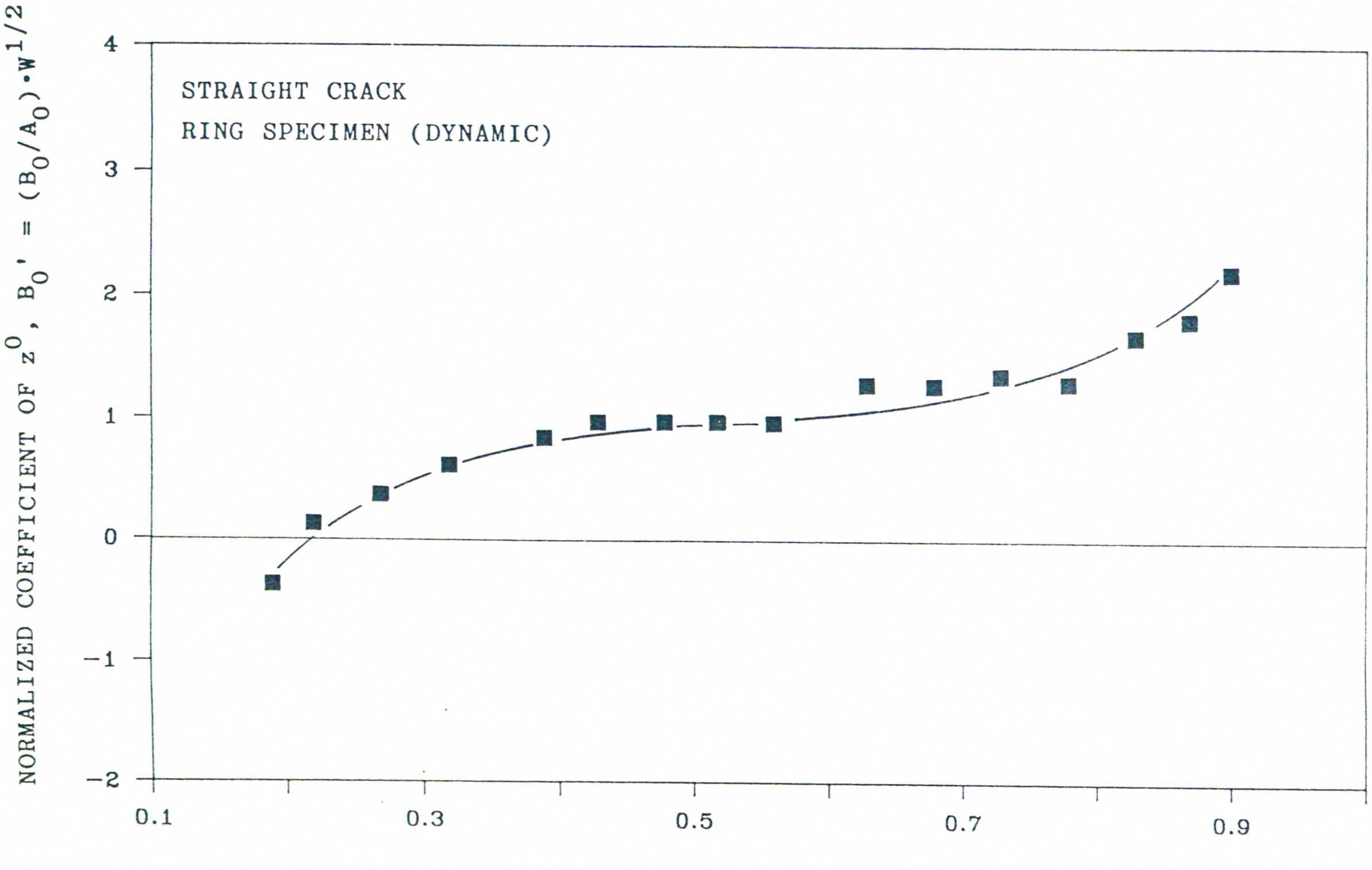

Figure 5.3 The variations with a/W of B_0', the normalized coefficient of z^0, for crack propagation across a ring segment.

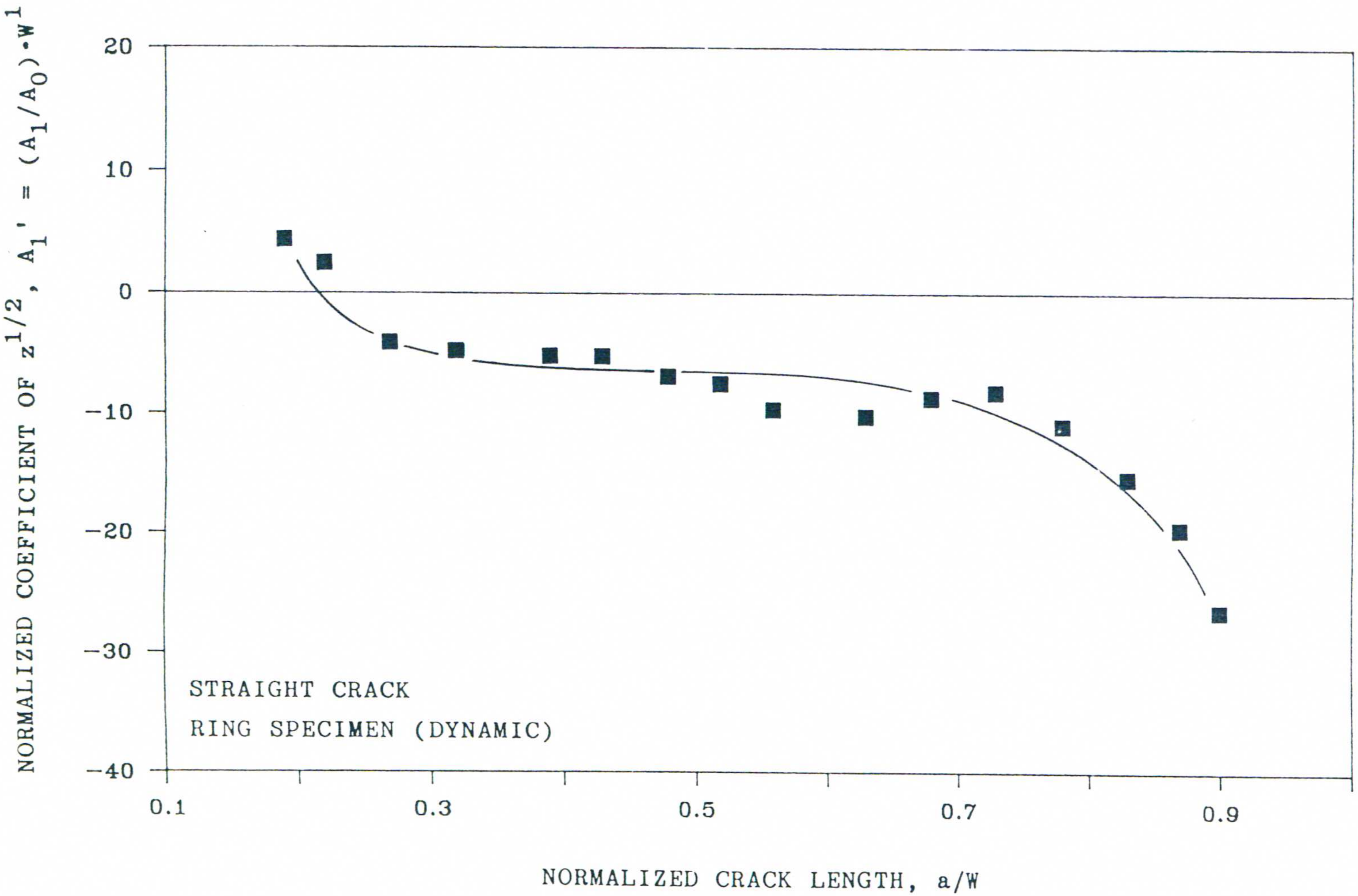

Figure 5.4 The variations with a/W of A_1', the normalized coefficient of $z^{1/2}$, for crack propagation across a ring segment.

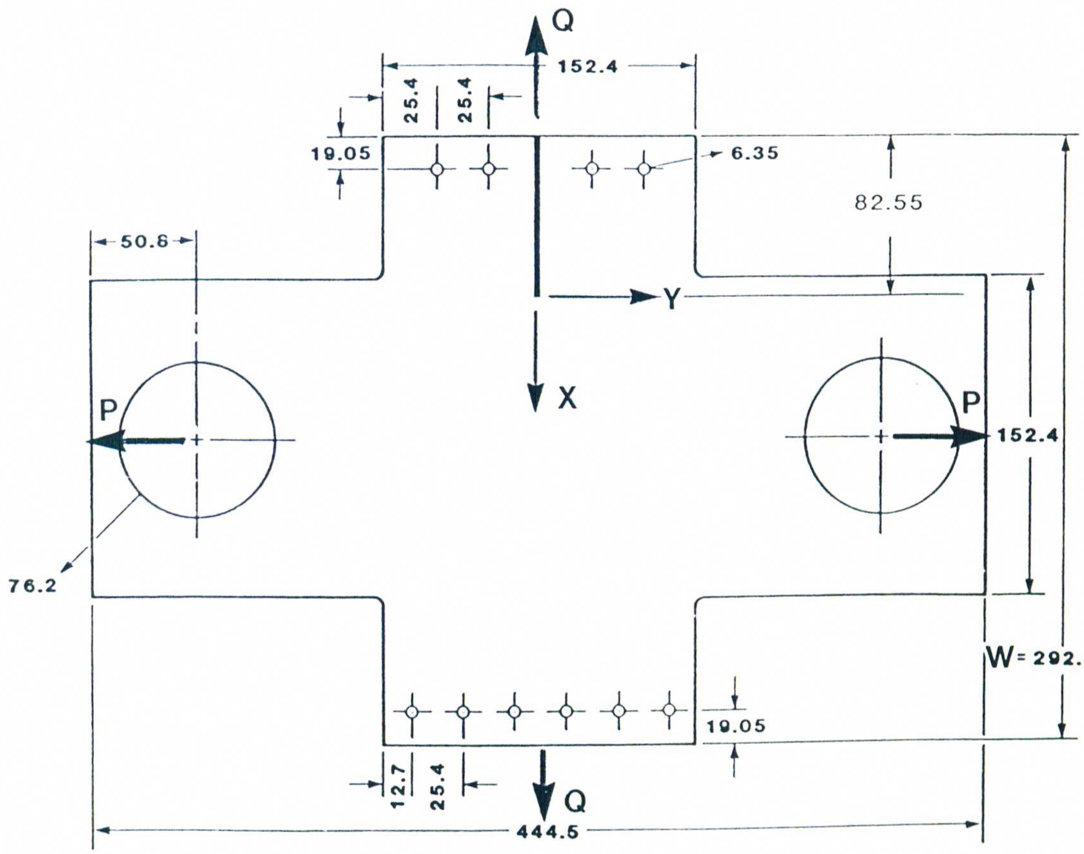

Figure 5.5 The geometry and loading of the biaxially-loaded, cross-shaped fracture specimen used for studies of rapidly propagating, smoothly curving cracks. (Dimensions in mm.)

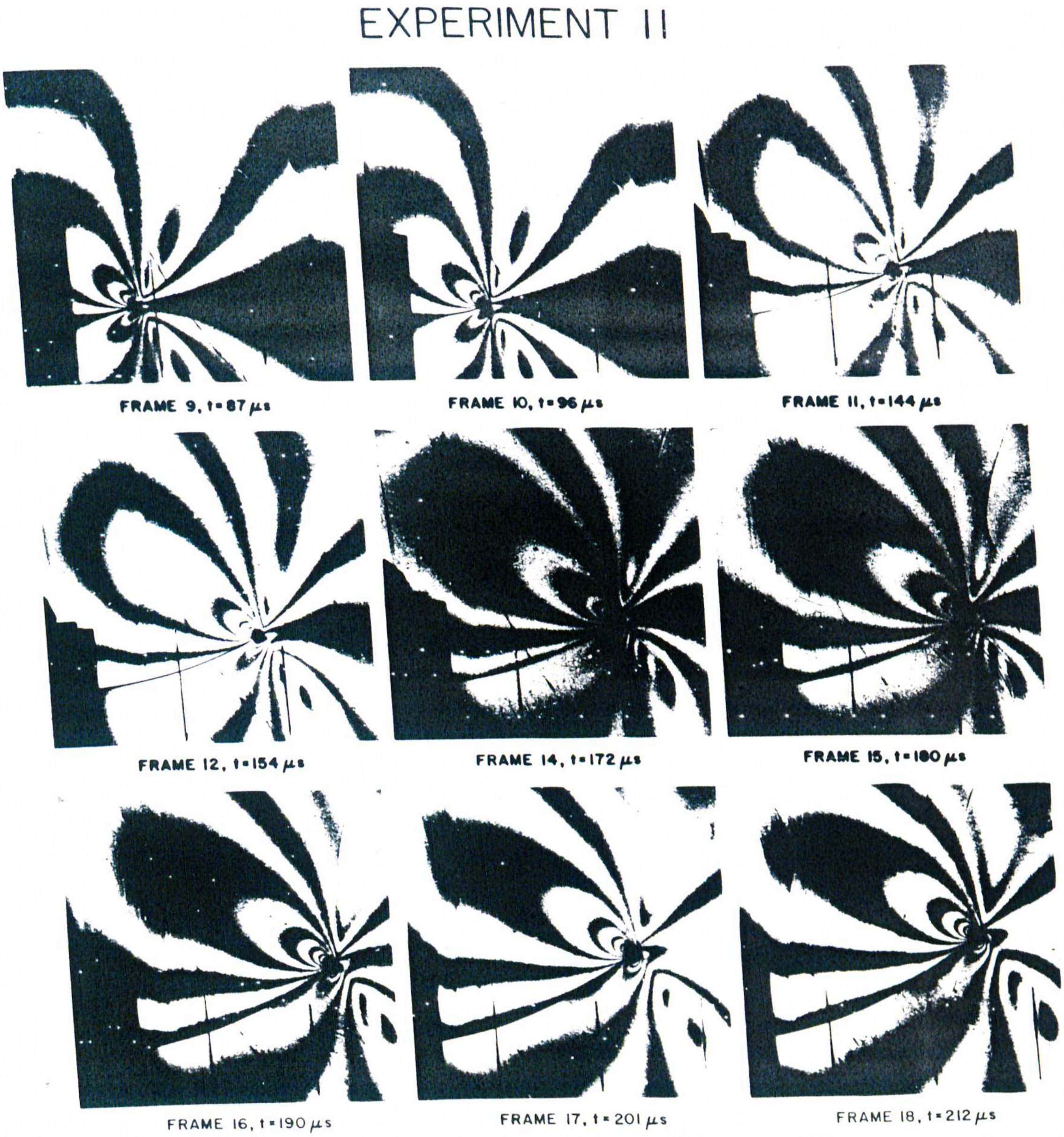

Figure 5.6 A sequence of frames recorded using a Cranz-Schardin camera showing the stress field surrounding the rapidly propagating curving crack of Experiment 11.

EXPERIMENT 12

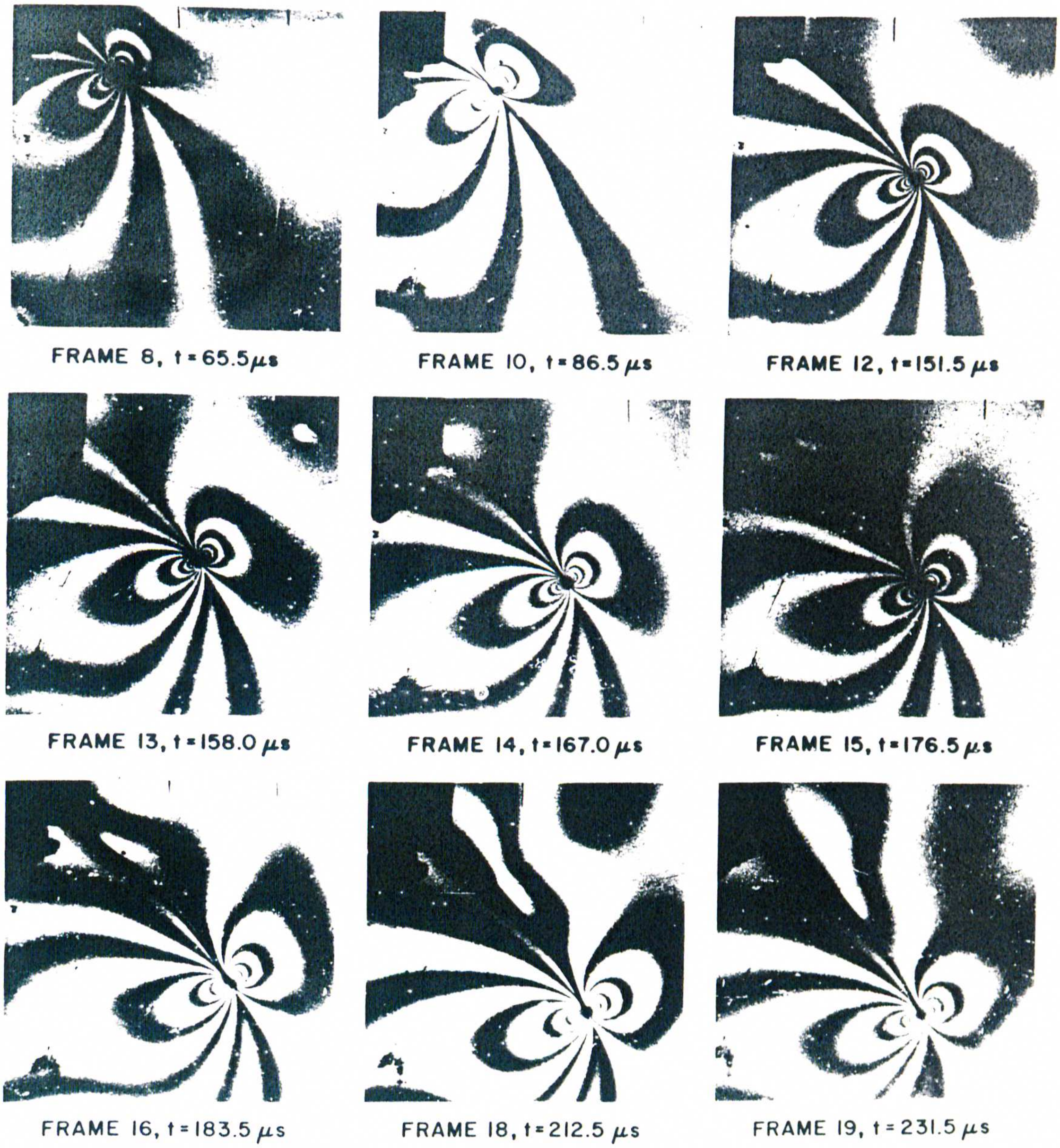

Figure 5.7 A sequence of frames recorded using a Cranz-Schardin camera showing the stress field surrounding the rapidly propagating curving crack of Experiment 12.

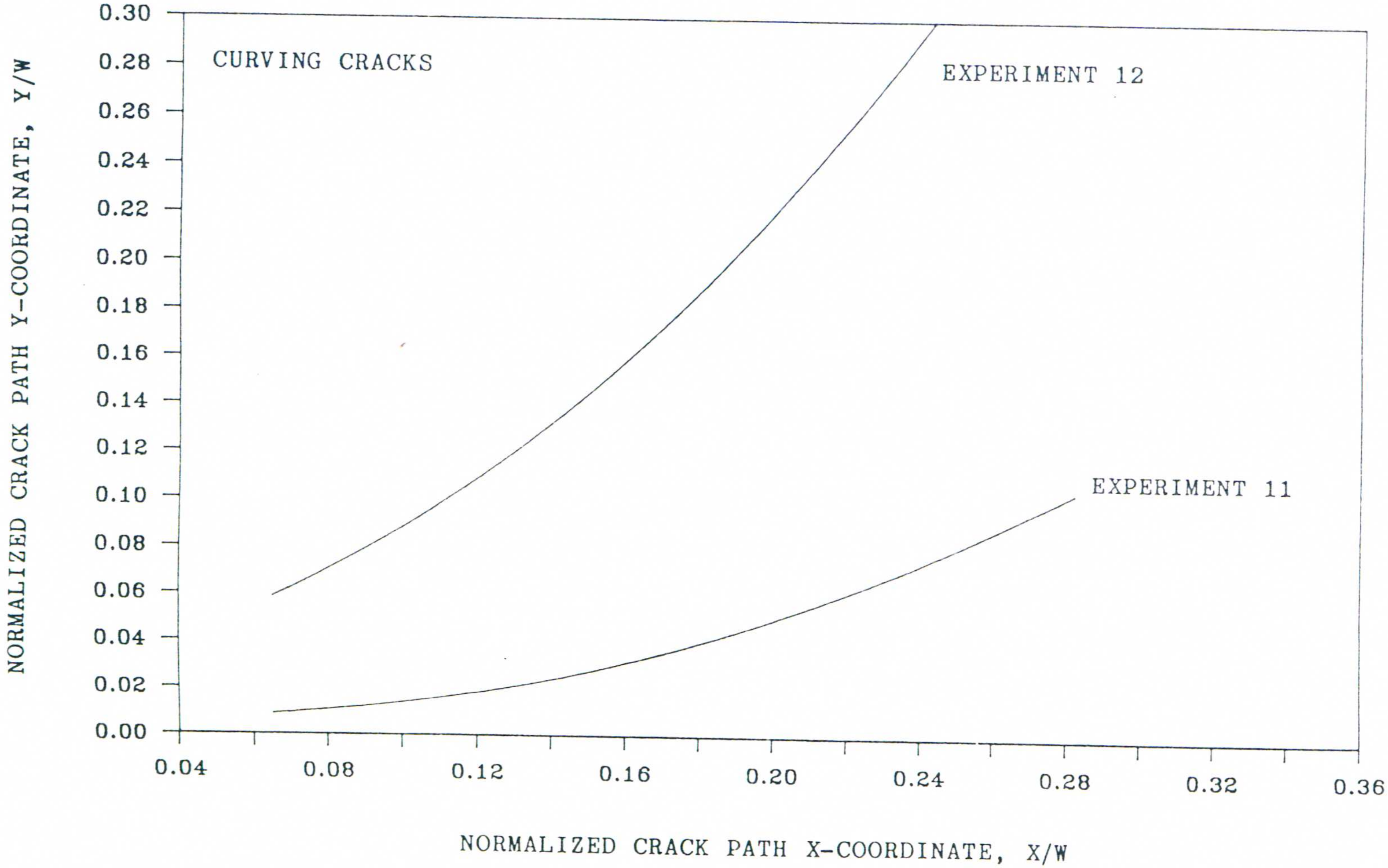

Figure 5.8 The crack paths for the rapidly propagating curving cracks of Experiments 11 and 12.

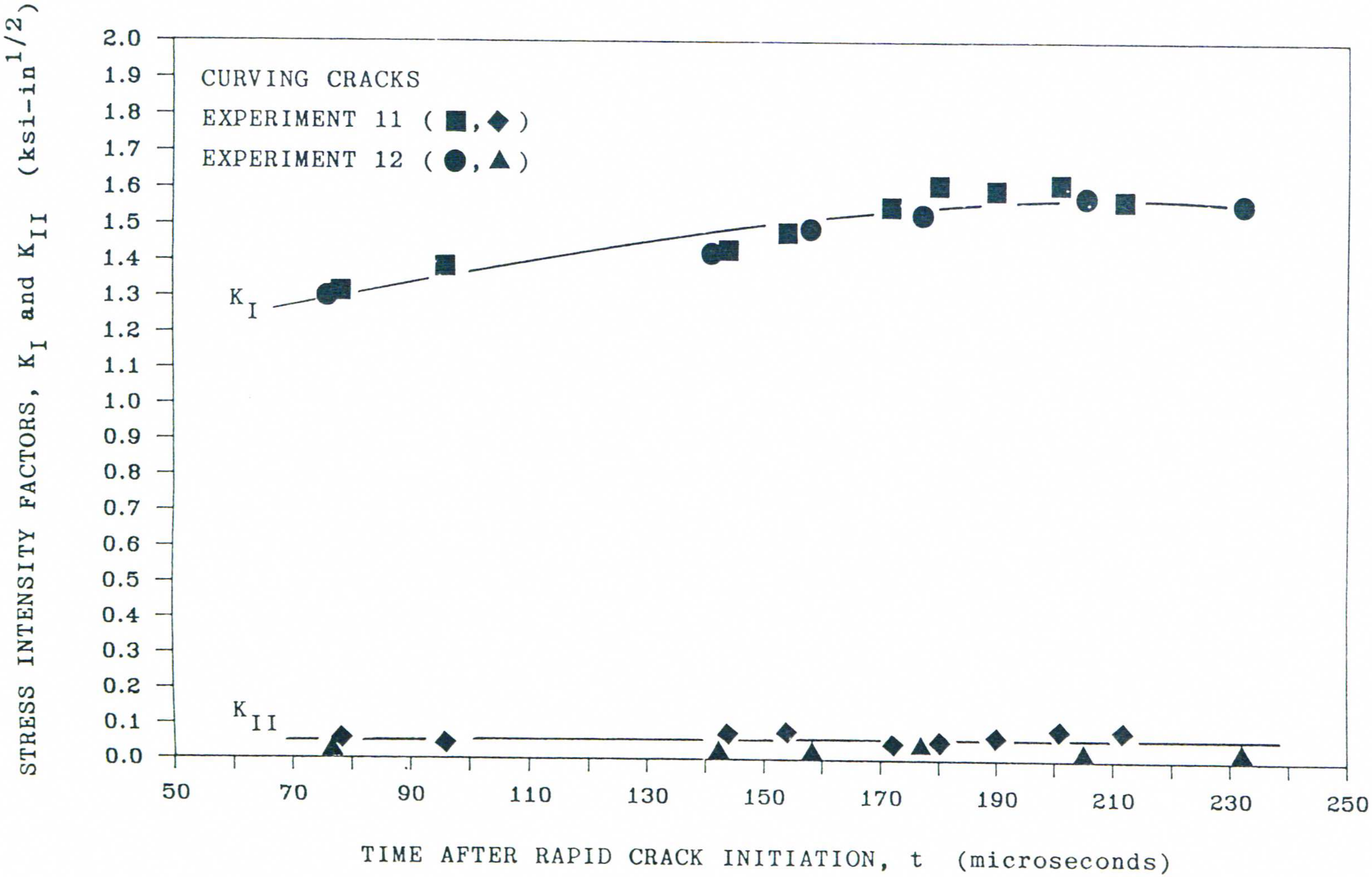

Figure 5.9 Results for the stress intensity factors, K_I and K_{II}, as functions of the elapsed time after rapid crack initiation, for the curving cracks of Experiments 11 and 12.

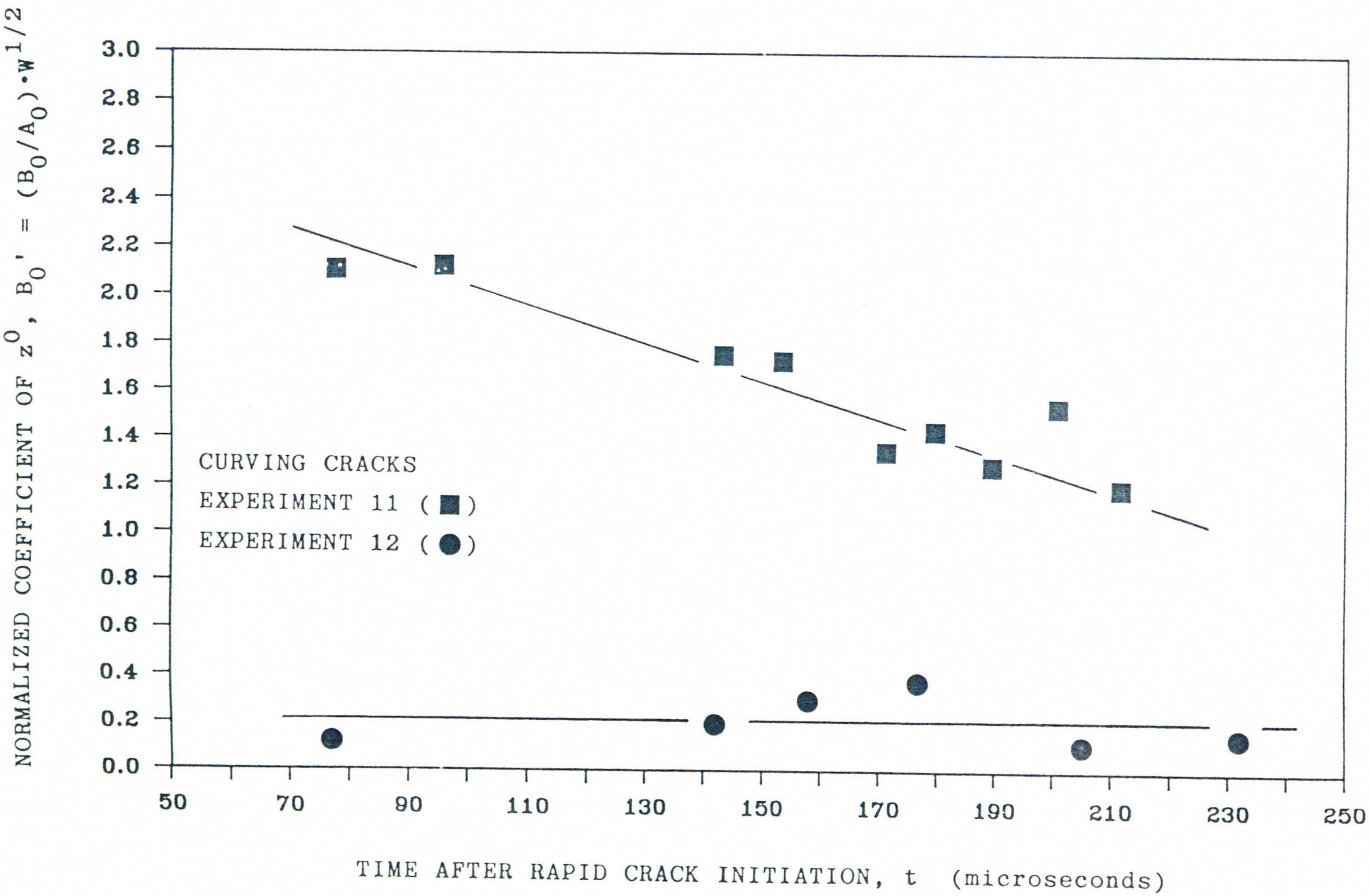

Figure 5.10 The normalized coefficient of z^0, B_0', as a function of the elapsed time after rapid crack initiation, for the curving cracks of Experiments 11 and 12.

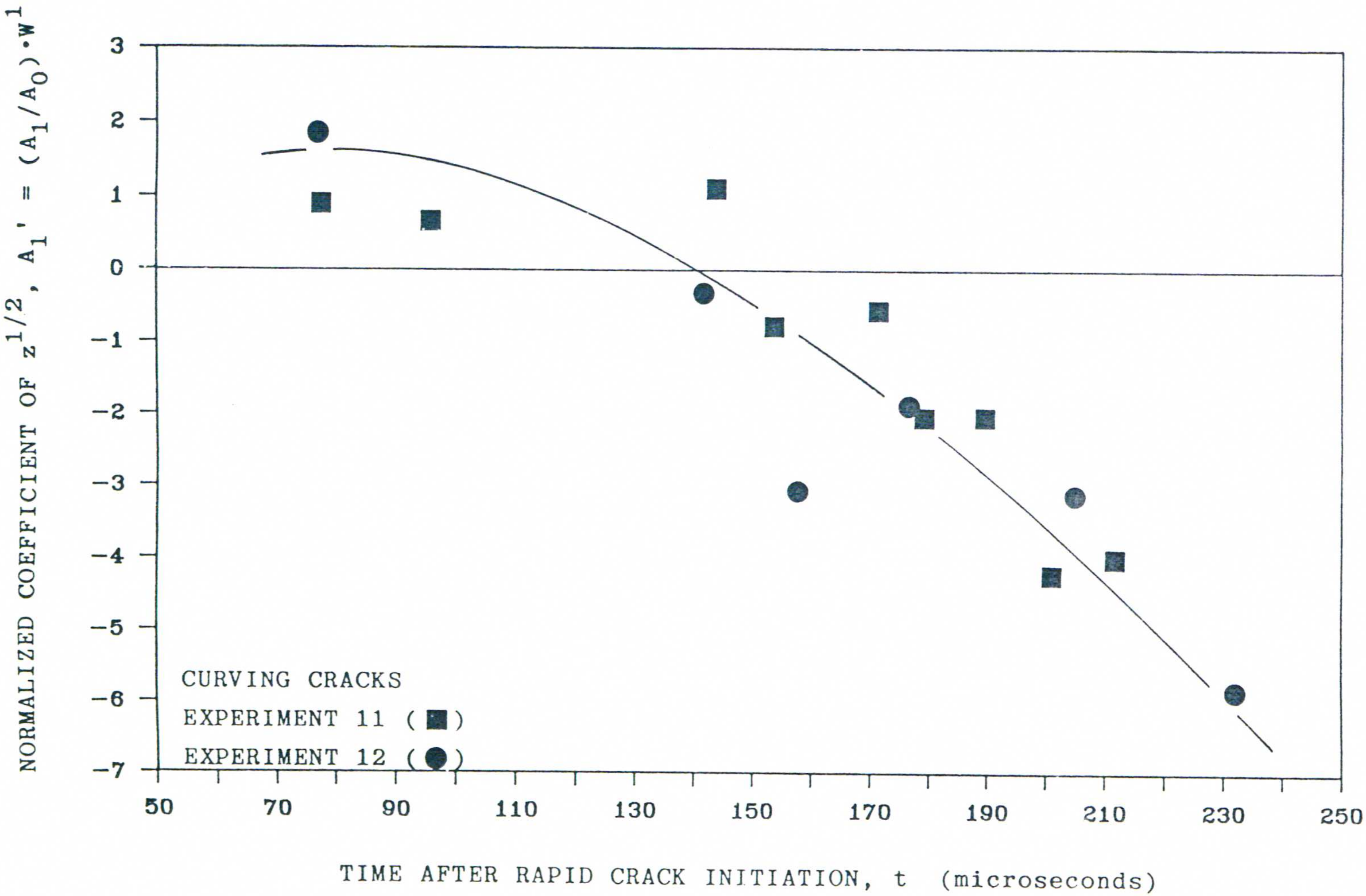

Figure 5.11 The normalized opening mode coefficient of $z^{1/2}$, A_1', as a function of the elapsed time after rapid crack initiation, for the curving cracks of Experiments 11 and 12.

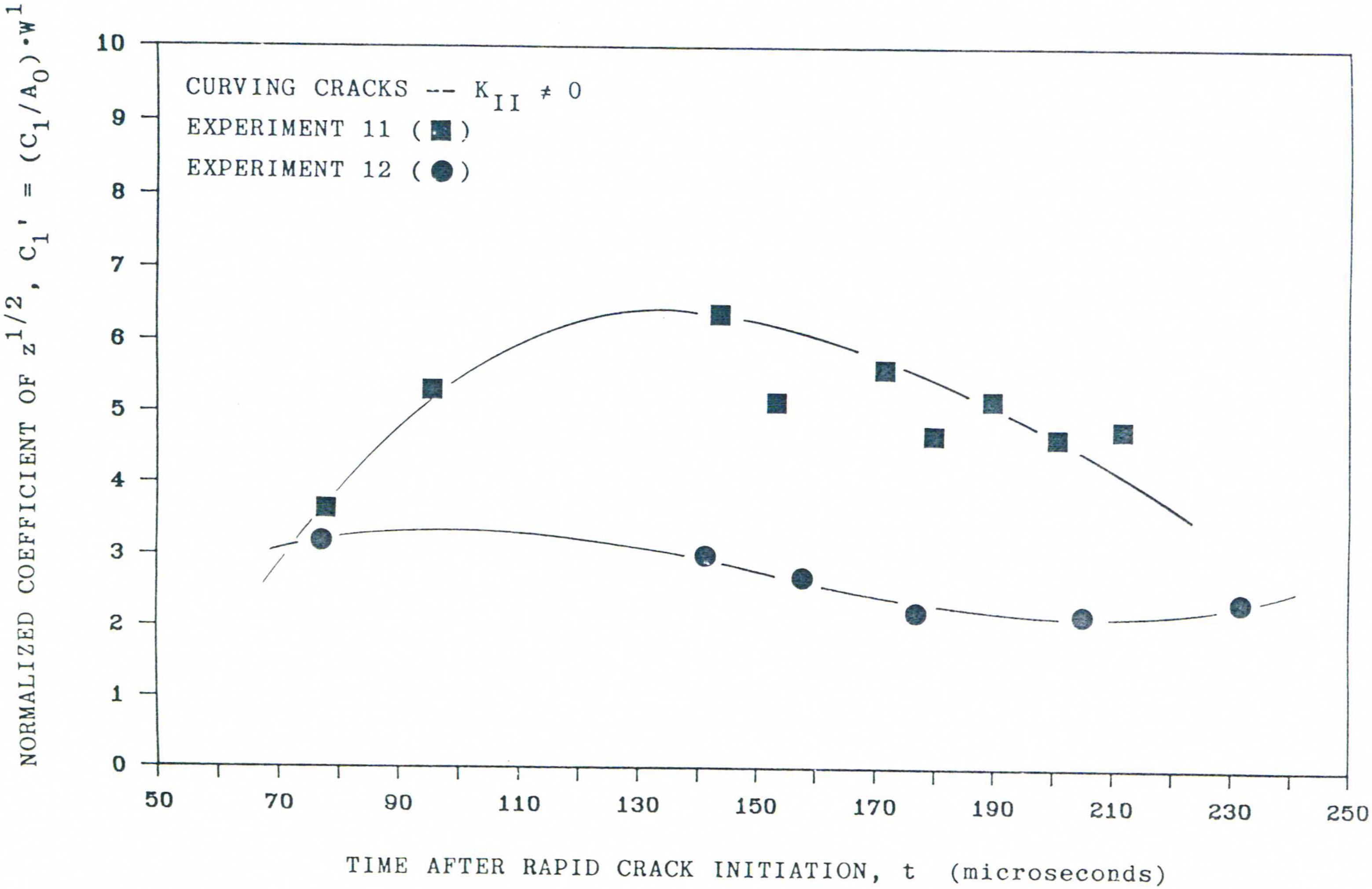

Figure 5.12 The normalized shear mode coefficient of $z^{1/2}$, C_1', as a function of the elapsed time after rapid crack initiation, for the curving cracks of Experiments 11 and 12.

CHAPTER 6

DISCUSSION OF RESULTS

Stress field representations suitable for modelling the stress field surrounding the tip of a crack in a finite-sized body were developed in Chapter 3 of this dissertation for both stationary and running cracks, under opening mode or combined loading conditions. Techniques for determining the crack-tip stress field parameters of interest from full-field experimental data were presented and their application to dynamic photoelastic fracture patterns was discussed in Chapter 4. The ability to model the stress state in a large region around the tip of a propagating crack with a high degree of confidence and accuracy was demonstrated for both straight and curving cracks, and the advantages of adopting a careful and systematic approach to the analysis of running crack stress fields were readily apparent from illustrations such as Figures 4.2, 4.3, 4.5, and 4.6.

Dynamic photoelastic experiments of opening mode cracking in a ring segment and curvilinear crack propagation in a biaxially-loaded, cross-shaped fracture specimen provided the data base for the next part of this study, in which the running crack fringe patterns from these experiments were analyzed using the parameter determination methodology discussed previously. The results obtained for both the singular and lower-order, non-singular stress field coefficients were presented in Chapter 5. Several items that merit further discussion can be identified from these results and these are presented and discussed in the sections that follow.

6.1 Higher Order Terms in Static and Dynamic Situations

It was pointed out in the Introduction that it was desired to compare quasi-static and running crack propagation behaviors so as to allow the influence of higher order terms to be examined in a dynamic setting. The results for the variation with crack tip position of the coefficients of the lowest-order, non-singular stress terms (r^0 and $r^{1/2}$), B_0 and A_1, were presented in the previous chapter (Figures 5.3 and 5.4) for a crack propagating across a ring specimen with the geometry shown in Figure 5.1.

A photoelastic model with the same geometry and loading was prepared and the crack extended in a quasi-static manner by a series of sawcuts over the range of crack lengths from $a/W = 0.10$ to $a/W = 0.90$, in increments of 0.10. The isochromatic fringe patterns associated with each crack tip location were recorded and analyzed using the techniques discussed earlier, to obtain up to the first six coefficients of the series stress field representation of equations (3.5) and (3.6), in a manner similar to [**6.1**].

Figures 6.1 and 6.2 compare the results for the normalized coefficients, B_0' and A_1', from the static and dynamic experiments. The strong influence of the specimen boundaries on the local crack-tip stress field is apparent for very short ($a/W \leqslant 0.3$) and very deep ($a/W \geqslant 0.8$) crack lengths and the variations with crack position of these coefficients can be seen to be similar in both cases. At the short crack lengths, both B_0' and A_1' display a change in sign and rapid changes as the crack length varies over the range $a/W = 0.2$ to

$a/W = 0.3$. At the long crack lengths, there is again a sharp change in the coefficients with crack length and both B_0' and A_1' almost double in magnitude as the crack extends from $a/W = 0.8$ to $a/W = 0.9$. Such behavior is in agreement with the observations that have been made previously for stationary cracks in different mode I fracture specimens [6.1, 6.2, 6.3].

The two sets of data display a clear separation at the shorter crack lengths, where the crack was propagating at a high velocity ($c/c_2 \approx 1/3$) in the dynamic case. However, the static and dynamic values for the non-singular stress field coefficients merge as the crack speed decreases to much lower values ($c/c_2 \approx 1/10$). This suggests that information regarding the relative magnitude and influence of non-singular stresses that is obtained from studies of stationary cracks such as [6.1 - 6.3] could be used in a dynamic setting without significant error, when the crack speed is moderate.

6.2 Effect of Higher Order Terms on the Accuracy of K-Determination

The importance of using higher order models that retain terms beyond the r^0, or constant stress, term when evaluating the stress field parameters of interest from experimental data is clearly seen in Figure 6.3. This figure compares the relationships between the crack tip stress intensity factor, K_I, and the crack speed, c, that would be inferred for the model material, Homalite 100, from the near-field and higher-order analyses of the running crack isochromatic fringe patterns for crack propagation in a ring specimen.

The retention of the terms of order $r^{1/2}$ and larger in the stress field model results in both a reduction in data scatter and a significant change in the extrapolated value of K corresponding to zero crack speed, K_a, which changes from 380 psi$\sqrt{in}$ to 430 psi$\sqrt{in}$, or more than 10%. The first result obviously has implications for the confidence with which such data can be used in further work. The second would have a strong influence on the results from any studies of crack propagation and arrest behavior that were performed using finite element computer codes, since such computations require a relationship of this kind as input data for predictive calculations [6.4, 6.5].

6.3 Examination of a $K_{II} = 0$ Criterion for a Smoothly Curving Crack

When a crack propagates along a curvilinear path, the isochromatic fringes associated with the advancing crack tip can show considerable asymmetry, as evidenced by the high speed photographs shown in Figures 5.6 and 5.7 for two such cases. This lack of symmetry is generally ascribed to the presence of a combined opening and shear mode stress field. However, it has been uncertain as to whether or not the contribution from the shear mode stress field includes a mode II stress singularity, K_{II}.

Analytical studies of crack initiation under combined loading conditions [6.6] and studies of quasi-static, curvilinear crack propagation [6.7, 6.8] have shown good agreement with experimental data when the analytical predictions have used a criterion that the strain energy release rate be a maximum to determine the direction of each locally straight segment used to model the crack trajectory. It has also been shown [6.8, 6.9] that, for quasi-static situations, the requirement that the strain energy release rate be maximized along the preferred crack path is equivalent to the statement that $K_{II} = 0$.

The possibility that K_{II} may be zero for a propagating crack has been discussed previously, though somewhat superficially and in a qualitative fashion [6.10]. It has also been demonstrated, through the use of computer-generated fringe patterns, that asymmetry in the crack tip isochromatic pattern can be obtained from a superposition of mode II non-singular stress terms with a mode I singularity, even in the absence of K_{II} [6.11]. Recently, the results from studies of curvilinear crack propagation and crack interaction problems using finite element methods [6.12, 6.13] showed that the use of a $K_{II} = 0$ criterion to determine the direction of each locally straight segment of forward crack extension provided a good match between computational and experimental results for the crack trajectory.

The results for the stress field parameters obtained in this study (Figure 5.9) showed that the apparent value of the shear mode stress singularity, K_{II}, calculated from local collocation analyses using higher order stress field models was small (2-5% of the instantaneous K_I). Furthermore, careful examination of enlargements of the crack-tip isochromatics such as those shown in Figures 6.4 and 6.5 indicated that, while in the former case, the asymmetry of the stress field persisted to within the limits of resolution of the recording system, in the latter example, the fringes on either side of the crack path clearly showed an increasing degree of symmetry as one approached the crack tip. This suggested, in a qualitative sense, that the crack-tip stress field could be one consisting of an opening-mode singularity, coupled with both opening and shear mode non-singular stresses. This in turn would imply that the values of K_{II} being calculated by the least-squares analysis algorithm were "false" fitting parameters compensating for small experimental errors in the input data rather than "true" parameters intrinsic to the crack-tip stress field under consideration.

Each data set for the fringe patterns from the two curving crack experiments analyzed in this study was therefore re-analyzed with a modified stress field model in which $K_{II} \equiv 0$ and all other details of the analysis procedure remained the same as before. Figure 6.6 shows the results from the modified analysis for the behavior of the fringe order error and the leading singular and non-singular stress field coefficients for the same fringe pattern (Experiment 11, Frame 12) that was discussed in some detail in Section 4.3. A comparison of Figure 6.6 with Figure 4.5 reveals that similar, stable behavior of the error term and the stress field coefficients was also obtained with the new model. Furthermore, the final results for the opening mode coefficients, K_I, B_0', and A_1', did not change in either magnitude or sign. The major difference between the two analyses was found to be the elevation (by about 30%) of the coefficient of $r^{1/2}$ in the shear mode stress field, C_1', which now became the first non-symmetric term in the series stress field representation.

The ability to achieve a good match with the experimental data using a model in which $K_{II} \equiv 0$ was further confirmed by Figure 6.7, which compares the experimental fringe pattern for this example with the reconstructed patterns corresponding to best-fit coefficient sets from the two sets of analyses. It is quite evident that either coefficient set provides an acceptable representation of the crack-tip stress field over a region of reasonable size, with an analysis model of similar order ($r^{3/2}$) being required in each case.

Figure 6.8 shows the results for C_1', the normalized coefficient of the $r^{1/2}$ term in the shear mode stress field, that were obtained from the modified analysis for each frame of Experiments 11 and 12. The general trends are seen to be the same as those obtained previously (Figure 5.12) but the magnitude of the coefficient increased to larger values with the elimination of K_{II}. The results for the next higher order (r^1) shear mode stress field coefficient, D_1, have not been shown here. However, these results displayed similar behavior, with higher values being assigned to that coefficient also, when the stress field representation assumed K_{II} to be zero. However, the degree of change was of order 5-20%, less than the corresponding change in C_1', which was of order 15-40%. The results for the opening mode coefficients, K_I, B_0', and A_1', remained essentially unchanged between the two analyses.

The results from the present study substantiate the idea that $K_{II} \equiv 0$. A plausible scenario for crack propagation along a curvilinear path would then state that, for a crack propagating in a brittle, isotropic material, the crack changes direction so as to continously eliminate any shear mode singularity, when the crack path is smoothly curving and the loading is applied by mechanical means. It could be argued that inhomogenities at fine scale would tend to provide a propagating crack some degree of choice with regard to the preferred direction of crack extension, and that all such directions would not necessarily correspond to the zero-K_{II} condition that has been postulated. However, it is assumed here that micromechanisms of this type would be confined within the limits of the infinitesmal region of K-domination and the comments made here are from a more global, or macroscopic, viewpoint.

Clearly, the discussion presented above has important implications insofar as the development of criteria for the preferred direction of cracking is concerned. A previous attempt at developing a crack curving criterion [6.14] chose to ascribe all of the observed non-symmetric behavior to K_{II}. The work described in [6.14] employed a stress field representation in terms of the opening mode parameters, K_I and σ_{ox}, and K_{II}, which were determined using local collocation techniques and dynamic photoelastic data. A criterion for crack curving was then developed in terms of these same three stress field coefficients, but no attempt was made to relate the crack trajectory curvature with any of the stress field parameters in a careful manner.

The need for including terms of order $r^{1/2}$ and larger before achieving accurate modelling of the crack-tip stress field has been demonstrated and discussed in Chapter 4 of the present study. It has also been shown that at least one coefficient beyond the term of interest must be retained before local collocation methods can provide accurate values for a particular coefficient. A lack of attention to this point in [6.14] effectively meant that the accuracy of the values computed for K_I and σ_{0x} was questionable, as were the computed non-zero results for K_{II} on which the proposed criterion was based. The criterion for crack curving that was presented was thus based on calculated parameters that had, at best, only empirical significance.

Transient mixed-mode crack-tip stress fields that include a contribution from a mode II singularity could perhaps occur when the crack propagation event is due to, or is accompanied by, stress wave loading generated through the use of explosives or projectile impact [6.15 - 6.17]. However, such loading conditions invariably result in sudden changes in the crack trajectory and the problem becomes more one of 'crack kinking' rather than of 'crack curving'.

Some results reported in [6.18] for an impact loaded fracture specimen are particularly interesting from this standpoint. Figure 5 of [6.18] showed two high speed photographs of the running crack stress field, taken 49 μsec apart. In Frame 15, the local stress state for the propagating crack was very close to pure shear. In the next frame, Frame 16, the crack was seen to have changed direction very sharply at the point where the stress state became almost pure mode II and then proceeded to propagate essentially perpendicular to its original direction. In other words, the crack had very quickly oriented itself so that the crack tip would be under opening mode conditions. Other examples of crack tips subjected to essentially pure shear loading were also presented in [6.18]. However, in all of those cases, the cracks had already arrested and crack reinitiation and further propagation did not occur, thus allowing the almost pure mode II loading to persist for some time.

6.4 The Relationship Between the Curvature of the Crack Path and the Components of the Crack-Tip Stress Field in a Local Region

The preceding discussion has offered evidence to support the contention that a smoothly curving crack in a brittle, isotropic material will propagate so as to maintain a $K_{II} = 0$ condition at the tip of the advancing crack. A logical next step would then be to establish a relationship between a parameter descriptive of the crack trajectory, such as the curvature of the crack path, and the remaining components of the crack-tip stress field in the close vicinity of the crack tip.

As discussed in the Introduction to this dissertation, any infinitesmal segment of a general curve in space can always be considered to be a straight line, without loss of generality. However, representation of a finite, non-zero curvature at any point along a trajectory requires that the form of the function used to model the trajectory yield a non-zero second derivative, i.e., higher order effects must be taken into account. This would suggest that the relationship that is sought could perhaps be found through a careful examination of the variations in the non-singular stress field parameters that accompany changes in the curvature of the crack path.

Figure 6.9 shows the normalized curvature of the crack path, $(R/W)^{-1}$, as a function of the normalized coordinate, X/W, of the crack path for the two experimental examples (Experiments 11 and 12) that have been analyzed in detail in the present study. The curvature behavior of the two examples can be seen to be quite different. For Experiment 11, the curvature increases steadily from its initial value to a maximum, and then decreases gradually as the crack path becomes more straight. In Experiment 12, on the other hand, the curvature is essentially constant for the initial portion of the path, following which it begins to decrease, as the crack path becomes closer to a straight line. (Recall that a straight line has zero curvature.)

Figure 6.10 shows the data for the curvature corresponding to each frame recorded by the high speed camera for the two experiments, as a function of the elapsed time after rapid crack initiation. These results were first compared with Figure 5.9, which showed the behavior as a function of time of the stress intensity factors, K_I and K_{II}, that were calculated when the stress field model included a K_{II}-term. The comparison failed to show any readily apparent connection between the curvature, which varied along each crack path and was different for the two crack paths, and the value of K_{II}, which remained small and essentially constant at 2-5% of K_I for both experiments.

The insensitivity of the apparent K_{II} value to changes in crack path curvature is consistent with the earlier contention that there is no shear mode singularity associated with curvilinear crack propagation along a smoothly curving path. Any non-zero value of K_{II} that is calculated based on local stress field information is therefore a consequence of either an attempt by a least-squares algorithm to accomodate minor experimental errors in input data specification or the result of an inadequate number of terms being retained in the series representation.

On the other hand, a comparison of Figure 6.10 with the opening and shear mode non-singular terms (Figures 5.10, 5.11, 5.12, and 6.8) revealed a direct correspondence between the variations in the curvature of the crack path and the value of the normalized coefficient, C_1', of the $r^{1/2}$-term of the shear mode stress field. The coefficient C_1' is shown as a function of the curvature of the crack path in Figure 6.11 for the two experiments. While there is some scatter in the data, an increasing trend in the magnitude of C_1' with an increase in crack path curvature is readily apparent, i.e., the larger the shear mode $r^{1/2}$-term becomes, the more sharply the crack is seen to be curving. Furthermore, the available results suggest that an extrapolated trend curve would pass through the origin of the coordinate axes -- a not inconsequential point, since the straight crack condition corresponding to zero curvature would have no shear associated with it and the stress field coefficient in question would be identically zero.

The present results establish that there does exist a relationship between the curvature of the path followed by a smoothly curving crack and the leading non-singular shear mode coefficient of the crack-tip stress field. The existence of such a relationship between non-singular stress components and the crack path curvature was not totally unexpected, since it had already been anticipated to some degree from geometric arguments, and these results provide a firm basis for further explanatory discussions and investigations of the general crack trajectory problem from the standpoint of a relationship between the manner in which the crack curves and the stress field in the local neighborhood of the tip of the propagating crack.

It would be tempting to claim a direct proportionality between the instantaneous value of the shear mode $r^{1/2}$-term at a given location along the crack path and the curvature of the crack path at the same point. That such a proportionality may exist is suggested by Figure 6.12, in which the shear mode $r^{1/2}$ coefficient, C_1, is once again shown in normalized form, as a function of the curvature of the crack path. The only difference between Figures 6.11 and 6.12 is that, in Figure 6.12, the characteristic length dimension used for normalization purposes is the instantaneous radius of curvature of the crack path itself, rather than some other dimension related to the specimen geometry, such as the specimen width, W, which was used for normalization purposes in Figure 6.11 and earlier. However, such a statement could be premature at this stage and would perhaps be better formulated following additional study of the influence on such a relationship of, at least, the next higher order terms, r^1 and $r^{3/2}$, as well as other factors that may become apparent.

REFERENCES

6.1 Chona, R., **Non-Singular Stress Effects in Fracture Test Specimens -- A Photoelastic Study**, M.S. Thesis, University of Maryland (1985).

6.2 Sanford, R.J. and R. Chona, "Characterizing Fracture Mechanics Specimens by Photoelastic Methods," (1987) -- Manuscript in Preparation.

6.3 Franke, J.A., **Non-Singular Stress Effects in a Single-Edge-Notched Specimen**, MS Paper, University of Maryland (1985).

6.4 Schwartz, C.W., R. Chona, W.L. Fourney and G.R. Irwin, **SAMCR: A Two-Dimensional Dynamic Finite Element Code for the Stress Analysis of Moving CRacks, NUREG/CR-3891 (ORNL/Sub 7778/3)**, University of Maryland (November 1984).

6.5 Irwin, G.R., W.L. Fourney, C.W. Schwartz and R. Chona, "Analysis of Dynamic Fracture Events," **Proceedings of the 1985 SEM Spring Conference on Experimental Mechanics**, Las Vegas, Nevada, pp. 872-884 (June 1985).

6.6 Hussain, M.A., Pu, S.L. and Underwood, J.H., "Strain Energy Release Rate for a Crack Under Combined Mode I and Mode II," **Fracture Analysis**, G.R. Irwin, editor, **ASTM STP 560**, pp. 2-28 (1974).

6.7 Wu, C.H., "Fracture Under Combined Loads by Maximum-Energy-Release-Rate Criterion, **Journal of Applied Mechanics**, **45**, pp. 553-558 (1978).

6.8 Hayashi, K. and S. Nemat-Nasser, "Energy Release Rate and Crack Kinking," **International Journal of Solids and Structures**, 17, pp. 107-114 (1981).

6.9 Sumi, Y., S. Nemat-Nasser and L.M. Keer, "On Crack Branching and Curving in a Finite Body," **International Journal of Fracture**, 21, pp. 67-79 (1983); Erratum: **International Journal of Fracture**, 24, p. 159 (1984).

6.10 Rossmanith, H.P., "How Mixed is Dynamic Mixed-Mode Crack Propagation? - A Dynamic Photoelastic Study," **Journal of the Mechanics and Physics of Solids**, 31, pp. 251-260 (1983).

6.11 Ramulu, M., Kobayashi, A.S. and Barker, D.B., "Analysis of Dynamic Mixed-Mode Isochromatics," **Experimental Mechanics**, 25, pp. 344-353 (1985).

6.12 Swenson, D.V., **Modeling Mixed-Mode Dynamic Crack Propagation Using Finite Elements, Report No.** 85-10, Department of Structural Engineering, Cornell University, Ithaca, New York (December 1985).

6.13 Swenson, D.V. and A.R. Ingraffea, "A Finite Element Model of Dynamic Crack Propagation with an Application to Intersecting Cracks," **Proceedings of the Fourth International Conference on Numerical Methods in Fracture Mechanics**, A.R. Luxmoore, et al., editors, Pineridge Press, Swansea, U.K., pp. 191-204 (1987).

6.14 Ramulu, M., **Dynamic Crack Curving and Branching**, PhD Dissertation, University of Washington (1982).

6.15 Kobayashi, A.S. and C.F. Chan, "A Dynamic Photoelastic Analysis of Dynamic-Tear-Test Specimen," **Experimental Mechanics**, 16, pp. 176-181 (1976).

6.16 Rossmanith, H.P. and A. Shukla, "Dynamic Photoelastic Investigation of Interaction of Stress Waves with Running Cracks," **Experimental Mechanics**, 21, pp. 415-422 (1981).

6.17 Dally, J.W. and D.B. Barker, "Dynamic Measurements of Initiation Toughness Under High Loading Rates," (1987) -- Submitted for publication.

6.18 Ramulu, M., A.S. Kobayashi and B.S.-J. Kang, "Dynamic Crack Branching -- A Photoelastic Evaluation," **Fracture Mechanics: Fifteenth Symposium**, R.J. Sanford, editor, **ASTM STP 833**, pp. 130-148 (1984).

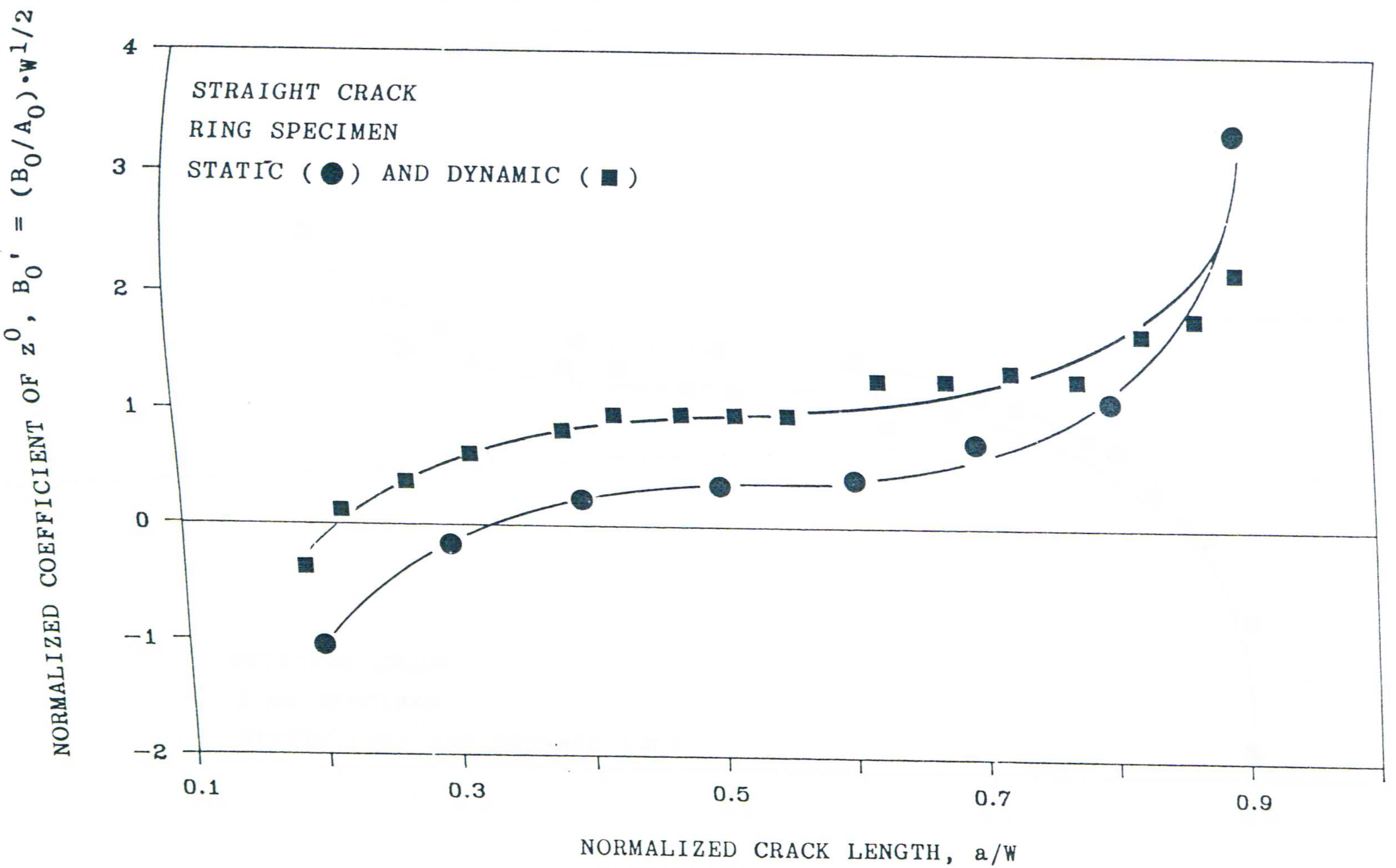

Figure 6.1 The variations with a/W of B_0', the normalized coefficient of z^0, for quasi-static and rapid crack extension across a ring segment.

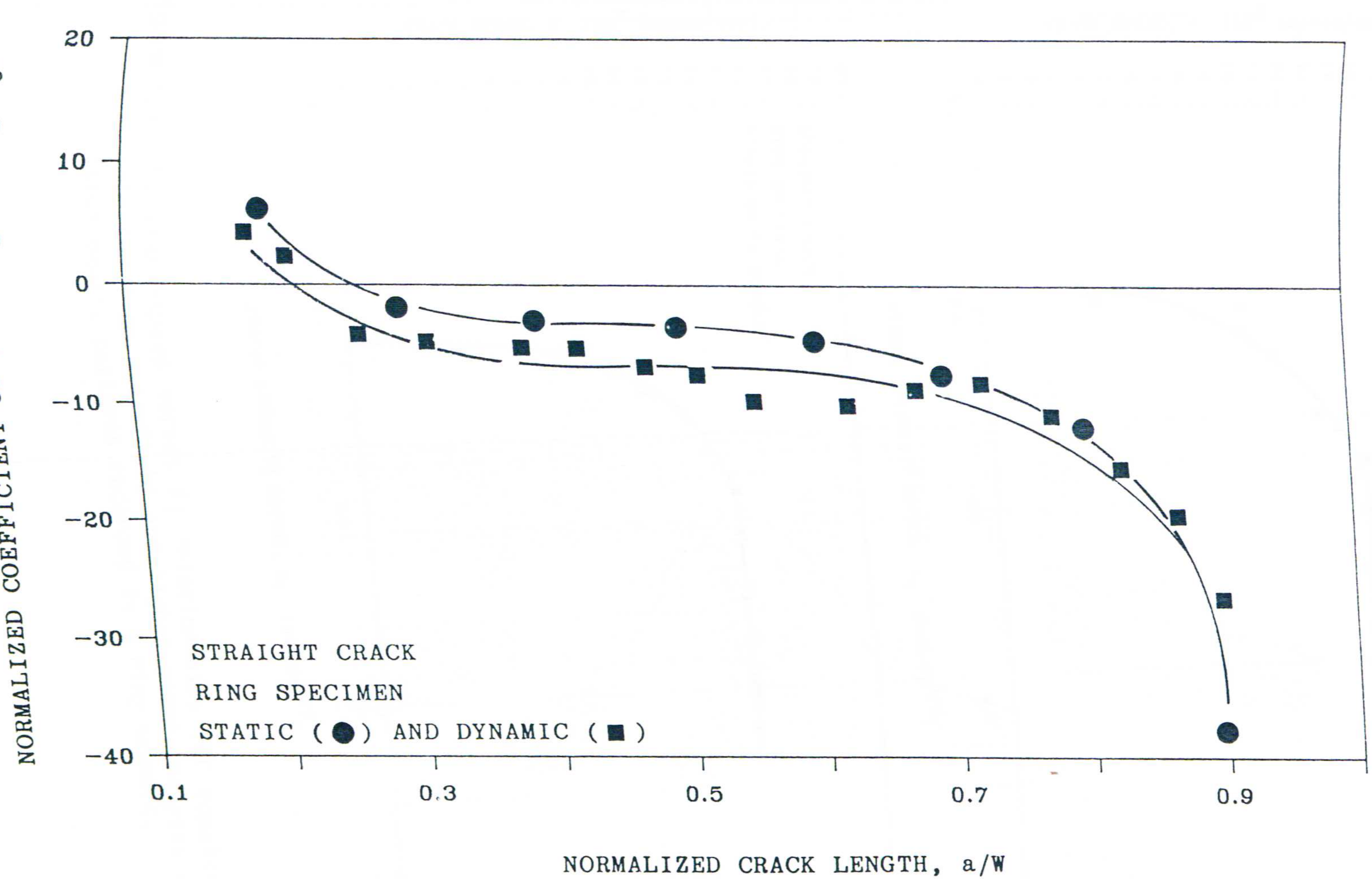

Figure 6.2 The variations with a/W of A_1', the normalized coefficient of $z^{1/2}$, for quasi-static and rapid crack extension across a ring segment.

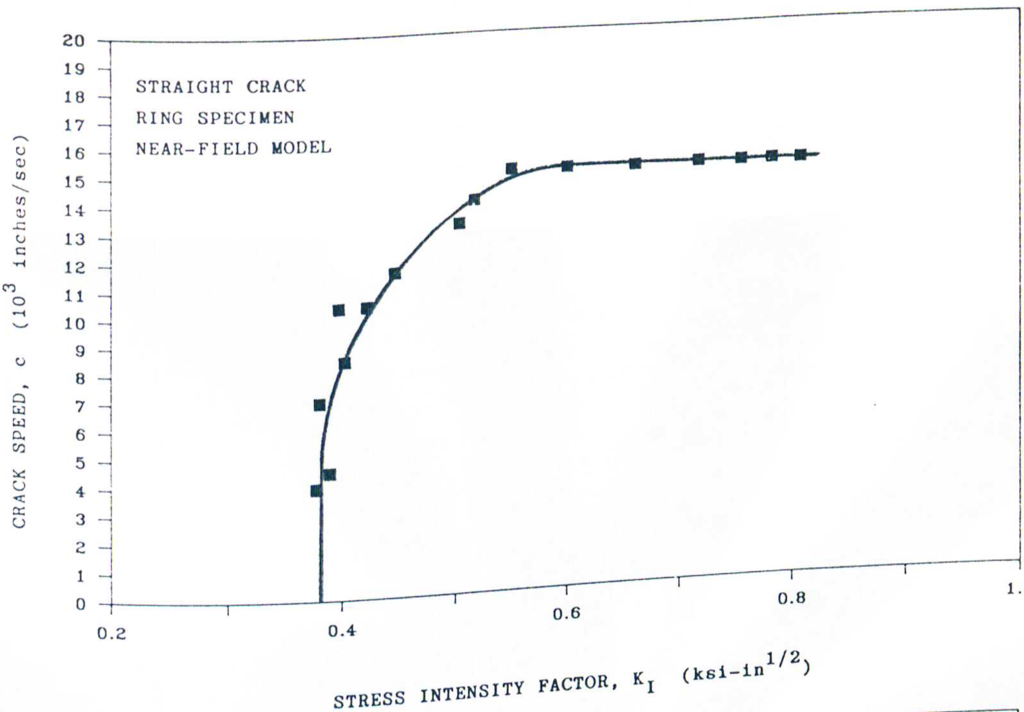

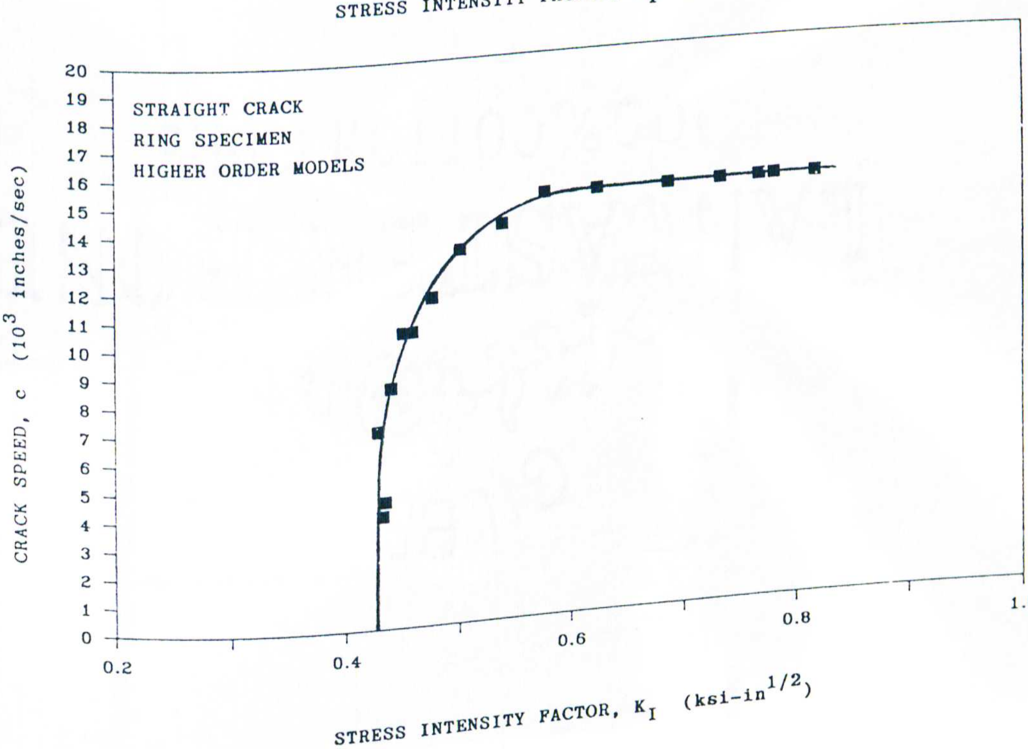

Figure 6.3 The crack-speed versus K_I relationships for Homalite 100 inferred from near-field and higher-order analyses of the isochromatic patterns recorded in a ring segment.

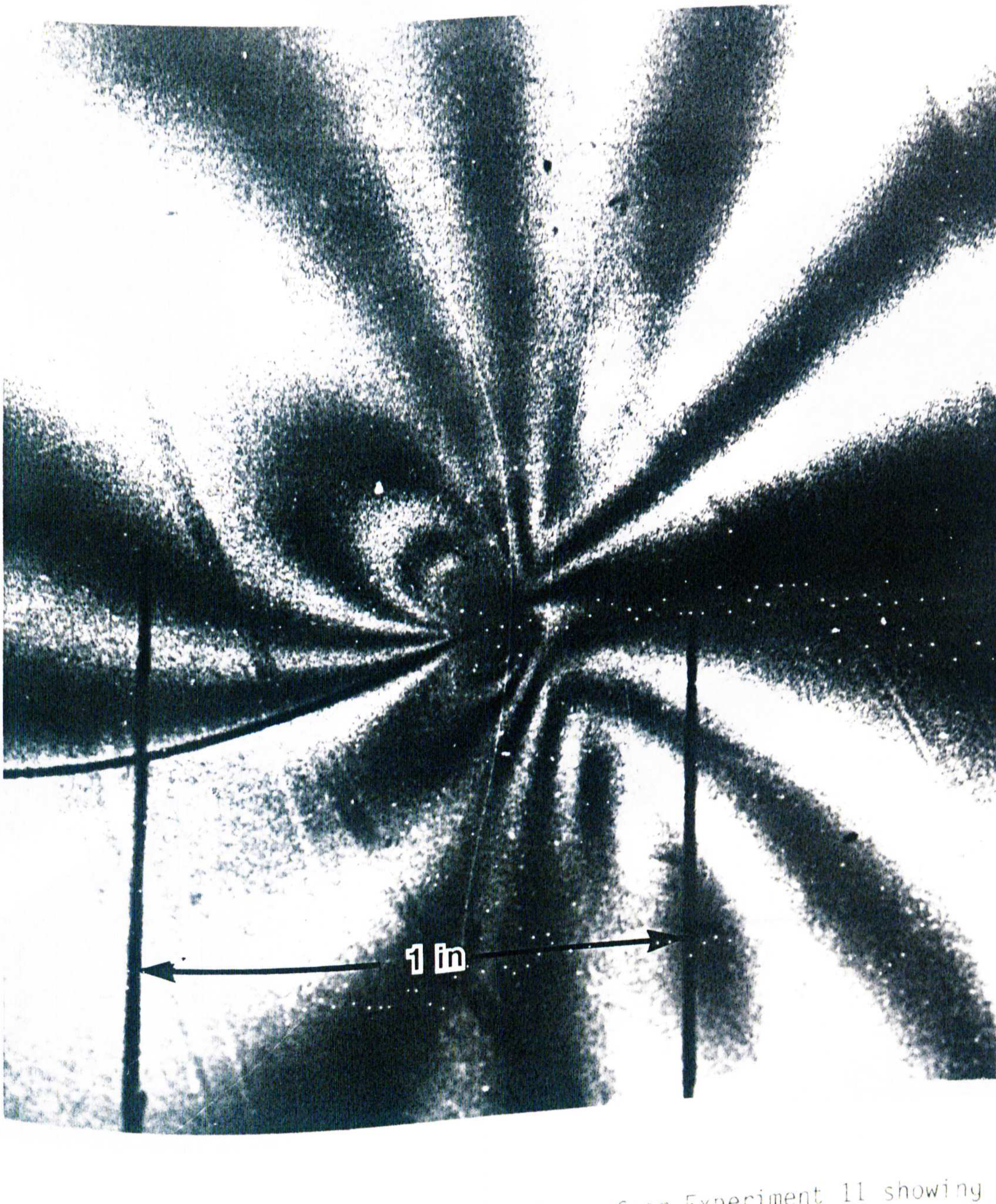

Figure 6.4 Enlargement of a single frame from Experiment 11 showing a crack-tip isochromatic pattern that retains considerable asymmetry as one approaches the crack tip.

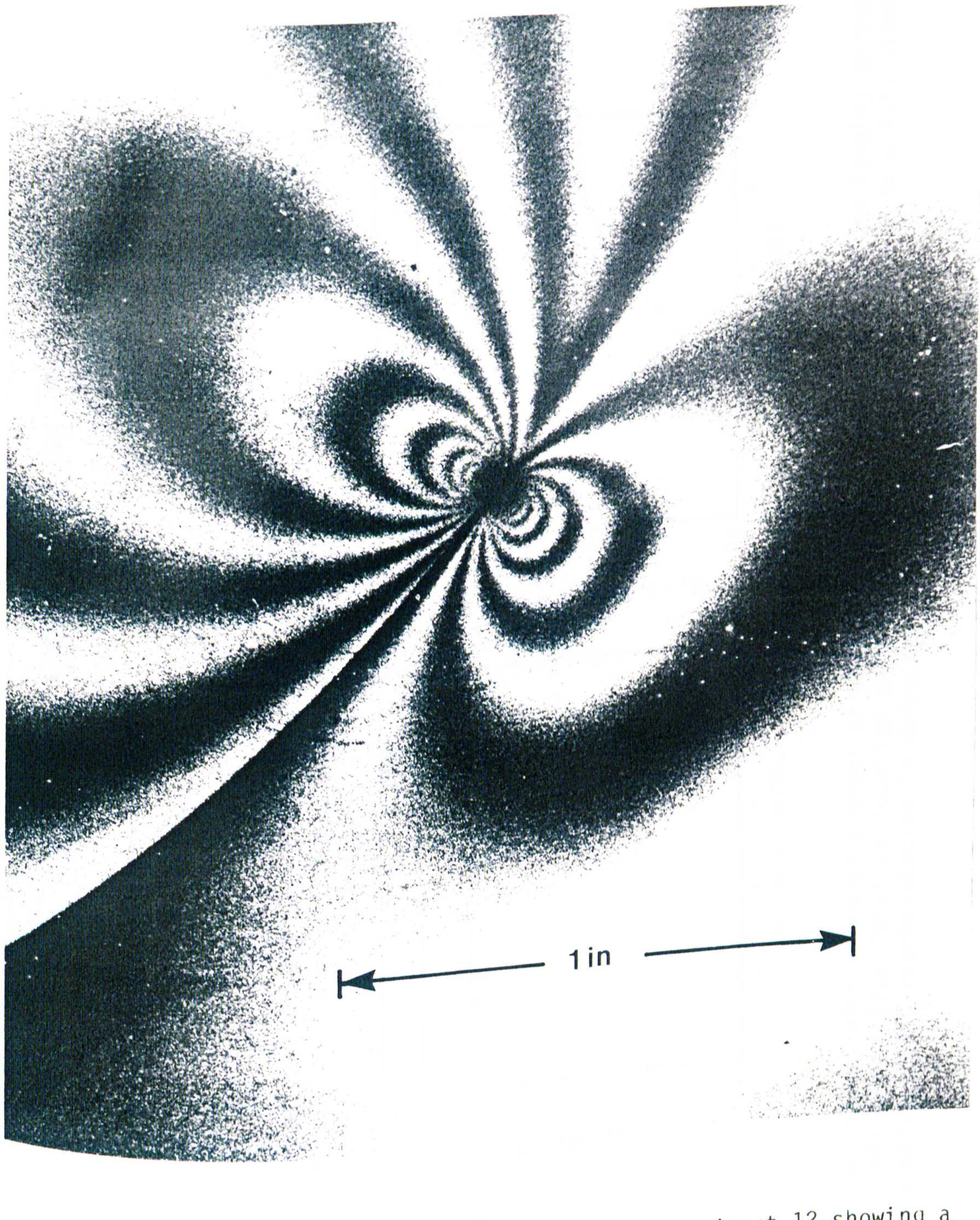

Figure 6.5 Enlargement of a single frame from Experiment 12 showing a crack-tip isochromatic pattern that becomes increasingly symmetric as one approaches the crack tip.

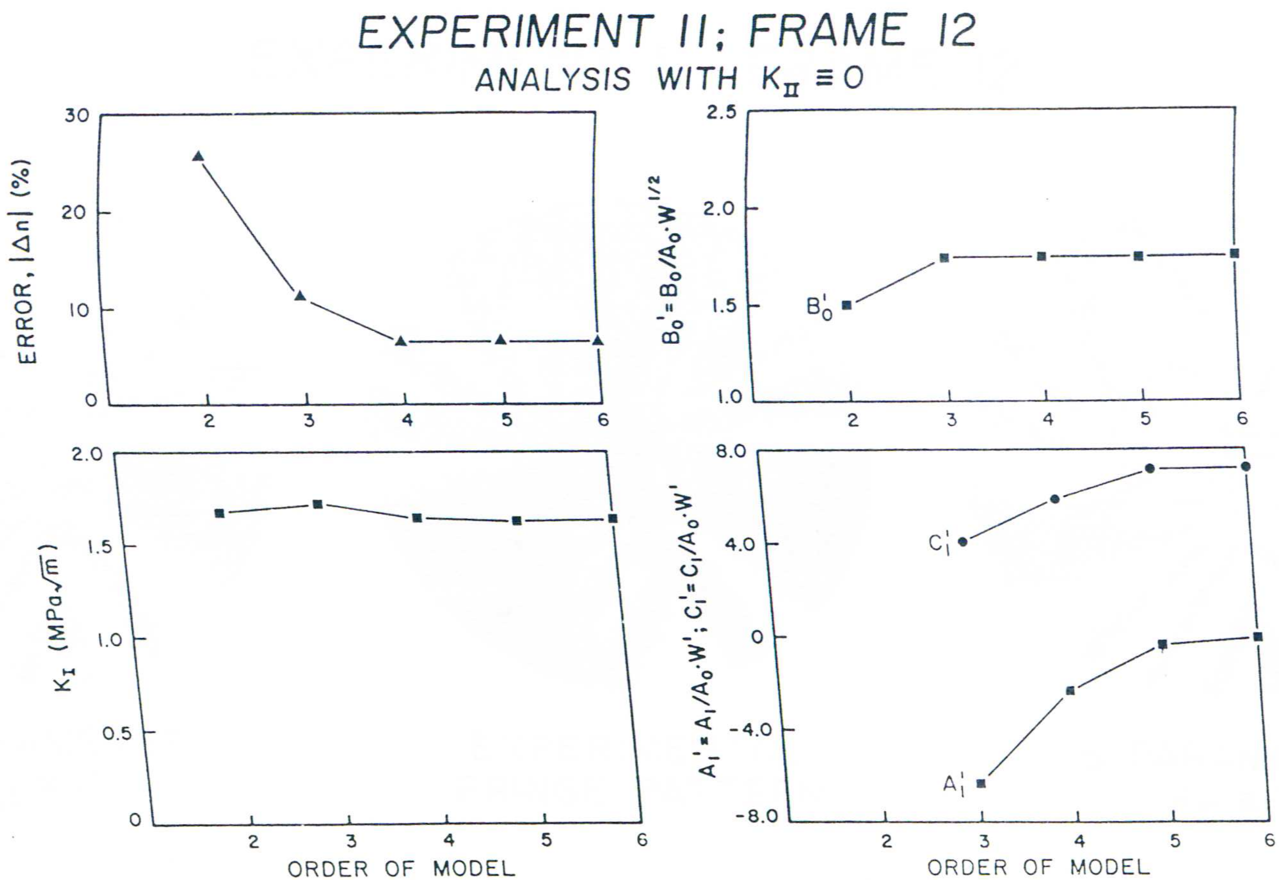

Figure 6.6 The changes with increasing order of analysis model in the error term and leading series coefficients from local collocation analyses of the fringe pattern of Figure 4.4, using a stress field representation in which $K_{II} \equiv 0$.

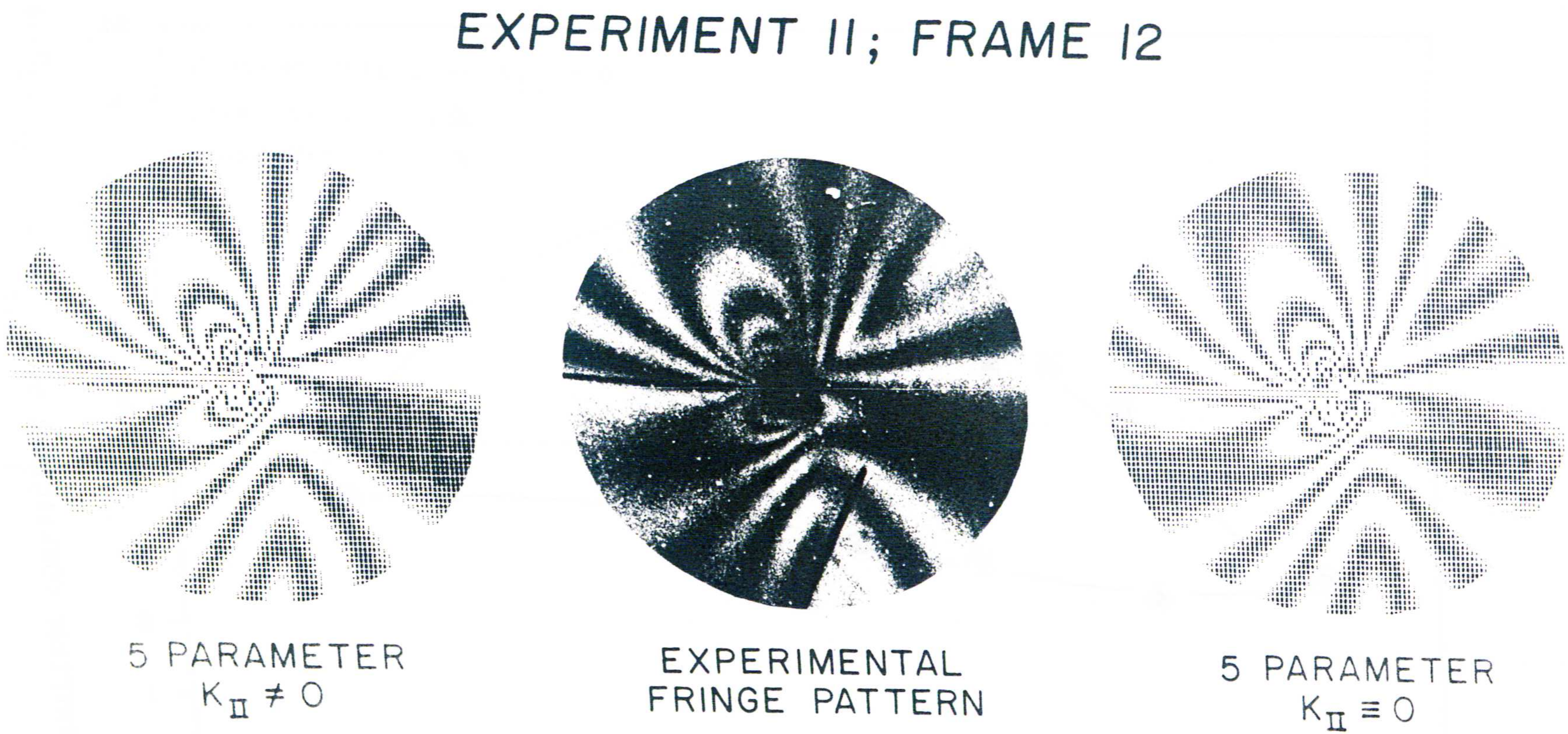

Figure 6.7 The experimental fringe pattern for Frame 12 of Experiment 11 showing the data acquisition region of radius equal to 0.50 inches and the reconstructed (computer generated) isochromatic patterns corresponding to 5 Parameter (5th Order) Models with and without K_{II}. The 5 Parameter Model retains terms upto $r^{3/2}$.

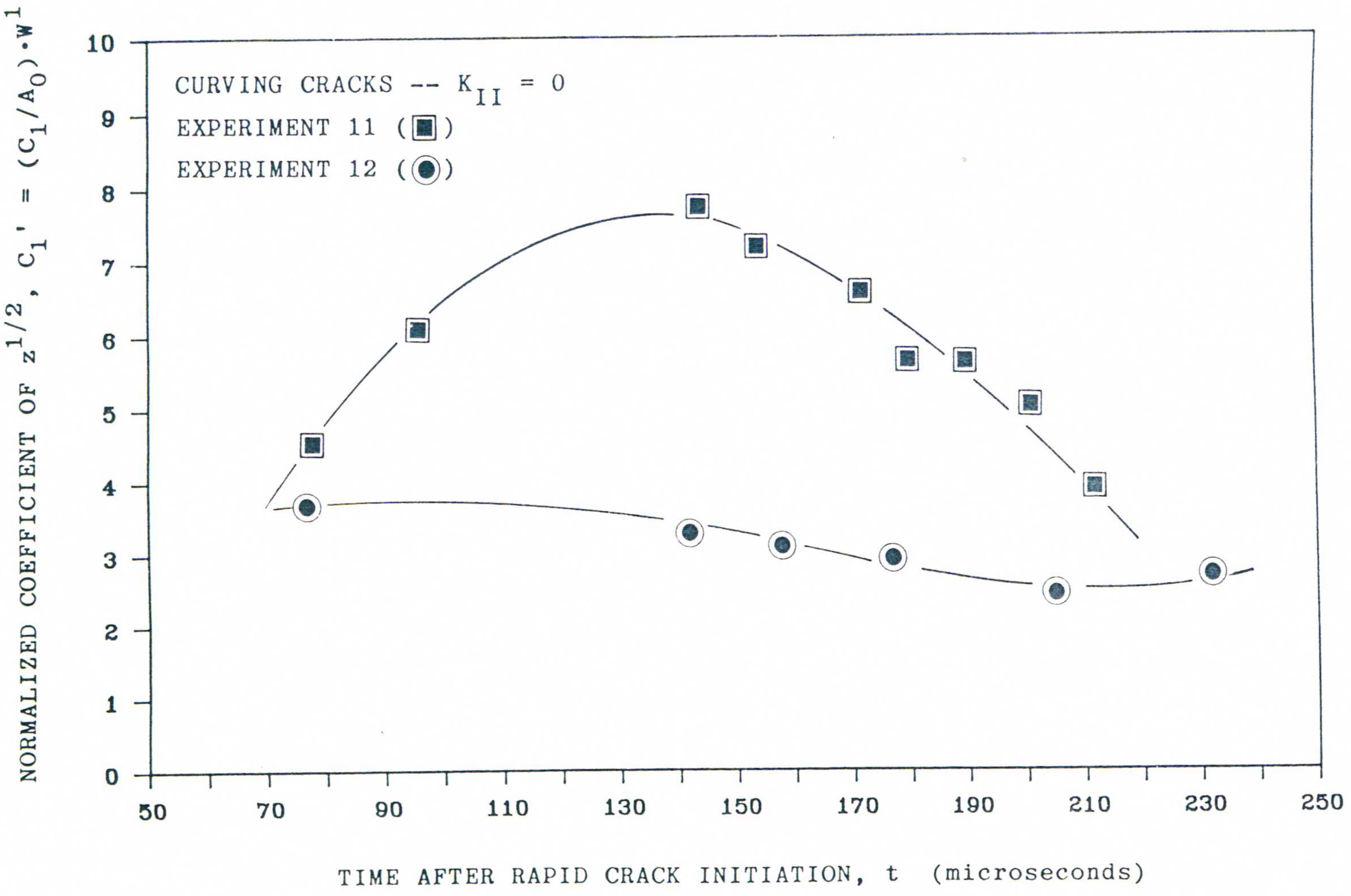

Figure 6.8 The normalized shear mode coefficient of $z^{1/2}$, C_1', as a function of time, for Experiments 11 and 12, using a stress field representation in which $K_{II} \equiv 0$.

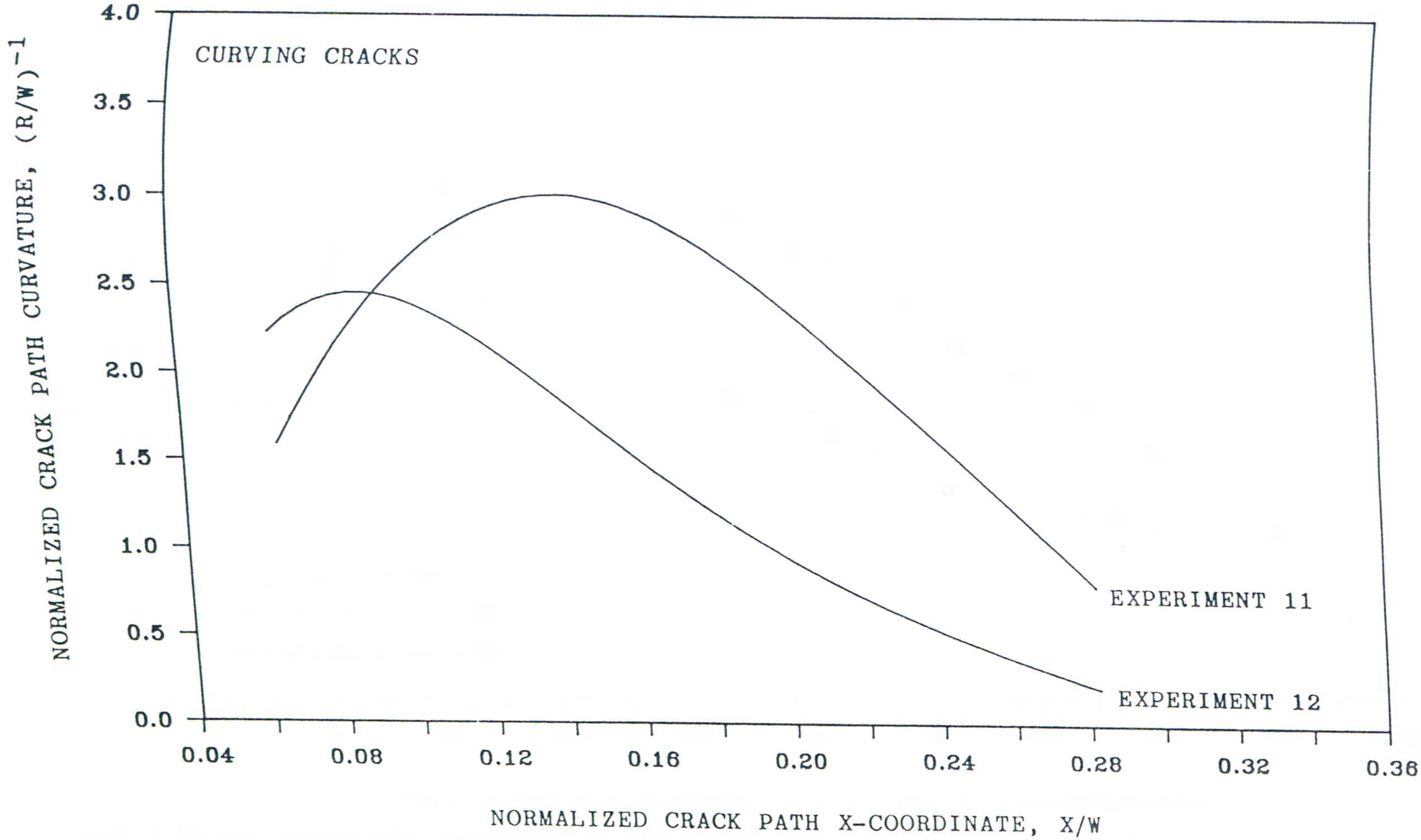

Figure 6.9 The normalized curvature of the crack path, $(R/W)^{-1}$, for Experiments 11 and 12, as a function of the normalized X-coordinate, X/W, of position along the path.

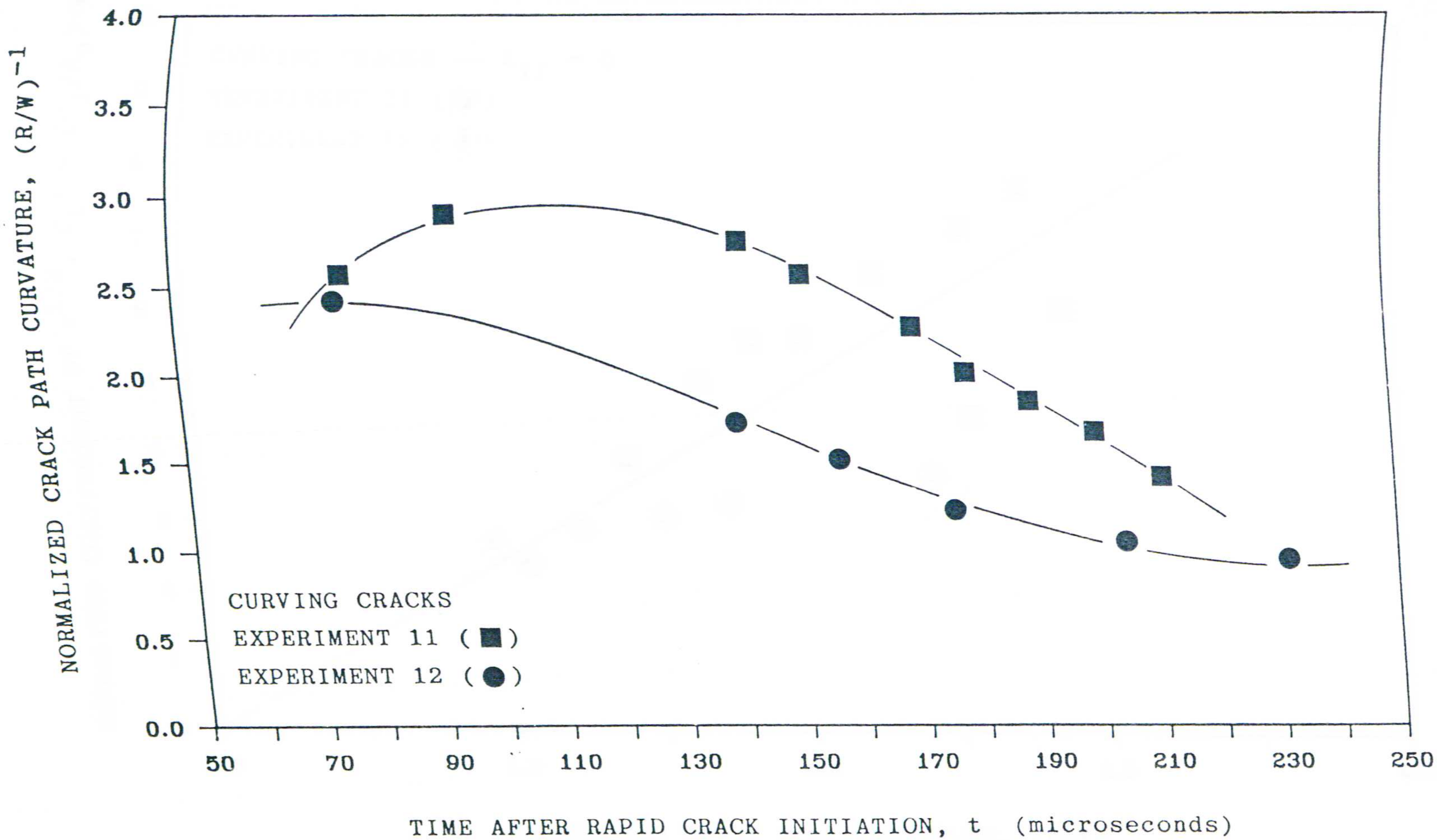

Figure 6.10 The normalized curvature of the crack path, $(R/W)^{-1}$, for Experiments 11 and 12, as a function of time, showing locations at which isochromatic data was recorded.

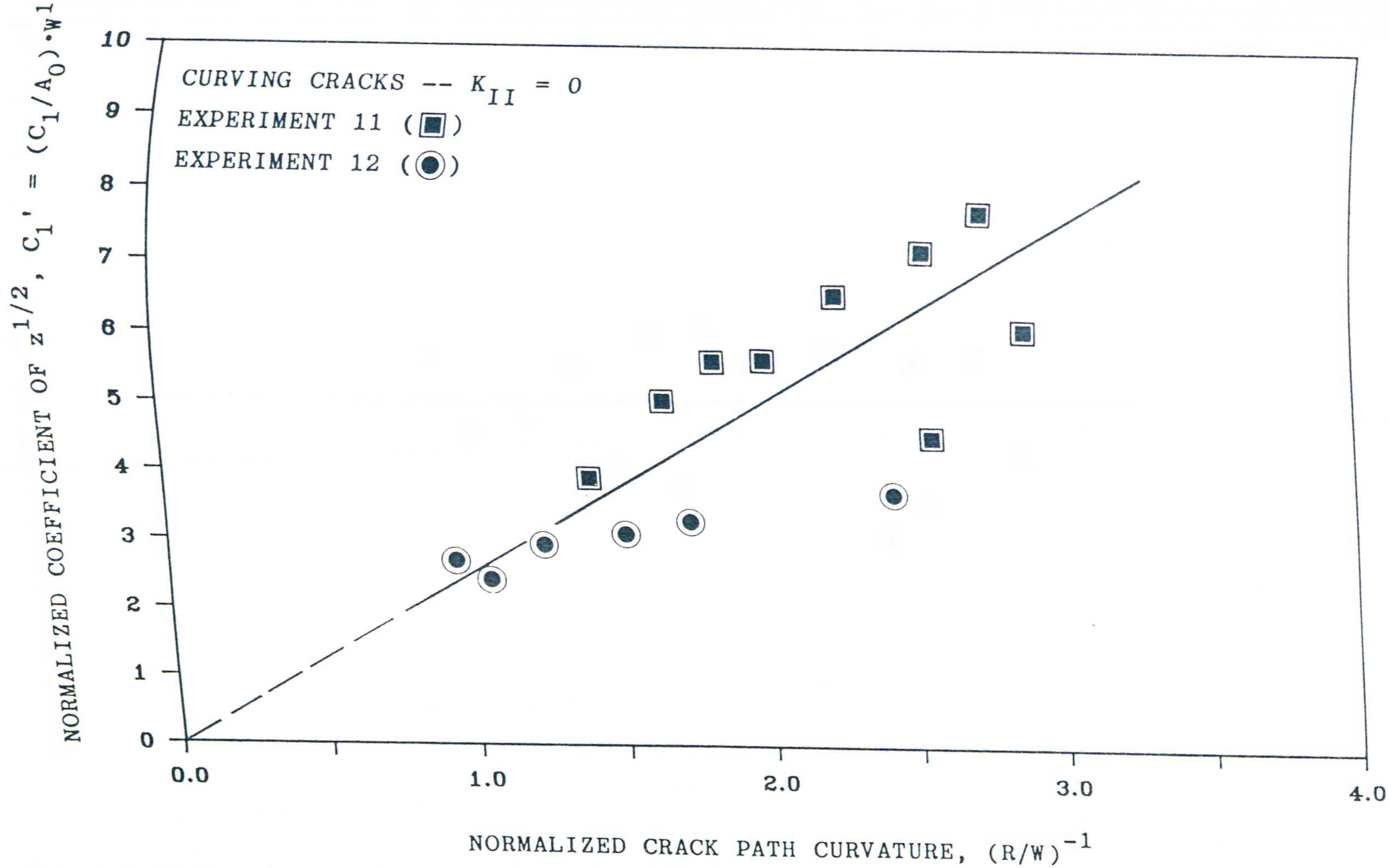

Figure 6.11 The normalized shear mode coefficient of $z^{1/2}$, C_1', as a function of the curvature of the crack path, for the curving crack trajectories of Experiments 11 and 12.

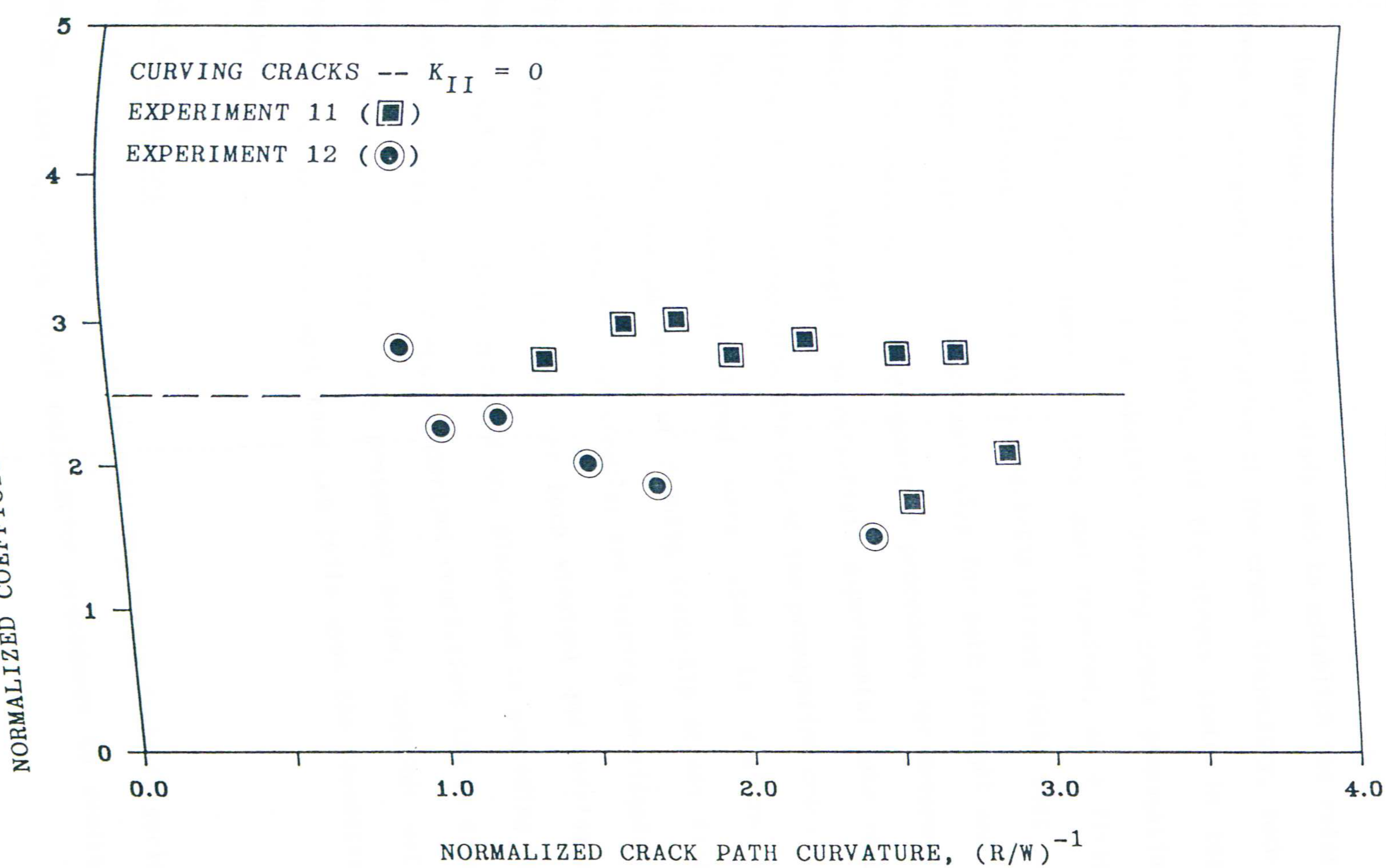

Figure 6.12 The shear mode coefficient of $z^{1/2}$, C_1', normalized with respect to the instantaneous radius of curvature of the crack path, as a function of the curvature of the crack path.

CHAPTER 7

CLOSURE

The primary goal of this study was to establish the relationship between a parameter descriptive of the crack trajectory, such as the curvature of the crack path, and the stress state in the close vicinity of the tip of a smoothly curving crack propagating in a finite body. Fulfillment of this goal required, as a first step, representations of the running crack-tip stress field that would be valid over a region of reasonable size for both straight and curving cracks, followed by the development of procedures for determining the parameters of interest from full-field experimental data related to the stress field surrounding the tip of the propagating crack.

The techniques developed were used to analyze dynamic photoelastic fringe patterns of running crack-tip stress fields and results were obtained for the singular and leading non-singular stress field parameters of interest for both straight and curving cracks. These results have been detailed and discussed in preceding sections of this dissertation. Certain important conclusions can be drawn from these results and these are presented below, together with some suggestions for future work that can build upon the foundation that has been laid here.

7.1 Conclusions

(1) Representations of the crack-tip stress field in series form can be combined with local collocation procedures to evaluate the

stress intensity factor(s) and other related stress field parameters of interest in a reliable and accurate manner from full-field experimental data, thus allowing the stress state surrounding the tip of a stationary or propagating crack to be modelled with a high degree of confidence in terms of these parameters.

(2) Non-singular stress field components of order $r^{1/2}$ must be retained in the series stress field representation even when the goal is accurate determination of the singular term(s) alone. In general, reliable values for a specific singular or non-singular stress field coefficient can only be obtained once the model used to describe the stress field retains at least one term beyond the point of interest in the particular series, Z or Y.

(3) The order of terms that must be retained so as to successfully match the stress state over a region of given size for a specific crack tip location in a particular geometry can be established by examining the changes in the stress field parameters with increasing order of analysis model, and by comparing the stress state predicted by a given set of coefficients with the experimentally observed stress state over the same region.

(4) The leading non-singular stress field coefficients for a particular geometry vary systematically with crack tip position for both stationary and running cracks under opening mode loading, and take on larger values when the crack tip is close to a boundary of the specimen. The results for stationary and propagating cracks approach one another as the crack speed decreases to moderate values.

(5) The singularity associated with the tip of a crack propagating continously along a smoothly varying, curvilinear path in a brittle, isotropic material is that of opening mode, K_I, and the shear mode singular term, K_{II}, is identically zero everywhere along the crack path, in the absence of stress wave loading conditions.

(6) The curvature of the path followed by a smoothly curving crack is related to the magnitude of the coefficient of the leading non-singular ($r^{1/2}$) component of the shear mode stress field, with larger values of this coefficient, C_1, being associated with a more sharply curving crack.

7.2 Suggestions for Future Work

The methodology developed in this study could be used fruitfully to pursue further investigations of running crack-tip stress fields and to evaluate stress field parameters using data from sources other than photoelasticity, such as moire interferometry, holography, or strain gages. Certain specific areas of study that would follow naturally from the present work are discussed below.

(1) The results for stationary and propagating cracks obtained for the opening mode case using a ring segment suggest that it may be possible to take the relative values for the non-singular stress field coefficients (normalized with regard to the magnitude of the singularity and the in-plane specimen dimensions) from static situations and obtain the corresponding dynamic coefficients by introducing an appropriate normalization factor that accounts for the influences of crack speed. This would certainly be useful since it

would allow the non-singular terms determined for stationary cracks to be applied to a wide variety of running crack situations. This would be particularly helpful when the experimental data cannot easily be used to calculate these coefficients directly, as in the case of the method of caustics, or for example, when using a limited number of strain gages to study dynamic crack propagation in metals.

(2) The importance of retaining terms of order $r^{1/2}$ when attempting to accurately determine the relationship between the crack speed and the instantaneous crack-tip stress intensity factor was discussed. There has been considerable discussion (and controversy) over the past decade on whether such a relationship is a unique property for a given material, and a great deal of the discussion has focussed on and been fueled by the differences in the results that are obtained experimentally using different specimen geometries and different methods. Since the magnitudes of the various higher order terms are themselves functions of the crack tip position, specimen geometry, and loading conditions, a careful re-examination of the problem from this standpoint may be fruitful and helpful in resolving this issue.

(3) The curving crack examples that were studied in this dissertation were both cases of constant speed crack propagation in identical specimens. This was, in fact, an important factor in the selection of these particular examples for detailed analysis, since it was desired to examine the non-singular effects relative to the crack path with a minimum of additional complexities that could be

introduced by varying crack speeds, differences in specimen geometry, and specimen size effects. Clearly, similar studies for non-constant crack speed situations would yield additional useful information. The question of specimen size effects bears on the choice of an appropriate characteristic length dimension for normalization purposes as evidenced by Figures 6.11 and 6.12. Finally, variations in specimen geometry could certainly be expected to play a role on the trajectory followed by a propagating crack.

(4) It was also pointed out in the previous discussion that it would be premature at the present time to try and relate all of the observed variations in the curvature of the crack path to the changes in the shear mode $r^{1/2}$ term alone. Examination of the trajectory problem with regard to influence of the next few higher order terms (independent of the issues raised in the preceding paragraph) would be needed before an exact relationship could be determined.

APPENDIX A

CRACK-TIP STRESS FIELD EXPRESSIONS

General expressions were obtained in Chapter 3 of this dissertation, using complex variables, for the in-plane Cartesian stress components for the case of a single-ended, stress-free crack propagating at a constant speed under plane-strain opening and shear mode loading conditions. These results are expressed in terms of real variables and combined to form the general solution to the elastodynamic crack problem in the sections that follow.

A.1 Opening Mode

The Cartesian stress components for the opening mode case were expressed as

$$\sigma_{xx_I} = \frac{(1+\lambda_2{}^2)}{4\lambda_1\lambda_2 - (1+\lambda_2{}^2)^2}\{(1+2\lambda_1{}^2-\lambda_2{}^2)\ \mathrm{Re}\ Z_1 - \frac{4\lambda_1\lambda_2}{1+\lambda_2{}^2}\ \mathrm{Re}\ Z_2 + (1+2\lambda_1{}^2-\lambda_2{}^2)\ \mathrm{Re}\ Y_1 - (1+\lambda_2{}^2)\ \mathrm{Re}\ Y_2\} \tag{A.1}$$

$$\sigma_{yy_I} = \frac{(1+\lambda_2{}^2)}{4\lambda_1\lambda_2 - (1+\lambda_2{}^2)^2}\{-(1+\lambda_2{}^2)\ \mathrm{Re}\ Z_1 + \frac{4\lambda_1\lambda_2}{1+\lambda_2{}^2}\ \mathrm{Re}\ Z_2 - (1+\lambda_2{}^2)\ \mathrm{Re}\ Y_1 + (1+\lambda_2{}^2)\ \mathrm{Re}\ Y_2\} \tag{A.2}$$

$$\tau_{xy_I} = \frac{(1+\lambda_2{}^2)}{4\lambda_1\lambda_2 - (1+\lambda_2{}^2)^2}\{-2\lambda_1\ \mathrm{Im}\ Z_1 + 2\lambda_1\ \mathrm{Im}\ Z_2 - 2\lambda_1\ \mathrm{Im}\ Y_1 + \frac{(1+\lambda_2{}^2)^2}{2\lambda_2}\ \mathrm{Im}\ Y_2\} \tag{A.3}$$

where the velocity-coupled complex stress functions, Z_1 and Z_2, and Y_1 and Y_2, were defined as

$$Z_1 = \sum_{n=0}^{\infty} A_n z_1^{n-1/2} \qquad Z_2 = \sum_{n=0}^{\infty} A_n z_2^{n-1/2} \tag{A.4}$$

$$Y_1 = \sum_{m=0}^{\infty} B_m z_1^{m} \qquad Y_2 = \sum_{m=0}^{\infty} B_m z_2^{m} \tag{A.5}$$

with z_1 and z_2 being the velocity-transformed coordinates defined in Figure 3.2 as

$$z_1 = x + i\lambda_1 y = \rho_1 e^{i\phi_1} \qquad z_2 = x + i\lambda_2 y = \rho_2 e^{i\phi_2} \tag{A.6}$$

with

$$\lambda_1 = [\, 1 - (c/c_1)^2 \,]^{1/2} \qquad \lambda_2 = [\, 1 - (c/c_2)^2 \,]^{1/2} \tag{A.7}$$

Substituting equation (A.6) in equation (A.4) gives

$$\begin{aligned} Z_1 &= (\mathrm{Re}\, Z_1) + i(\mathrm{Im}\, Z_1) \\ &= \sum_{n=0}^{\infty} A_n \rho_1^{n-1/2} \cos(n-1/2)\phi_1 + i \sum_{n=0}^{\infty} A_n \rho_1^{n-1/2} \sin(n-1/2)\phi_1 \end{aligned} \tag{A.8}$$

and

$$\begin{aligned} Z_2 &= (\mathrm{Re}\, Z_2) + i(\mathrm{Im}\, Z_2) \\ &= \sum_{n=0}^{\infty} A_n \rho_2^{n-1/2} \cos(n-1/2)\phi_2 + i \sum_{n=0}^{\infty} A_n \rho_2^{n-1/2} \sin(n-1/2)\phi_2 \end{aligned} \tag{A.9}$$

Similarly, substituting equation (A.6) in equation (A.5) gives

$$Y_1 = (\mathrm{Re}\, Y_1) + i(\mathrm{Im}\, Y_1) \tag{A.10}$$

$$= \sum_{m=0}^{\infty} B_m \rho_1^{m} \cos m\phi_1 + i \sum_{m=0}^{\infty} B_m \rho_1^{m} \sin m\phi_1$$

and

$$Y_2 = (\mathrm{Re}\, Y_2) + i(\mathrm{Im}\, Y_2) \tag{A.11}$$

$$= \sum_{m=0}^{\infty} B_m \rho_2^{m} \cos m\phi_2 + i \sum_{m=0}^{\infty} B_m \rho_2^{m} \sin m\phi_2$$

Substituting equations (A.8)-(A.11) in equations (A.1)-(A.3) results in the following expressions for the opening mode elastodynamic stress components in terms of the real variables, A_n, B_m, ρ_1, ρ_2, ϕ_1, and ϕ_2:

$$\sigma_{xx_I} = \frac{(1+\lambda_2^{\,2})}{4\lambda_1\lambda_2 - (1+\lambda_2^{\,2})^2} \Big\{ (1+2\lambda_1^{\,2}-\lambda_2^{\,2}) \sum_{n=0}^{\infty} A_n \rho_1^{\,n-1/2} \cos(n-1/2)\phi_1$$

$$- \frac{4\lambda_1\lambda_2}{1+\lambda_2^{\,2}} \sum_{n=0}^{\infty} A_n \rho_2^{\,n-1/2} \cos(n-1/2)\phi_2$$

$$+ (1+2\lambda_1^{\,2}-\lambda_2^{\,2}) \sum_{m=0}^{\infty} B_m \rho_1^{\,m} \cos m\phi_1$$

$$- (1+\lambda_2^{\,2}) \sum_{m=0}^{\infty} B_m \rho_2^{\,m} \cos m\phi_2 \Big\} \tag{A.12}$$

$$\sigma_{yy_I} = \frac{(1+\lambda_2{}^2)}{4\lambda_1\lambda_2 - (1+\lambda_2{}^2)^2} \Big\{ -(1+\lambda_2{}^2) \sum_{n=0}^{\infty} A_n \rho_1{}^{n-1/2} \cos(n-1/2)\phi_1$$

$$+ \frac{4\lambda_1\lambda_2}{1+\lambda_2{}^2} \sum_{n=0}^{\infty} A_n \rho_2{}^{n-1/2} \cos(n-1/2)\phi_2$$

$$- (1+\lambda_2{}^2) \sum_{m=0}^{\infty} B_m \rho_1{}^m \cos m\phi_1$$

$$+ (1+\lambda_2{}^2) \sum_{m=0}^{\infty} B_m \rho_2{}^m \cos m\phi_2 \Big\} \quad (A.13)$$

$$\tau_{xy_I} = \frac{(1+\lambda_2{}^2)}{4\lambda_1\lambda_2 - (1+\lambda_2{}^2)^2} \Big\{ -2\lambda_1 \sum_{n=0}^{\infty} A_n \rho_1{}^{n-1/2} \sin(n-1/2)\phi_1$$

$$+ 2\lambda_1 \sum_{n=0}^{\infty} A_n \rho_2{}^{n-1/2} \sin(n-1/2)\phi_2$$

$$- 2\lambda_1 \sum_{m=0}^{\infty} B_m \rho_1{}^m \sin m\phi_1$$

$$+ \frac{(1+\lambda_2{}^2)^2}{2\lambda_2} \sum_{m=0}^{\infty} B_m \rho_2{}^m \sin m\phi_2 \Big\} \quad (A.14)$$

A.2 Shear Mode

The expressions for the stress components which represent the elastodynamic shear mode counterpart to equations (A.1)-(A.3) were obtained previously as

$$\sigma_{xx_{II}} = \frac{2\lambda_2}{4\lambda_1\lambda_2 - (1+\lambda_2^2)^2} \{ (1+2\lambda_1^2-\lambda_2^2) \text{ Re } Y_1^* - \frac{4\lambda_1\lambda_2}{1+\lambda_2^2} \text{ Re } Y_2^*$$

$$+ (1+2\lambda_1^2-\lambda_2^2) \text{ Re } Z_1^* - (1+\lambda_2^2) \text{ Re } Z_2^* \} \quad (A.15)$$

$$\sigma_{yy_{II}} = \frac{2\lambda_2}{4\lambda_1\lambda_2 - (1+\lambda_2^2)^2} \{ - (1+\lambda_2^2) \text{ Re } Y_1^* + \frac{4\lambda_1\lambda_2}{1+\lambda_2^2} \text{ Re } Y_2^*$$

$$- (1+\lambda_2^2) \text{ Re } Z_1^* + (1+\lambda_2^2) \text{ Re } Z_2^* \} \quad (A.16)$$

$$\tau_{xy_{II}} = \frac{2\lambda_2}{4\lambda_1\lambda_2 - (1+\lambda_2^2)^2} \{ - 2\lambda_1 \text{ Im } Y_1^* + 2\lambda_1 \text{ Im } Y_2^*$$

$$- 2\lambda_1 \text{ Im } Z_1^* + \frac{(1+\lambda_2^2)^2}{2\lambda_2} \text{ Im } Z_2^* \} \quad (A.17)$$

where the antisymmetric, velocity-coupled, complex stress functions, Z_1^* and Z_2^*, and Y_1^* and Y_2^*, were defined as

$$Z_1^* = \sum_{n=0}^{\infty} -i\, C_n\, z_1^{n-1/2} \qquad Z_2^* = \sum_{n=0}^{\infty} -i\, C_n\, z_2^{n-1/2} \quad (A.18)$$

$$Y_1^* = \sum_{m=0}^{\infty} -i\, D_m\, z_1^{m} \qquad Y_2^* = \sum_{m=0}^{\infty} -i\, D_m\, z_2^{m} \quad (A.19)$$

with z_1 and z_2, and λ_1 and λ_2 defined as before.

Substituting equation (A.6) in equation (A.18) gives

$$Z_1^* = (\text{Re } Z_1^*) + i(\text{Im } Z_1^*) \tag{A.20}$$

$$= \sum_{n=0}^{\infty} C_n \rho_1^{n-1/2} \sin(n-1/2)\phi_1 + i \sum_{n=0}^{\infty} -C_n \rho_1^{n-1/2} \cos(n-1/2)\phi_1$$

and

$$Z_2^* = (\text{Re } Z_2^*) + i(\text{Im } Z_2^*) \tag{A.21}$$

$$= \sum_{n=0}^{\infty} C_n \rho_2^{n-1/2} \sin(n-1/2)\phi_2 + i \sum_{n=0}^{\infty} -C_n \rho_2^{n-1/2} \cos(n-1/2)\phi_2$$

Similarly, substituting equation (A.6) in equation (A.19) gives

$$Y_1^* = (\text{Re } Y_1^*) + i(\text{Im } Y_1^*) \tag{A.22}$$

$$= \sum_{m=0}^{\infty} D_m \rho_1^{m} \sin m\phi_1 + i \sum_{m=0}^{\infty} -D_m \rho_1^{m} \cos m\phi_1$$

and

$$Y_2^* = (\text{Re } Y_2^*) + i(\text{Im } Y_2^*) \tag{A.23}$$

$$= \sum_{m=0}^{\infty} D_m \rho_2^{m} \sin m\phi_2 + i \sum_{m=0}^{\infty} -D_m \rho_2^{m} \cos m\phi_2$$

The desired expressions for the elastodynamic shear mode stress components in terms of the real variables, C_n, D_m, ρ_1, ρ_2, ϕ_1, and ϕ_2 can then be written as

$$\sigma_{xx_{II}} = \frac{2\lambda_2}{4\lambda_1\lambda_2 - (1+\lambda_2{}^2)^2}\Big\{ (1+2\lambda_1{}^2-\lambda_2{}^2) \sum_{n=0}^{\infty} C_n \rho_1{}^{n-1/2} \sin(n-1/2)\phi_1$$

$$- (1+\lambda_2{}^2) \sum_{n=0}^{\infty} C_n \rho_2{}^{n-1/2} \sin(n-1/2)\phi_2$$

$$+ (1+2\lambda_1{}^2-\lambda_2{}^2) \sum_{m=0}^{\infty} D_m \rho_1{}^m \sin m\phi_1$$

$$- \frac{4\lambda_1\lambda_2}{1+\lambda_2{}^2} \sum_{n=0}^{\infty} D_m \rho_2{}^m \sin m\phi_2 \Big\} \quad (A.24)$$

$$\sigma_{yy_{II}} = \frac{2\lambda_2}{4\lambda_1\lambda_2 - (1+\lambda_2{}^2)^2}\Big\{ - (1+\lambda_2{}^2) \sum_{n=0}^{\infty} C_n \rho_1{}^{n-1/2} \sin(n-1/2)\phi_1$$

$$+ (1+\lambda_2{}^2) \sum_{n=0}^{\infty} C_n \rho_2{}^{n-1/2} \sin(n-1/2)\phi_2$$

$$- (1+\lambda_2{}^2) \sum_{m=0}^{\infty} D_m \rho_1{}^m \sin m\phi_1$$

$$+ \frac{4\lambda_1\lambda_2}{1+\lambda_2{}^2} \sum_{n=0}^{\infty} D_m \rho_2{}^m \sin m\phi_2 \Big\} \quad (A.25)$$

$$\tau_{xy_{II}} = \frac{2\lambda_2}{4\lambda_1\lambda_2 - (1+\lambda_2^2)^2} \{ \quad 2\lambda_1 \sum_{n=0}^{\infty} C_n \rho_1^{n-1/2} \cos(n-1/2)\phi_1$$

$$- \frac{(1+\lambda_2^2)^2}{2\lambda_2} \sum_{n=0}^{\infty} C_n \rho_2^{n-1/2} \cos(n-1/2)\phi_2$$

$$+ 2\lambda_1 \sum_{m=0}^{\infty} D_m \rho_1^{m} \cos m\phi_1$$

$$- 2\lambda_1 \sum_{m=0}^{\infty} D_m \rho_2^{m} \cos m\phi_2 \} \quad (A.26)$$

A.3 Combined Loading

Superposition of the stress components given in equations (A.12)-(A.14) and (A.24)-(A.26) provides the general solution for the stress field for a crack propagating at a constant speed under combined opening and forward shear loading. The resulting expressions for the stresses are presented below.

(A.27)

$$\sigma_{xx} = \sigma_{xx_I} + \sigma_{xx_{II}}$$

$$= \frac{(1+\lambda_2^2)}{4\lambda_1\lambda_2 - (1+\lambda_2^2)^2} \{ \sum_{n=0}^{\infty} A_n [(1+2\lambda_1^2-\lambda_2^2)\rho_1^{n-1/2}\cos(n-1/2)\phi_1 - \frac{4\lambda_1\lambda_2}{1+\lambda_2^2} \rho_2^{n-1/2}\cos(n-1/2)\phi_2]$$

$$+ \sum_{m=0}^{\infty} B_m [(1+2\lambda_1^2-\lambda_2^2)\rho_1^{m}\cos m\phi_1 - (1+\lambda_2^2)\rho_2^{m}\cos m\phi_2] \}$$

$$+ \frac{2\lambda_2}{4\lambda_1\lambda_2 - (1+\lambda_2{}^2)^2} \{ \sum_{n=0}^{\infty} C_n [(1+2\lambda_1{}^2-\lambda_2{}^2)\rho_1{}^{n-1/2}\sin(n-1/2)\phi_1 - (1+\lambda_2{}^2)\rho_2{}^{n-1/2}\sin(n-1/2)\phi_2]$$

$$+ \sum_{m=0}^{\infty} D_m [(1+2\lambda_1{}^2-\lambda_2{}^2)\rho_1{}^m \sin m\phi_1 - \frac{4\lambda_1\lambda_2}{1+\lambda_2{}^2}\rho_2{}^m \sin m\phi_2] \}$$

(A.28)

$$\sigma_{yy} = \sigma_{yy_I} + \sigma_{yy_{II}}$$

$$= \frac{(1+\lambda_2{}^2)}{4\lambda_1\lambda_2 - (1+\lambda_2{}^2)^2} \{ \sum_{n=0}^{\infty} A_n [- (1+\lambda_2{}^2)\rho_1{}^{n-1/2}\cos(n-1/2)\phi_1 + \frac{4\lambda_1\lambda_2}{1+\lambda_2{}^2}\rho_2{}^{n-1/2}\cos(n-1/2)\phi_2]$$

$$+ \sum_{m=0}^{\infty} B_m [- (1+\lambda_2{}^2)\rho_1{}^m \cos m\phi_1 + (1+\lambda_2{}^2)\rho_2{}^m \cos m\phi_2] \}$$

$$+ \frac{2\lambda_2}{4\lambda_1\lambda_2 - (1+\lambda_2{}^2)^2} \{ \sum_{n=0}^{\infty} C_n [- (1+\lambda_2{}^2)\rho_1{}^{n-1/2}\sin(n-1/2)\phi_1 + (1+\lambda_2{}^2)\rho_2{}^{n-1/2}\sin(n-1/2)\phi_2]$$

$$+ \sum_{m=0}^{\infty} D_m [- (1+\lambda_2{}^2)\rho_1{}^m \sin m\phi_1 + \frac{4\lambda_1\lambda_2}{1+\lambda_2{}^2}\rho_2{}^m \sin m\phi_2] \}$$

$$\tau_{xy} = \tau_{xy_I} + \tau_{xy_{II}} \tag{A.29}$$

$$= \frac{(1+\lambda_2{}^2)}{4\lambda_1\lambda_2 - (1+\lambda_2{}^2)^2} \left\{ \sum_{n=0}^{\infty} A_n \left[-2\lambda_1 \rho_1{}^{n-1/2} \sin(n-1/2)\phi_1 + 2\lambda_1 \rho_2{}^{n-1/2} \sin(n-1/2)\phi_2 \right] + \sum_{m=0}^{\infty} B_m \left[-2\lambda_1 \rho_1{}^m \sin m\phi_1 + \frac{(1+\lambda_2{}^2)^2}{2\lambda_2} \rho_2{}^m \sin m\phi_2 \right] \right\}$$

$$+ \frac{2\lambda_2}{4\lambda_1\lambda_2 - (1+\lambda_2{}^2)^2} \left\{ \sum_{n=0}^{\infty} C_n \left[2\lambda_1 \rho_1{}^{n-1/2} \cos(n-1/2)\phi_1 - \frac{(1+\lambda_2{}^2)^2}{2\lambda_2} \rho_2{}^{n-1/2} \cos(n-1/2)\phi_2 \right] + \sum_{m=0}^{\infty} D_m \left[2\lambda_1 \rho_1{}^m \cos m\phi_1 - 2\lambda_1 \rho_2{}^m \cos m\phi_2 \right] \right\}$$

APPENDIX B

THE LOCAL COLLOCATION ALGORITHM

B.1 Governing Equation for the Isochromatic Fringe Pattern

When implementing local collocation methods for the analysis of isochromatic fringe pattern data, it is convenient to express the photoelastic fringe order, N, in terms of the maximum in-plane shear stress, τ_{max}, as

$$
\begin{aligned}
(N f_\sigma / 2t)^2 &= \tau_{max}^2 \\
&= [(\sigma_{yy} - \sigma_{xx})/2]^2 + \tau_{xy}^2 \\
&= D^2 + T^2
\end{aligned}
\qquad (B.1)
$$

where f_σ is the fringe sensitivity of the birefringent model material, t is the model thickness, $D = (\sigma_{yy} - \sigma_{xx})/2$ and $T = \tau_{xy}$.

Using equations (A.27)-(A.29) of Appendix A, the terms D and T can be expressed as

$$
\begin{aligned}
D &= (\sigma_{yy} - \sigma_{xx})/2 \\
&= \frac{(1+\lambda_2^2)}{4\lambda_1\lambda_2 - (1+\lambda_2^2)^2} \Big\{ \sum_{n=0}^{\infty} A_n \Big[-(1+\lambda_1^2)\, \rho_1^{n-1/2} \cos(n-1/2)\phi_1 \\
&\qquad + \frac{4\lambda_1\lambda_2}{1+\lambda_2^2}\, \rho_2^{n-1/2} \cos(n-1/2)\phi_2 \Big] \\
&\qquad + \sum_{m=0}^{\infty} B_m \Big[-(1+\lambda_1^2)\, \rho_1^{m} \cos m\phi_1 \\
&\qquad + (1+\lambda_2^2)\, \rho_2^{m} \cos m\phi_2 \Big] \Big\}
\end{aligned}
\qquad (B.2)
$$

$$+ \frac{2\lambda_2}{4\lambda_1\lambda_2 - (1+\lambda_2{}^2)^2} \{ \sum_{n=0}^{\infty} C_n [- (1+\lambda_1{}^2) \ \rho_1{}^{n-1/2} \sin(n-1/2)\phi_1 + (1+\lambda_2{}^2) \ \rho_2{}^{n-1/2} \sin(n-1/2)\phi_2]$$

$$+ \sum_{m=0}^{\infty} D_m [- (1+\lambda_1{}^2) \ \rho_1{}^m \sin m\phi_1 + \frac{4\lambda_1\lambda_2}{1+\lambda_2{}^2} \ \rho_2{}^m \sin m\phi_2] \}$$

(B.3)

and $T = \tau_{xy}$

$$= \frac{(1+\lambda_2{}^2)}{4\lambda_1\lambda_2 - (1+\lambda_2{}^2)^2} \{ \sum_{n=0}^{\infty} A_n [- 2\lambda_1 \ \rho_1{}^{n-1/2} \sin(n-1/2)\phi_1 + 2\lambda_1 \ \rho_2{}^{n-1/2} \sin(n-1/2)\phi_2]$$

$$+ \sum_{m=0}^{\infty} B_m [- 2\lambda_1 \ \rho_1{}^m \sin m\phi_1 + \frac{(1+\lambda_2{}^2)^2}{2\lambda_2} \ \rho_2{}^m \sin m\phi_2] \}$$

$$+ \frac{2\lambda_2}{4\lambda_1\lambda_2 - (1+\lambda_2{}^2)^2} \{ \sum_{n=0}^{\infty} C_n [2\lambda_1 \ \rho_1{}^{n-1/2} \cos(n-1/2)\phi_1 - \frac{(1+\lambda_2{}^2)^2}{2\lambda_2} \ \rho_2{}^{n-1/2} \cos(n-1/2)\phi_2]$$

$$+ \sum_{m=0}^{\infty} D_m [2\lambda_1 \ \rho_1{}^m \cos m\phi_1 - 2\lambda_1 \ \rho_2{}^m \cos m\phi_2] \}$$

B.2 Mathematical Formulation of the Local Collocation Method

Equations (B.2) and (B.3), when substituted into equation (B.1) represent the general solution for the full-field isochromatic fringe pattern around a crack tip propagating at constant speed in the plane of a body subjected to combined opening and shear mode loading conditions. These expressions can be used to describe the stress state in any size region around the crack tip, with the size of the region and the degree of precision desired determining the number of terms, n=N and m=M, that must be retained in the truncated form of each of the infinite series in order to adequately describe the stress state over the given region.

The unknown constants, A_0, A_1, ..., A_N, B_0, B_1, ..., B_M, C_0, C_1, ..., C_N, D_1, D_2, ..., D_M, in these series can be determined using experimentally obtained isochromatic fringe data for any geometry and loading condition by employing standard, over-deterministic, non-linear, least-squares methods. (Recall that the term D_0 does not influence the stress components and therefore does not appear in this development.)

One such method utilizes an iterative procedure based on the Newton-Raphson method. Consider a set of functions of the form:

$$g_k(A_0, C_0, B_0, A_1, C_1, B_1, D_1, \ldots, A_N, C_N, B_M, D_M) = 0 \tag{B.4}$$

where k = 1, 2, ..., K , and K > 2(N+1)+2(M+1)-1. Taking the Taylor's series expansion of equation (B.4) gives:

$$
\begin{aligned}
(g_k)_{i+1} = (g_k)_i \; & + (\partial g_k/\partial A_0)_i \, \Delta A_0 + (\partial g_k/\partial C_0)_i \, \Delta C_0 \\
& + (\partial g_k/\partial B_0)_i \, \Delta B_0 \\
& + (\partial g_k/\partial A_1)_i \, \Delta A_1 + (\partial g_k/\partial C_1)_i \, \Delta C_1 \\
& + (\partial g_k/\partial B_1)_i \, \Delta B_1 + (\partial g_k/\partial D_1)_i \, \Delta D_1 \\
& + \;\ldots\ldots \qquad + \;\ldots\ldots \\
& + \;\ldots\ldots \qquad + \;\ldots\ldots \\
& + (\partial g_k/\partial A_N)_i \, \Delta A_N + (\partial g_k/\partial C_N)_i \, \Delta C_N \\
& + (\partial g_k/\partial B_M)_i \, \Delta B_M + (\partial g_k/\partial D_M)_i \, \Delta D_M
\end{aligned} \qquad (B.5)
$$

where i refers to the ith iteration step, and ΔA_0, ΔC_0, ΔB_0, ΔA_1, ΔC_1, ΔB_1, ΔD_1, ..., ΔA_N, ΔC_N, ΔB_M, ΔD_M, are corrections to the previous estimates of A_0, C_0, B_0, A_1, C_1, B_1, D_1, ..., A_N, C_N, B_M, D_M, respectively.

Recognizing from equation (B.5) that the desired result is $(g_k)_{i+1} = 0$ yields an iterative equation of the form:

$$
\begin{aligned}
-(g_k) = \; & \\
& (\partial g_k/\partial A_0)_i \Delta A_0 + (\partial g_k/\partial C_0)_i \Delta C_0 + (\partial g_k/\partial B_0)_i \Delta B_0 + \\
& (\partial g_k/\partial A_1)_i \Delta A_1 + (\partial g_k/\partial C_1)_i \Delta C_1 + (\partial g_k/\partial B_1)_i \Delta B_1 + (\partial g_k/\partial D_1)_i \Delta D_1 + \\
& \ldots\ldots\ldots\ldots + \ldots\ldots\ldots\ldots + \ldots\ldots\ldots\ldots + \ldots\ldots\ldots\ldots + \\
& (\partial g_k/\partial A_N)_i \Delta A_N + (\partial g_k/\partial C_N)_i \Delta C_N + (\partial g_k/\partial B_M)_i \Delta B_M + (\partial g_k/\partial D_M)_i \Delta D_M
\end{aligned} \qquad (B.6)
$$

which can be rewritten in matrix notation as

$$[g] = [c][\Delta] \tag{B.7}$$

where

$$[g]^T = [-g_1, -g_2, \ldots, -g_K]$$

$$[\Delta]^T = [\Delta A_0, \Delta C_0, \Delta B_0, \Delta A_1, \Delta C_1, \Delta B_1, \Delta D_1, \ldots, \Delta A_N, \Delta C_N, \Delta B_M, \Delta D_M]$$

$$[c] = \begin{bmatrix} \partial g_1/\partial A_0 & \partial g_1/\partial C_0 & \partial g_1/\partial B_0 & \partial g_1/\partial A_1 & \cdots & \partial g_1/\partial B_M & \partial g_1/\partial D_M \\ \vdots & \vdots & \vdots & \vdots & & \vdots & \vdots \\ \partial g_K/\partial A_0 & \partial g_K/\partial C_0 & \partial g_K/\partial B_0 & \partial g_K/\partial A_1 & \cdots & \partial g_K/\partial B_M & \partial g_K/\partial D_M \end{bmatrix}$$

$[g]^T$ is the transpose of the matrix $[g]$, and $[\Delta]^T$ is the transpose of the matrix $[\Delta]$.

Since matrix $[c]$ is not square, $K > 2(N+1)+2(M+1)-1$, equation (B.7) has no unique solution. However, it can be shown that a solution in the least-squares sense can be obtained from an auxiliary equation of the form:

$$[\Delta] = [d]^{-1}[c]^T[g] \tag{B.8}$$

where $[d] = [c]^T[c]$ and $[c]^T$ is the transpose of the matrix $[c]$.

Use of an algorithm of this type for isochromatic fringe pattern analysis requires that equation (B.1) be recast in the form:

$$g_k = D_k^{\,2} + T_k^{\,2} - (N_k f_\sigma/2t)^2 = 0 \tag{B.9}$$

where the subscript, 'k', denotes the value of the function at the point in the field having position coordinates (r_k, θ_k), and at which the fringe order is N_k. A total of K such equations are clearly needed, with the total number of data points, K, exceeding the total number of unknown coefficients to be determined, that is, K > 2(N+1)+2(M+1)-1.

B.3 Implementation of the Method

The procedure for determining the best-fit set of coefficients for a given fringe pattern can be summarized as follows:

(a) from the experimental fringe pattern, define a region for data acquisition purposes and select a sufficiently large number of data points with coordinates (r_k, θ_k, N_k), distributed over the entire region;

(b) assume initial values for the unknowns, A_0, C_0, B_0, ..., A_N, C_N, B_M, D_M;

(c) compute the elements of the matrices [g] and [c] for each data point;

(d) compute the matrix [Δ] from equation (B.8);

(e) revise the estimates of the unknowns, i.e.,

$$(A_0)_{i+1} = (A_0)_i + \Delta A_0$$
$$(C_0)_{i+1} = (C_0)_i + \Delta C_0$$

$$(B_0)_{i+1} = (B_0)_i + \Delta B_0$$
$$(A_1)_{i+1} = (A_1)_i + \Delta A_1$$
$$(C_1)_{i+1} = (C_1)_i + \Delta C_1$$
$$(B_1)_{i+1} = (B_1)_i + \Delta B_1$$
$$(D_1)_{i+1} = (D_1)_i + \Delta D_1$$
$$\vdots \qquad \vdots \qquad \vdots$$
$$(A_N)_{i+1} = (A_N)_i + \Delta A_N$$
$$(C_N)_{i+1} = (C_N)_i + \Delta C_N$$
$$(B_M)_{i+1} = (B_M)_i + \Delta B_M$$
$$(D_M)_{i+1} = (D_M)_i + \Delta D_M$$

(f) repeat steps (c), (d), and (e) above, until $[\Delta]$ becomes acceptably small.

Several comments on the implementation of the method are given below. These are based on the experience gained from this and previous studies, and are offered insofar as they may be helpful to other investigators.

First, the total number of data points required, K, must exceed the total number of unknown coefficients to be determined, i.e., K > 2(N+1)+2(M+1)-1. It has generally been found that the algorithm performs well when the degree of redundancy, or overdetermination, exceeds 3 to 4. On the other hand, a degree of redundancy of 10 or greater does not appear to improve the results significantly.

Second, it has been found that analyzing the same data set with sequentially higher order models provides useful information as to the number of coefficients needed to adequately describe the stress state over the region of data acquisition -- this is an important point, since the number of coefficients that must be retained is not generally known **a priori.** Examination of the behavior of the error term, $|\Delta N|$, defined in Chapter 4, and the behavior of the leading coefficients is particularly helpful in this regard, and two illustrative examples have been discussed previously in some detail. It is recommended that the analysis be started with a model of order 2 (retaining terms upto r^0 -- A_0, C_0, B_0) and successively increasing the order of the model by powers of $r^{1/2}$. The analysis can then be started with an initial estimate for A_0 only and the results for the coefficients from the 2nd order model can be used as initial estimates for the 3rd order model, and so on.

Third, the computational procedure is greatly simplified, if it is recognized that the column elements of the matrix [c] are of the form:

$$\partial g_k / \partial A_n = 2D_k(\partial D/\partial A_n)_k + 2T_k(\partial T/\partial A_n)_k$$
$$\partial g_k / \partial C_n = 2D_k(\partial D/\partial C_n)_k + 2T_k(\partial T/\partial C_n)_k$$
$$\partial g_k / \partial B_m = 2D_k(\partial D/\partial B_m)_k + 2T_k(\partial T/\partial B_m)_k$$
$$\partial g_k / \partial D_m = 2D_k(\partial D/\partial D_m)_k + 2T_k(\partial T/\partial D_m)_k$$

Each of the required partial derivatives are then easily obtained in their general form from equations (B.2) and (B.3).

Fourth, it should be recognized that since the leading term, D_0, in the series Y* does not influence the stress components in any way, its inclusion in the formulation detailed above would result in a column with entries identically equal to zero in the matrix [c]. The matrix [d] formed by taking $[c]^T[c]$ would thus be a singular matrix, which cannot be inverted. Some care must therefore be exercised in the logic of the computer program(s) that are used to implement the general solution scheme outlined above.

Finally, the stress field expressions and the formulation of the method have both been given for the general case of a propagating crack under combined opening and shear mode conditions. The same methodology can be used for pure opening mode conditions and for stationary cracks under single or combined modes of loading. For the dynamic opening mode case, the formulation given here can be employed directly, after deleting all references to terms involving C_n and D_m. The total number of unknown coefficients in this case is obviously $(N+1)+(M+1)$. In the case of stationary cracks, the appropriate stress field expressions from Chapter 3 must be used to obtain expressions similar to equations (B.2) and (B.3) before implementation of the method. Note that, while the elastodynamic solutions do reduce to their static counterparts in the limit as the crack speed goes to zero, this limit cannot be obtained computationally by simply specifying a zero crack speed in the dynamic equations.

Implementation of the local collocation method can be performed on either a main-frame or microcomputer system in a straightforward manner. In the present study, a microcomputer-based digitizing system was used to obtain the required data from photographs of the isochromatic fringe patterns to be analyzed. This data was then transferred to a Sperry/1100 main-frame system, on which the analysis algorithms were implemented using BASIC. Listings of sample programs used on the Sperry system for analysis and for reconstruction of the fringe pattern using the best-fit coefficients are given in Appendix C.

APPENDIX C

LISTINGS OF COMPUTER PROGRAMS
USED TO IMPLEMENT THE LOCAL COLLOCATION METHOD
AND TO RECONSTRUCT THE FRINGE PATTERNS FOR A GIVEN COEFFICIENT SET
USING A SPERRY 1100 SERIES MAIN-FRAME COMPUTER SYSTEM

C.1 BASIC Program Listing for Dynamic Mixed-Mode Analysis with K_{II}

```
00100 STRINGS500
00110 P$='*==================================================================*'
00120 U$='      %%          %%%%.%%%         %%.%%%%            %%%.%%%%'
00130 V$=' A% = %%%%%.%%    A%/AO = %%%.%%%      C% = %%%%%.%%    C%/AO = %%%.%%%'
00140 W$=' B% = %%%%%.%%    B%/AO = %%%.%%%      D% = %%%%%.%%    D%/AO = %%%.%%%'
00150 Y$=' ITER. NO.      ERROR      DELTA N (FRGS)   DELTA N (PCT)'
00160 REM PROGRAM TO COMPUTE UPTO A EIGHT PARAMETER (15 COEFFICIENT) MODEL
00170 REM AND OUTPUT THE COEFFICIENTS OF THE SERIES SOLUTION TO THE
00180 REM DYNAMIC MIXED MODE CRACK PROBLEM.
00190 REM PROGRAM USES THE NEWTON-RAPHSON NON-LINEAR LEAST SQUARES
00200 REM TECHNIQUE FOLLOWING THE METHOD DUE TO
00210 REM R. J. SANFORD.
00220 REM UPTO 200 DATA POINTS MAY BE SPECIFIED AND SHOULD BE ENTERED
00230 REM AS DATA STATEMENTS 2500--.
00240 DIM Z(200,3),N(200),R(200),Q(200)
00250 DIM A(15,1),B(15,200),C(200,15),D(15,15),E(15,15),F(15,1),G(200,1)
00260 DIM H(15,1), S(200,15),U(200,15),M(40,4),T(16)
00270 INPUT K1,K2,K3,K4,K5,K6,K7,K8,CO,C1,C2
00280 READ Z$
00290 PRINT Z$
00300 PRINT 'NUMBER OF DATA POINTS=';K1
00310 PRINT 'LOWEST ORDER MODEL=';K2
00320 PRINT 'HIGHEST ORDER MODEL=';K3
00330 PRINT 'NUMBER OF ITERATIONS=';K4
00340 PRINT 'MATERIAL FRINGE CONSTANT=';K5
00350 PRINT 'MODEL THICKNESS=';K6
00360 PRINT 'INITIAL ESTIMATE OF K-I =';K7
00370 PRINT 'INITIAL ESTIMATE OF K-II =';K8
00380 PRINT 'CRACK SPEED (INCHES/SEC)=';CO
00390 PRINT 'P-WAVE SPEED (INCHES/SEC)=';C1
00400 PRINT 'S-WAVE SPEED (INCHES/SEC)=';C2
00410 PRINT 'C/C1=';CO/C1;'C/C2=';CO/C2
00420 C3=SQR(1.0-(CO/C1)**2)
00430 C4=SQR(1.0-(CO/C2)**2)
00440 C5=(1.0+C4**2)/(4.0*C3*C4 - (1.0+C4**2)**2)
00450 C6=2.0*C4/(4.0*C3*C4 - (1.0+C4**2)**2)
00460 C7=1.0+2.0*C3**2-C4**2
00470 C8=4.0*C3*C4/(1.0+C4**2)
00480 C9=1.0+C4**2
00490 D1=((1.0+C4**2)**2)/2.0/C4
00500 MAT Z=ZER(K1,3)
00510 MAT N=ZER(K1)
00520 MAT Q=ZER(K1)
00530 MAT R=ZER(K1)
00540 MAT S=ZER(K1,2*K3-1)
00550 MAT U=ZER(K1,2*K3-1)
00560 MAT READ Z
00570 N1=0
00580 FOR J1=1 TO K1
00590 R(J1)=Z(J1,1)
00600 Q(J1)=Z(J1,2)
00610 N(J1)=Z(J1,3)
00620 N1=N1+N(J1)
00630 NEXT J1
00640 FOR J2=1 TO K1
00650 T=Q(J2)*3.141592654/180.0
00660 R=R(J2)
00670 X1=R*COS(T)
00680 X2=X1
00690 Y1=R*SIN(T)*C3
00700 Y2=R*SIN(T)*C4
00710 R1=SQR(X1**2+Y1**2)
00720 R2=SQR(X2**2+Y2**2)
00730 IF X1 >= 0 THEN 740 ELSE 770
00740 T1=ATN(Y1/X1)
00750 T2=ATN(Y2/X2)
00760 GO TO 830
00770 IF Y1>= 0 THEN 780 ELSE 810
00780 T1=ATN(Y1/X1)+3.141592654
00790 T2=ATN(Y2/X2)+3.141592654
00800 GO TO 830
00810 T1=ATN(Y1/X1)-3.141592654
00820 T2=ATN(Y2/X2)-3.141592654
00830 REM
00840 FOR J3=1 TO K3
00850 IF J3 <= 2 THEN 860 ELSE 890
00860 J7=2*J3-1
00870 J8=J7+1
00880 GO TO 910
00890 J7=2*J3-2
00900 J8=J7+1
00910 J5=(J3-2)/2
00920 P1=R1**J5
00930 P2=R2**J5
00940 S1=COS(J5*T1)
00950 S2=COS(J5*T2)
00960 U1=SIN(J5*T1)
00970 U2=SIN(J5*T2)
00980 J4=INP(J3/2)*2
00990 IF J4=J3 THEN 1050 ELSE 1000
01000 S(J2,J7)=0.5*C5*(-(C9+C7)*P1*S1 + 2.0*C8*P2*S2)
```

```
01010 U(J2,J7)=C5*(-2.0*C3*P1*U1 + 2.0*C3*P2*U2)
01020 S(J2,J8)=0.5*C6*(-(C9+C7)*P1*U1 + 2.0*C9*P2*U2)
01030 U(J2,J8)=-C6*(-2.0*C3*P1*S1 + D1*P2*S2)
01040 GO TO 1100
01050 S(J2,J7)=0.5*C5*(-(C9+C7)*P1*S1 + 2.0*C9*P2*S2)
01060 U(J2,J7)=C5*(-2.0*C3*P1*U1 + D1*P2*U2)
01070 IF J3=2 THEN 1100 ELSE 1080
01080 S(J2,J8)=0.5*C6*(-(C9+C7)*P1*U1 + 2.0*C8*P2*U2)
01090 U(J2,J8)=-C6*(-2.0*C3*P1*S1 + 2.0*C3*P2*S2)
01100 NEXT J3
01110 NEXT J2
01120 PRINT P$
01130 PRINT K2;'PARAMETER MODEL -- DYNAMIC MIXED-MODE SOLUTION'
01140 PRINT '  ';Z$
01150 PRINT P$
01160 PRINT
01170 IF I3=K4 THEN 1190 ELSE 1180
01180 IF A(1,1)=0 THEN 1190 ELSE 1220
01190 MAT A = ZER(2*K2-1,1)
01200 A(1,1)=K7*K6/K5/SQR(2*3.141592654)
01210 A(2,1)=K8*K6/K5/SQR(2*3.141592654)
01220 MAT A=DIM(2*K2-1,1)
01230 A(2*K2-1,1)=0
01240 MAT B = ZER(2*K2-1,K1)
01250 MAT C = ZER(K1,2*K2-1)
01260 MAT D = ZER(2*K2-1,2*K2-1)
01270 MAT E = ZER(2*K2-1,2*K2-1)
01280 MAT F = ZER(2*K2-1,1)
01290 MAT G = ZER(K1,1)
01300 MAT H = ZER(2*K2-1,1)
01310 MAT M = ZER(K4,4)
01320 MAT T = ZER(2*K2)
01330 N8=N1/K1
01340 REM
01350 REM BEGIN ITERATIVE SOLUTION
01360 REM
01370 PRINT ' AVERAGE INPUT FRINGE ORDER='; N8
01380 PRINT
01390 PRINT Y$
01400 FOR I3=1 TO K4
01410 E1=0
01420 N3=0
01430 FOR I4=1 TO K1
01440 F1=0
01450 F2=0
01460 F3=0
01470 F4=0
01480 FOR I5=1 TO K2
01490 IF I5 <= 2 THEN 1500 ELSE 1530
01500 I7=2*I5-1
01510 I8=I7+1
01520 GO TO 1550
01530 I7=2*I5-2
01540 I8=I7+1
01550 F1=F1+A(I7,1)*S(I4,I7)
01560 F2=F2+A(I7,1)*U(I4,I7)
01570 IF I5 = 2 THEN 1600 ELSE 1580
01580 F3=F3+A(I8,1)*S(I4,I8)
01590 F4=F4+A(I8,1)*U(I4,I8)
01600 NEXT I5
01610 G(I4,1)=((N(I4)/2)**2)-(F1+F3)**2-(F2+F4)**2
01620 E1=E1+G(I4,1)**2
01630 N4=2*SQR((F1+F3)**2+(F2+F4)**2)
01640 N3=N3+ABS(N(I4)-N4)
01650 FOR I6=1 TO K2
01660 IF I6 <= 2 THEN 1670 ELSE 1700
01670 I7=2*I6-1
01680 I8=I7+1
01690 GO TO 1720
01700 I7=2*I6-2
01710 I8=I7+1
01720 C(I4,I7)=2*(F1+F3)*S(I4,I7) + 2*(F2+F4)*U(I4,I7)
01730 IF I6 = 2 THEN 1750 ELSE 1740
01740 C(I4,I8)=2*(F1+F3)*S(I4,I8) + 2*(F2+F4)*U(I4,I8)
01750 NEXT I6
01760 NEXT I4
01770 MAT B=TRN(C)
01780 MAT D=B*C
01790 MAT E=INV(D)
01800 MAT F=B*G
01810 MAT H=E*F
01820 MAT A=A+H
01830 N7=N3/K1
01840 M(I3,1)=I3
01850 M(I3,2)=E1
01860 M(I3,3)=N7
01870 M(I3,4)=N7/N8*100
01880 IF I3=1 THEN 1910 ELSE 1890
01890 J1=ABS(1-M(I3,2)/M(I3-1,2))
01900 IF J1<=.002 THEN 1930 ELSE 1910
```

```
01910 NEXT I3
01920 I3=I3-1
01930 FOR I4=1 TO I3
01940 PRINT IN IMAGE U$: M(I4,1),M(I4,2),M(I4,3),M(I4,4)
01950 NEXT I4
01960 PRINT
01970 PRINT
01980 T(1)=A(1,1)
01990 T(2)=A(2,1)
02000 T(3)=A(3,1)
02010 T(4)=0
02020 IF K2 >= 3 THEN 2030 ELSE 2070
02030 FOR I6=3 TO K2
02040 T(2*I6-1)=A(2*I6-2,1)
02050 T(2*I6)=A(2*I6-1,1)
02060 NEXT I6
02070 FOR I7=1 TO K2
02080 I1=(I7-1)/2
02090 I2=I7/2-1
02100 I3=K5/K6
02110 I8=2*I7-1
02120 I9=2*I7
02130 IF I7 = INP(I7/2)*2 THEN 2160 ELSE 2140
02140 PRINT IN IMAGE V$: I1,T(I8)*I3,I1,T(I8)/T(1),I1,T(I9)*I3,I1,T(I9)/T(1)
02150 GO TO 2170
02160 PRINT IN IMAGE W$: I2,T(I8)*I3,I2,T(I8)/T(1),I2,T(I9)*I3,I2,T(I9)/T(1)
02170 NEXT I7
02180 PRINT
02190 PRINT P$
02200 K2=K2+1
02210 IF K2 <= K3 THEN GO TO 1130
99999 END
```

C.2 BASIC Program Listing for Dynamic Mixed-Mode Analysis with $K_{II} \equiv 0$

```
00100 STRINGS500
00110 P$='*==================================================================*'
00120 U$='    %%          %%%%.%%%          %%.%%%%              %%%.%%%%'
00130 V$=' A% = %%%%%.%%    A%/AO = %%%.%%%          C% = %%%%%.%%    C%/AO = %%%.%%%'
00140 W$=' B% = %%%%%.%%    B%/AO = %%%.%%%          D% = %%%%%.%%    D%/AO = %%%.%%%'
00150 Y$=' ITER. NO.      ERROR      DELTA N (FRGS)   DELTA N (PCT)'
00160 REM PROGRAM TO COMPUTE UPTO A EIGHT PARAMETER (14 COEFFICIENT) MODEL
00170 REM AND OUTPUT THE COEFFICIENTS OF THE SERIES SOLUTION TO THE
00180 REM DYNAMIC MIXED MODE CRACK PROBLEM; WITH K-II FORCED TO BE ZERO.
00190 REM PROGRAM USES THE NEWTON-RAPHSON NON-LINEAR LEAST SQUARES
00200 REM TECHNIQUE FOLLOWING THE METHOD DUE TO
00210 REM R. J. SANFORD.
00220 REM UPTO 200 DATA POINTS MAY BE SPECIFIED AND SHOULD BE ENTERED
00230 REM AS DATA STATEMENTS 2500--.
00240 DIM Z(200,3),N(200),R(200),Q(200)
00250 DIM A(14,1),B(14,200),C(200,14),D(14,14),E(14,14),F(14,1),G(200,1)
00260 DIM H(14,1),  S(200,14),U(200,14),M(40,4),T(16)
00270 INPUT K1,K2,K3,K4,K5,K6,K7,K8,C0,C1,C2
00280 READ Z$
00290 PRINT Z$
00300 PRINT 'NUMBER OF DATA POINTS=';K1
00310 PRINT 'LOWEST ORDER MODEL=';K2
00320 PRINT 'HIGHEST ORDER MODEL=';K3
00330 PRINT 'NUMBER OF ITERATIONS=';K4
00340 PRINT 'MATERIAL FRINGE CONSTANT=';K5
00350 PRINT 'MODEL THICKNESS=';K6
00360 PRINT 'INITIAL ESTIMATE OF K-I =';K7
00370 PRINT 'INITIAL ESTIMATE OF K-II =';K8
00380 PRINT 'CRACK SPEED (INCHES/SEC)=';C0
00390 PRINT 'P-WAVE SPEED (INCHES/SEC)=';C1
00400 PRINT 'S-WAVE SPEED (INCHES/SEC)=';C2
00410 PRINT 'C/C1=';C0/C1;'C/C2=';C0/C2
00420 C3=SQR(1.0-(C0/C1)**2)
00430 C4=SQR(1.0-(C0/C2)**2)
00440 C5=(1.0+C4**2)/(4.0*C3*C4 - (1.0+C4**2)**2)
00450 C6=2.0*C4/(4.0*C3*C4 - (1.0+C4**2)**2)
00460 C7=1.0+2.0*C3**2-C4**2
00470 C8=4.0*C3*C4/(1.0+C4**2)
00480 C9=1.0+C4**2
00490 D1=((1.0+C4**2)**2)/2.0/C4
00500 MAT Z=ZER(K1,3)
00510 MAT N=ZER(K1)
00520 MAT Q=ZER(K1)
00530 MAT R=ZER(K1)
00540 MAT S=ZER(K1,2*K3-2)
00550 MAT U=ZER(K1,2*K3-2)
00560 MAT READ Z
00570 N1=0
00580 FOR J1=1 TO K1
00590 R(J1)=Z(J1,1)
00600 Q(J1)=Z(J1,2)
00610 N(J1)=Z(J1,3)
00620 N1=N1+N(J1)
00630 NEXT J1
00640 FOR J2=1 TO K1
00650 T=Q(J2)*3.141592654/180.0
00660 R=R(J2)
00670 X1=R*COS(T)
00680 X2=X1
00690 Y1=R*SIN(T)*C3
00700 Y2=R*SIN(T)*C4
00710 R1=SQR(X1**2+Y1**2)
00720 R2=SQR(X2**2+Y2**2)
00730 IF X1 >= 0 THEN 740 ELSE 770
00740 T1=ATN(Y1/X1)
00750 T2=ATN(Y2/X2)
00760 GO TO 830
00770 IF Y1>= 0 THEN 780 ELSE 810
00780 T1=ATN(Y1/X1)+3.141592654
00790 T2=ATN(Y2/X2)+3.141592654
00800 GO TO 830
00810 T1=ATN(Y1/X1)-3.141592654
00820 T2=ATN(Y2/X2)-3.141592654
00830 REM
00840 FOR J3=1 TO K3
00850 IF J3 = 1 THEN 860 ELSE 880
00860 J7=2*J3-1
00870 GO TO 930
00880 IF J3 = 2 THEN 890 ELSE 910
00890 J7=2*J3-2
00900 GO TO 930
00910 J7=2*J3-3
00920 J8=J7+1
00930 J5=(J3-2)/2
00940 P1=R1**J5
00950 P2=R2**J5
00960 S1=COS(J5*T1)
00970 S2=COS(J5*T2)
00980 U1=SIN(J5*T1)
00990 U2=SIN(J5*T2)
01000 J4=INP(J3/2)*2
```

```
01010 IF J4=J3 THEN 1080 ELSE 1020
01020 S(J2, J7)=0.5*C5*(-(C9+C7)*P1*S1 + 2.0*C8*P2*S2)
01030 U(J2, J7)=C5*(-2.0*C3*P1*U1 + 2.0*C3*P2*U2)
01040 IF J3 = 1 THEN 1070 ELSE 1050
01050 S(J2, J8)=0.5*C6*(-(C9+C7)*P1*U1 + 2.0*C9*P2*U2)
01060 U(J2, J8)=-C6*(-2.0*C3*P1*S1 + D1*P2*S2)
01070 GO TO 1130
01080 S(J2, J7)=0.5*C5*(-(C9+C7)*P1*S1 + 2.0*C9*P2*S2)
01090 U(J2, J7)=C5*(-2.0*C3*P1*U1 + D1*P2*U2)
01100 IF J3=2 THEN 1130 ELSE 1110
01110 S(J2, J8)=0.5*C6*(-(C9+C7)*P1*U1 + 2.0*C8*P2*U2)
01120 U(J2, J8)=-C6*(-2.0*C3*P1*S1 + 2.0*C3*P2*S2)
01130 NEXT J3
01140 NEXT J2
01150 PRINT P$
01160 PRINT K2; 'PARAMETER MODEL -- DYNAMIC MIXED-MODE SOLUTION -- K-II = 0'
01170 PRINT ' '; Z$
01180 PRINT P$
01190 PRINT
01200 IF I3=K4 THEN 1220 ELSE 1210
01210 IF A(1, 1)=0 THEN 1220 ELSE 1240
01220 MAT A = ZER(2*K2-2, 1)
01230 A(1, 1)=K7*K6/K5/SQR(2*3.141592654)
01240 MAT A=DIM(2*K2-2, 1)
01250 A(2*K2-2, 1)=0
01260 MAT B = ZER(2*K2-2, K1)
01270 MAT C = ZER(K1, 2*K2-2)
01280 MAT D = ZER(2*K2-2, 2*K2-2)
01290 MAT E = ZER(2*K2-2, 2*K2-2)
01300 MAT F = ZER(2*K2-2, 1)
01310 MAT G = ZER(K1, 1)
01320 MAT H = ZER(2*K2-2, 1)
01330 MAT M = ZER(K4, 4)
01340 MAT T = ZER(2*K2)
01350 N8=N1/K1
01360 REM
01370 REM BEGIN ITERATIVE SOLUTION
01380 REM
01390 PRINT ' AVERAGE INPUT FRINGE ORDER='; N8
01400 PRINT
01410 PRINT Y$
01420 FOR I3=1 TO K4
01430 E1=0
01440 N3=0
01450 FOR I4=1 TO K1
01460 F1=0
01470 F2=0
01480 F3=0
01490 F4=0
01500 FOR I5=1 TO K2
01510 IF I5 = 1 THEN 1520 ELSE 1540
01520 I7=2*I5-1
01530 GO TO 1590
01540 IF I5 = 2 THEN 1550 ELSE 1570
01550 I7=2*I5-2
01560 GO TO 1590
01570 I7=2*I5-3
01580 I8=I7+1
01590 F1=F1+A(I7, 1)*S(I4, I7)
01600 F2=F2+A(I7, 1)*U(I4, I7)
01610 IF I5 <= 2 THEN 1640 ELSE 1620
01620 F3=F3+A(I8, 1)*S(I4, I8)
01630 F4=F4+A(I8, 1)*U(I4, I8)
01640 NEXT I5
01650 G(I4, 1)=((N(I4)/2)**2)-(F1+F3)**2-(F2+F4)**2
01660 E1=E1+G(I4, 1)**2
01670 N4=2*SQR((F1+F3)**2+(F2+F4)**2)
01680 N3=N3+ABS(N(I4)-N4)
01690 FOR I6=1 TO K2
01700 IF I6 = 1 THEN 1710 ELSE 1730
01710 I7=2*I6-1
01720 GO TO 1780
01730 IF I6 = 2 THEN 1740 ELSE 1760
01740 I7=2*I6-2
01750 GO TO 1780
01760 I7=2*I6-3
01770 I8=I7+1
01780 C(I4, I7)=2*(F1+F3)*S(I4, I7) + 2*(F2+F4)*U(I4, I7)
01790 IF I6 <= 2 THEN 1810 ELSE 1800
01800 C(I4, I8)=2*(F1+F3)*S(I4, I8) + 2*(F2+F4)*U(I4, I8)
01810 NEXT I6
01820 NEXT I4
01830 MAT B=TRN(C)
01840 MAT D=B*C
01850 MAT E=INV(D)
01860 MAT F=B*G
01870 MAT H=E*F
01880 MAT A=A+H
01890 N7=N3/K1
01900 M(I3, 1)=I3
```

```
01910 M(I3,2)=E1
01920 M(I3,3)=N7
01930 M(I3,4)=N7/N8*100
01940 IF I3=1 THEN 1970 ELSE 1950
01950 J1=ABS(1-M(I3,2)/M(I3-1,2))
01960 IF J1<=.002 THEN 1990 ELSE 1970
01970 NEXT I3
01980 I3=I3-1
01990 FOR I4=1 TO I3
02000 PRINT IN IMAGE U$: M(I4,1),M(I4,2),M(I4,3),M(I4,4)
02010 NEXT I4
02020 PRINT
02030 PRINT
02040 T(1)=A(1,1)
02050 T(2)=0
02060 T(3)=A(2,1)
02070 T(4)=0
02080 IF K2 >= 3 THEN 2090 ELSE 2130
02090 FOR I6=3 TO K2
02100 T(2*I6-1)=A(2*I6-3,1)
02110 T(2*I6)=A(2*I6-2,1)
02120 NEXT I6
02130 FOR I7=1 TO K2
02140 I1=(I7-1)/2
02150 I2=I7/2-1
02160 I3=K5/K6
02170 I8=2*I7-1
02180 I9=2*I7
02190 IF I7 = INP(I7/2)*2 THEN 2220 ELSE 2200
02200 PRINT IN IMAGE V$: I1,T(I8)*I3,I1,T(I8)/T(1),I1,T(I9)*I3,I1,T(I9)/T(1)
02210 GO TO 2230
02220 PRINT IN IMAGE W$: I2,T(I8)*I3,I2,T(I8)/T(1),I2,T(I9)*I3,I2,T(I9)/T(1)
02230 NEXT I7
02240 PRINT
02250 PRINT P$
02260 K2=K2+1
02270 IF K2 <= K3 THEN GO TO 1160
99999 END
```

C.3 Sample Data Set from Frame 11, Experiment 12, Curving Crack

```
2500 REM DATA FROM EXPT-12, FRAME 11, ARUN SHUKLA
2501 DATA DATA FROM 1/2 INCH RADIUS; EXPT. 12; FRAME 11
2502 DATA 0.500, 6.17, 0.5
2503 DATA 0.448, 5.70, 0.5
2504 DATA 0.369, 5.56, 0.5
2505 DATA 0.253, 4.42, 0.5
2506 DATA 0.232, 15.7, 0.5
2507 DATA 0.312, 20.4, 0.5
2508 DATA 0.397, 24.6, 0.5
2509 DATA 0.497, 28.2, 0.5
2510 DATA 0.498, 47.7, 1.5
2511 DATA 0.429, 45.3, 1.5
2512 DATA 0.344, 42.3, 1.5
2513 DATA 0.250, 37.6, 1.5
2515 DATA 0.209, -18.5, 1.5
2516 DATA 0.290, -21.6, 1.5
2517 DATA 0.385, -25.8, 1.5
2518 DATA 0.487, -29.6, 1.5
2519 DATA 0.445, -151.8, 1.5
2520 DATA 0.364, -157.5, 1.5
2521 DATA 0.273, -160.1, 1.5
2522 DATA 0.181, -165.2, 1.5
2523 DATA 0.491, 147.2, 1.5
2524 DATA 0.427, 149.8, 1.5
2525 DATA 0.341, 152.4, 1.5
2526 DATA 0.231, 156.4, 1.5
2527 DATA 0.233, 170.6, 0.5
2528 DATA 0.328, 167.9, 0.5
2529 DATA 0.412, 166.4, 0.5
2530 DATA 0.495, 165.9, 0.5
2532 DATA 0.268, 57.0, 2.5
2533 DATA 0.355, 63.2, 2.5
2534 DATA 0.488, 70.1, 2.5
2535 DATA 0.491, 124.6, 2.5
2536 DATA 0.414, 129.2, 2.5
2537 DATA 0.322, 133.6, 2.5
2538 DATA 0.252, 139.1, 2.5
2541 DATA 0.187, -45.2, 2.5
2542 DATA 0.241, -55.9, 2.5
2543 DATA 0.272, -67.1, 2.5
2544 DATA 0.285, -84.7, 2.5
2545 DATA 0.283, -103.4, 2.5
2546 DATA 0.282, -120.2, 2.5
2547 DATA 0.239, -135.5, 2.5
2548 DATA 0.174, -146.6, 2.5
2550 DATA 0.227, 72.7, 3.5
2551 DATA 0.286, 83.8, 3.5
2552 DATA 0.316, 94.7, 3.5
2553 DATA 0.294, 108.7, 3.5
2554 DATA 0.248, 119.0, 3.5
2557 DATA 0.177, -98.5, 3.5
2558 DATA 0.165, -80.6, 3.5
```

C.4 Sample Output for Dynamic Mixed-Mode Analysis Retaining K_{II}

```
DATA FROM 1/2 INCH RADIUS; EXPT. 12; FRAME 11; URI -- 5/85
NUMBER OF DATA POINTS= 50
LOWEST ORDER MODEL= 2
HIGHEST ORDER MODEL= 8
NUMBER OF ITERATIONS= 40
MATERIAL FRINGE CONSTANT= 150
MODEL THICKNESS= .413
INITIAL ESTIMATE OF K-I = 1000
INITIAL ESTIMATE OF K-II = 100
CRACK SPEED (INCHES/SEC)= 1
P-WAVE SPEED (INCHES/SEC)= 5.07
S-WAVE SPEED (INCHES/SEC)= 3
C/C1= .19723866 C/C2= .33333333
*=====================================================================*
 2 PARAMETER MODEL -- DYNAMIC MIXED-MODE SOLUTION
 DATA FROM 1/2 INCH RADIUS; EXPT. 12; FRAME 11; URI -- 5/85
*=====================================================================*

 AVERAGE INPUT FRINGE ORDER= 1.84

 ITER. NO.       ERROR      DELTA N (FRGS)   DELTA N (PCT)
     1          32.704          .6504           35.3452
     2          10.374          .3073           16.7034
     3           7.061          .2741           14.8992
     4           7.049          .2723           14.7964


 A0 =     566.83    A0/A0 =    1.000     C0 =    -12.67    C0/A0 =    -.022
 B0 =      27.98    B0/A0 =     .049     D0 =      0.00    D0/A0 =    0.000

*=====================================================================*
 3 PARAMETER MODEL -- DYNAMIC MIXED-MODE SOLUTION
 DATA FROM 1/2 INCH RADIUS; EXPT. 12; FRAME 11; URI -- 5/85
*=====================================================================*

 AVERAGE INPUT FRINGE ORDER= 1.84

 ITER. NO.       ERROR      DELTA N (FRGS)   DELTA N (PCT)
     1           7.049          .2721           14.7885
     2            .289          .0742            4.0299
     3            .163          .0555            3.0170
     4            .163          .0555            3.0175


 A0 =     571.43    A0/A0 =    1.000     C0 =    -16.48    C0/A0 =    -.029
 B0 =      40.79    B0/A0 =     .071     D0 =      0.00    D0/A0 =    0.000
 A1 =     -52.90    A1/A0 =    -.093     C1 =   -120.34    C1/A0 =    -.211

*=====================================================================*
 4 PARAMETER MODEL -- DYNAMIC MIXED-MODE SOLUTION
 DATA FROM 1/2 INCH RADIUS; EXPT. 12; FRAME 11; URI -- 5/85
*=====================================================================*

 AVERAGE INPUT FRINGE ORDER= 1.84

 ITER. NO.       ERROR      DELTA N (FRGS)   DELTA N (PCT)
     1            .163          .0555            3.0173
     2            .051          .0292            1.5876
     3            .050          .0295            1.6015
     4            .050          .0295            1.6035


 A0 =     567.80    A0/A0 =    1.000     C0 =     -6.54    C0/A0 =    -.012
 B0 =      32.70    B0/A0 =     .058     D0 =      0.00    D0/A0 =    0.000
 A1 =     -49.30    A1/A0 =    -.087     C1 =   -149.51    C1/A0 =    -.263
 B1 =       2.80    B1/A0 =     .005     D1 =    120.36    D1/A0 =     .212

*=====================================================================*
 5 PARAMETER MODEL -- DYNAMIC MIXED-MODE SOLUTION
 DATA FROM 1/2 INCH RADIUS; EXPT. 12; FRAME 11; URI -- 5/85
*=====================================================================*

 AVERAGE INPUT FRINGE ORDER= 1.84

 ITER. NO.       ERROR      DELTA N (FRGS)   DELTA N (PCT)
     1            .050          .0295            1.6034
     2            .043          .0273            1.4847
     3            .043          .0272            1.4799


 A0 =     567.11    A0/A0 =    1.000     C0 =     -6.86    C0/A0 =    -.012
 B0 =      32.98    B0/A0 =     .058     D0 =      0.00    D0/A0 =    0.000
 A1 =     -13.93    A1/A0 =    -.025     C1 =   -148.79    C1/A0 =    -.262
 B1 =     -17.89    B1/A0 =    -.032     D1 =    123.95    D1/A0 =     .219
 A2 =      42.88    A2/A0 =     .076     C2 =      5.55    C2/A0 =     .010
```

```
*==========================================================================*
6 PARAMETER MODEL -- DYNAMIC MIXED-MODE SOLUTION
DATA FROM 1/2 INCH RADIUS; EXPT. 12; FRAME 11; URI -- 5/85
*==========================================================================*

AVERAGE INPUT FRINGE ORDER= 1.84

ITER. NO.      ERROR      DELTA N (FRGS)   DELTA N (PCT)
   1           .043         .0272            1.4802
   2           .039         .0265            1.4424
   3           .039         .0262            1.4238

AO =    569.05    AO/AO =   1.000     CO =     -6.83    CO/AO =   -.012
BO =     37.13    BO/AO =    .065     DO =      0.00    DO/AO =   0.000
A1 =    -61.41    A1/AO =   -.108     C1 =   -149.55    C1/AO =   -.263
B1 =      1.49    B1/AO =    .003     D1 =    106.95    D1/AO =    .188
A2 =      6.47    A2/AO =    .011     C2 =     22.56    C2/AO =    .040
B2 =     14.11    B2/AO =    .025     D2 =    -35.53    D2/AO =   -.062

*==========================================================================*
7 PARAMETER MODEL -- DYNAMIC MIXED-MODE SOLUTION
DATA FROM 1/2 INCH RADIUS; EXPT. 12; FRAME 11; URI -- 5/85
*==========================================================================*

AVERAGE INPUT FRINGE ORDER= 1.84

ITER. NO.      ERROR      DELTA N (FRGS)   DELTA N (PCT)
   1           .039         .0262            1.4249
   2           .030         .0260            1.4134
   3           .029         .0240            1.3023
   4           .029         .0242            1.3139

AO =    568.64    AO/AO =   1.000     CO =     -5.04    CO/AO =   -.009
BO =     44.45    BO/AO =    .078     DO =      0.00    DO/AO =   0.000
A1 =   -151.08    A1/AO =   -.266     C1 =   -149.08    C1/AO =   -.262
B1 =     30.15    B1/AO =    .053     D1 =     93.36    D1/AO =    .164
A2 =     17.19    A2/AO =    .030     C2 =     55.48    C2/AO =    .098
B2 =    -48.47    B2/AO =   -.085     D2 =   -108.08    D2/AO =   -.190
A3 =     95.21    A3/AO =    .167     C3 =     54.53    C3/AO =    .096

*==========================================================================*
8 PARAMETER MODEL -- DYNAMIC MIXED-MODE SOLUTION
DATA FROM 1/2 INCH RADIUS; EXPT. 12; FRAME 11; URI -- 5/85
*==========================================================================*

AVERAGE INPUT FRINGE ORDER= 1.84

ITER. NO.      ERROR      DELTA N (FRGS)   DELTA N (PCT)
   1           .029         .0241            1.3122
   2           .028         .0220            1.1954
   3           .028         .0218            1.1845

AO =    568.68    AO/AO =   1.000     CO =     -5.31    CO/AO =   -.009
BO =     44.13    BO/AO =    .078     DO =      0.00    DO/AO =   0.000
A1 =   -142.57    A1/AO =   -.251     C1 =   -153.29    C1/AO =   -.270
B1 =     23.48    B1/AO =    .041     D1 =    107.00    D1/AO =    .188
A2 =     26.41    A2/AO =    .046     C2 =     53.45    C2/AO =    .094
B2 =    -37.56    B2/AO =   -.066     D2 =   -134.33    D2/AO =   -.236
A3 =     50.54    A3/AO =    .089     C3 =     83.02    C3/AO =    .146
B3 =     32.15    B3/AO =    .057     D3 =    -23.40    D3/AO =   -.041

*==========================================================================*
```

C.5 Sample Output for Dynamic Mixed-Mode Analysis with $K_{II} \equiv 0$

```
DATA FROM 1/2 INCH RADIUS; EXPT. 12; FRAME 11; URI -- 5/85
NUMBER OF DATA POINTS= 50
LOWEST ORDER MODEL= 2
HIGHEST ORDER MODEL= 8
NUMBER OF ITERATIONS= 40
MATERIAL FRINGE CONSTANT= 150
MODEL THICKNESS= .413
INITIAL ESTIMATE OF K-I = 1000
INITIAL ESTIMATE OF K-II = 100
CRACK SPEED (INCHES/SEC)= 1
P-WAVE SPEED (INCHES/SEC)= 5.07
S-WAVE SPEED (INCHES/SEC)= 3
C/C1= .19723866 C/C2= .33333333
*==========================================================================*
 2 PARAMETER MODEL -- DYNAMIC MIXED-MODE SOLUTION -- K-II = 0
 DATA FROM 1/2 INCH RADIUS; EXPT. 12; FRAME 11; URI -- 5/85
*==========================================================================*

 AVERAGE INPUT FRINGE ORDER= 1.84

 ITER. NO.      ERROR     DELTA N (FRGS)    DELTA N (PCT)
    1          30.932        .5949            32.3310
    2           8.806        .2747            14.9320
    3           7.354        .2672            14.5231
    4           7.352        .2680            14.5631


 AO =    567.79    AO/AO =    1.000     CO =     0.00    CO/AO =    0.000
 BO =     28.78    BO/AO =     .051     DO =     0.00    DO/AO =    0.000

*==========================================================================*
 3 PARAMETER MODEL -- DYNAMIC MIXED-MODE SOLUTION -- K-II = 0
 DATA FROM 1/2 INCH RADIUS; EXPT. 12; FRAME 11; URI -- 5/85
*==========================================================================*

 AVERAGE INPUT FRINGE ORDER= 1.84

 ITER. NO.      ERROR     DELTA N (FRGS)    DELTA N (PCT)
    1           7.352        .2680            14.5641
    2            .830        .1053             5.7224
    3            .712        .1049             5.6995
    4            .712        .1049             5.7031


 AO =    570.46    AO/AO =    1.000     CO =     0.00    CO/AO =    0.000
 BO =     37.51    BO/AO =     .066     DO =     0.00    DO/AO =    0.000
 A1 =    -45.64    A1/AO =    -.080     C1 =  -118.00    C1/AO =    -.207

*==========================================================================*
 4 PARAMETER MODEL -- DYNAMIC MIXED-MODE SOLUTION -- K-II = 0
 DATA FROM 1/2 INCH RADIUS; EXPT. 12; FRAME 11; URI -- 5/85
*==========================================================================*

 AVERAGE INPUT FRINGE ORDER= 1.84

 ITER. NO.      ERROR     DELTA N (FRGS)    DELTA N (PCT)
    1            .712        .1049             5.7031
    2            .081        .0400             2.1744
    3            .078        .0406             2.2049
    4            .078        .0406             2.2074


 AO =    565.28    AO/AO =    1.000     CO =     0.00    CO/AO =    0.000
 BO =     27.43    BO/AO =     .049     DO =     0.00    DO/AO =    0.000
 A1 =    -41.83    A1/AO =    -.074     C1 =  -161.99    C1/AO =    -.287
 B1 =      4.20    B1/AO =     .007     D1 =   172.60    D1/AO =     .305

*==========================================================================*
 5 PARAMETER MODEL -- DYNAMIC MIXED-MODE SOLUTION -- K-II = 0
 DATA FROM 1/2 INCH RADIUS; EXPT. 12; FRAME 11; URI -- 5/85
*==========================================================================*

 AVERAGE INPUT FRINGE ORDER= 1.84

 ITER. NO.      ERROR     DELTA N (FRGS)    DELTA N (PCT)
    1            .078        .0406             2.2075
    2            .069        .0438             2.3784
    3            .068        .0449             2.4411
    4            .068        .0451             2.4537

 AO =    559.39    AO/AO =    1.000     CO =     0.00    CO/AO =    0.000
 BO =     13.26    BO/AO =     .024     DO =     0.00    DO/AO =    0.000
 A1 =    118.13    A1/AO =     .211     C1 =  -178.60    C1/AO =    -.319
 B1 =    -40.51    B1/AO =    -.072     D1 =   253.52    D1/AO =     .453
 A2 =     63.81    A2/AO =     .114     C2 =   -20.52    C2/AO =    -.037
```

```
*==========================================================================*
 6 PARAMETER MODEL -- DYNAMIC MIXED-MODE SOLUTION -- K-II = 0
 DATA FROM 1/2 INCH RADIUS; EXPT. 12; FRAME 11; URI -- 5/85
*==========================================================================*

 AVERAGE INPUT FRINGE ORDER= 1.84

 ITER. NO.      ERROR      DELTA N (FRGS)   DELTA N (PCT)
     1           .068         .0452            2.4561
     2           .065         .0447            2.4312
     3           .065         .0445            2.4178


 A0 =    561.08   A0/A0 =    1.000    C0 =       0.00   C0/A0 =    0.000
 B0 =     16.06   B0/A0 =     .029    D0 =       0.00   D0/A0 =    0.000
 A1 =     81.83   A1/A0 =     .146    C1 =    -180.38   C1/A0 =    -.321
 B1 =    -24.18   B1/A0 =    -.043    D1 =     242.26   D1/A0 =     .432
 A2 =     30.60   A2/A0 =     .055    C2 =      -7.37   C2/A0 =    -.013
 B2 =     13.61   B2/A0 =     .024    D2 =     -29.80   D2/A0 =    -.053

*==========================================================================*
 7 PARAMETER MODEL -- DYNAMIC MIXED-MODE SOLUTION -- K-II = 0
 DATA FROM 1/2 INCH RADIUS; EXPT. 12; FRAME 11; URI -- 5/85
*==========================================================================*

 AVERAGE INPUT FRINGE ORDER= 1.84

 ITER. NO.      ERROR      DELTA N (FRGS)   DELTA N (PCT)
     1           .065         .0444            2.4113
     2           .061         .0400            2.1750
     3           .039         .0303            1.6447
     4           .039         .0305            1.6593
     5           .039         .0305            1.6583


 A0 =    565.62   A0/A0 =    1.000    C0 =       0.00   C0/A0 =    0.000
 B0 =     42.15   B0/A0 =     .075    D0 =       0.00   D0/A0 =    0.000
 A1 =   -185.91   A1/A0 =    -.329    C1 =    -160.68   C1/A0 =    -.284
 B1 =     56.46   B1/A0 =     .100    D1 =     140.31   D1/A0 =     .248
 A2 =     -1.41   A2/A0 =    -.002    C2 =      52.28   C2/A0 =     .092
 B2 =    -76.23   B2/A0 =    -.135    D2 =    -111.88   D2/A0 =    -.198
 A3 =    163.45   A3/A0 =     .289    C3 =      60.41   C3/A0 =     .107

*==========================================================================*
 8 PARAMETER MODEL -- DYNAMIC MIXED-MODE SOLUTION -- K-II = 0
 DATA FROM 1/2 INCH RADIUS; EXPT. 12; FRAME 11; URI -- 5/85
*==========================================================================*

 AVERAGE INPUT FRINGE ORDER= 1.84

 ITER. NO.      ERROR      DELTA N (FRGS)   DELTA N (PCT)
     1           .039         .0305            1.6584
     2           .038         .0302            1.6402
     3           .038         .0302            1.6411


 A0 =    565.53   A0/A0 =    1.000    C0 =       0.00   C0/A0 =    0.000
 B0 =     42.02   B0/A0 =     .074    D0 =       0.00   D0/A0 =    0.000
 A1 =   -183.09   A1/A0 =    -.324    C1 =    -163.69   C1/A0 =    -.289
 B1 =     53.68   B1/A0 =     .095    D1 =     150.40   D1/A0 =     .266
 A2 =      4.06   A2/A0 =     .007    C2 =      50.82   C2/A0 =     .090
 B2 =    -71.53   B2/A0 =    -.126    D2 =    -128.51   D2/A0 =    -.227
 A3 =    140.69   A3/A0 =     .249    C3 =      78.72   C3/A0 =     .139
 B3 =     18.95   B3/A0 =     .034    D3 =     -15.62   D3/A0 =    -.028

*==========================================================================*
```

C.6 FORTRAN Program Listing for Dynamic Mixed-Mode Isochromatic Plot

```
C PROGRAM TO GENERATE ISOCHROMATIC FRINGE PLOTS FOR DYNAMIC PROBLEMS.
C THIS PROGRAM GENERATES A USER DEFINED SIZE PLOT FOR LIGHT OR DARK FIELDS.
C PROGRAM USES THE CONSTANT SPEED EQUATIONS FOR COMBINED OPENING AND SHEAR MODES
C
      REAL L,M,IO,JO
      DIMENSION A(12),C(12)
      DIMENSION LABEL(80)
      DIMENSION FI(3),FII(3),FT(3)
      DIMENSION LEVEL1(120),LEVEL2(120),LEVEL3(120),LEVEL4(120)
C
C...  N = NUMBER OF PLOTS TO BE MADE WITH SAME VELOCITY, PLOT SIZE, AND
C...      VIEWING WINDOW (XMIN, XMAX, YMIN, YMAX)
C...  CO = CRACK VELOCITY (USE 250.0 IN/SEC FOR STATIC PROBLEMS)
C...  C1 = DILATATIONAL WAVE VELOCITY (USE 100,000.0 IN/SEC FOR STATIC PLOTS)
C...  C2 = SHEAR WAVE VELOCITY (USE 50,000.0 IN/SEC FOR STATIC PLOTS)
C...  FSIGMA = MATERIAL FRINGE CONSTANT (PSI-IN/FRINGE)
C...  H = SPECIMEN THICKNESS (INCHES)
C...  IO = PLOT SIZE ALONG WIDTH OF PAPER.  MUST BE LESS THAN 12 INCHES.  ALSO
C...       SHOULD BE SUCH THAT 10*IO WILL BE AN INTEGER, SINCE 10 CHARACTERS/IN
C...       IS ASSUMED IN THAT DIRECTION.
C...  JO = PLOT SIZE ALONG LENGTH OF PAPER.  CAN BE AS LARGE AS YOU WANT PROVIDED
C...       YOU CAN OVERRIDE PAGE SPACING - ON UNIVAC @HDG,N . M,88,0,0.  MUST BE
C...       SUCH THAT 8*JO WILL BE AN INTEGER, SINCE 8 CHARACTERS/IN IS ASSUMED
C...       IN THAT DIRECTION.
C...  XMIN = MINIMUM X-VALUE FOR PLOT WINDOW.
C...  XMAX = MAXIMUM X-VALUE FOR PLOT WINDOW.
C...  YMIN = MINIMUM Y-VALUE FOR PLOT WINDOW.
C...  YMAX = MAXIMUM Y-VALUE FOR PLOT WINDOW.
C...  PLOTTING STARTS AT TOP LEFT-HAND CORNER (XMIN,YMAX) AND GOES ALONG LINES
C...  OF CONSTANT Y.  I-DIRECTION CORRESPONDS TO X AND J-DIRECTION CORRESPONDS TO
C...  Y.
C
 99   FORMAT ( )
      READ(5,99)N
      READ (5,99) CO,C1,C2
      READ (5,99) FSIGMA, H
      READ (5,99) IO,JO
      READ(5,99) XMIN, XMAX, YMIN, YMAX
C
C...  WRITE OUT BASIC INFORMATION RELATING TO PLOTS.
C
      WRITE(6,300)N
 300  FORMAT('1',2X,'ISOCHROMATIC FRINGE PLOTS WITH THE FOLLOWING DATA',
     $ ' ; TOTAL OF',I3,' PLOTS',//)
      WRITE (6,301) CO,C1,C2
 301    FORMAT(2X,'CRACK VELOCITY=',F10.2,' INCHES/SEC',/,2X,
     $ 'C1=',F10.2,' INCHES/SEC',2X,'C2=',F10.2,' INCHES/SEC')
      WRITE (6,303) FSIGMA, H
 303    FORMAT(2X,'FSIGMA=',F10.2,' PSI-IN/FRINGE',5X,'THICKNESS=',F6.4,
     $ ' INCHES')
      IMAX=10*IO
      JMAX=8*JO
      XO=XMIN
      YO=YMAX
      DX=(XMAX-XMIN)/FLOAT(IMAX-1)
      DY=(YMAX-YMIN)/FLOAT(JMAX-1)
      WRITE(6,305) IO, JO
      WRITE(6,302)XMIN,XMAX,YMIN,YMAX
 302  FORMAT(2X,'XMIN=',F10.4,5X,'XMAX=',F10.4,5X,'YMIN=',F10.4,5X,
     $ 'YMAX=',F10.4)
      WRITE(6,304)XO,YO,DX,DY
 304  FORMAT(2X,'PLOT STARTS AT XO=',F10.4,5X,',YO=',F10.4,5X,/,2X,
     $ 'WITH A PLOT INCREMENT OF DX=',F10.6,5X,'IN THE X-DIRECTION',/,2X
     $ ,'AND A PLOT INCREMENT OF DY=',F10.6,5X,'IN THE Y-DIRECTION')
 305  FORMAT(//,2X,'PLOT SIZE IS =',F4.1,' X ',F4.1,' INCHES',//)
C
C...  CALCULATE VELOCITY FUNCTIONS NEEDED IN STRESS CALCULATIONS.
C
      C3=SQRT(1.0-(CO/C1)**2)
      C4=SQRT(1.0-(CO/C2)**2)
      C5=(1.0+C4**2)/(4.0*C3*C4 - (1.0+C4**2)**2)
      C6=2.0*C4/(4.0*C3*C4 - (1.0+C4**2)**2)
      C7=1.0+2.0*C3**2-C4**2
      C8=4.0*C3*C4/(1.0+C4**2)
      C9=1.0+C4**2
      C10=((1.0+C4**2)**2)/2.0/C4
C
C...  START DO-LOOP FOR EACH INDIVIDUAL PLOT.
C
      DO 5 K=1,N
C
C..  ZERO OUT COEFFICIENTS: A(1)-A(12) A(1)=AO, A(2)=BO,....,A(12)=B6.
C...  ZERO OUT COEFFICIENTS: C(1)-C(12) C(1)=CO, C(2)=DO,...,C(12)=D6.
C
      DO 6 K1=1,12
      A(K1)=0.0
      C(K1)=0.0
    6 CONTINUE
C
C...  READ IN COEFFICIENTS AND OTHER INFORMATION FOR PARTICULAR PLOT.
C...  N1 = 0 FOR DARK-FIELD (COSINE SQUARED) ; N1 = 1 FOR LIGHT-FIELD.
C...  N2 = NUMBER OF PARAMETERS TO BE READ IN FOR THIS PLOT.
C...  LABEL(I),I=1,80 = HEADING LABEL TO BE PRINTED AT TOP OF PLOT.
C...  A(I),I=1,N2 = COEFFICIENTS OF MODE I SOLUTION STARTING AT A(1).
C...  C(I),I=1,N2 = COEFFICIENTS OF MODE II SOLUTION STARTING AT C(1).
```

```
C
      READ(5,99)N1,N2
      READ(5,1000)(LABEL(I),I=1,80)
      READ(5,99)(A(I),I=1,N2)
      READ(5,99)(C(I),I=1,N2)
 1000 FORMAT(80A1)
      WRITE(6,1001)(LABEL(I),I=1,80)
 1001 FORMAT('1',80A1,/)
      WRITE(6,1002)(A(I),I=1,11,2)
      WRITE(6,1003)(A(I),I=2,12,2)
      WRITE(6,1004)(C(I),I=1,11,2)
      WRITE(6,1005)(C(I),I=2,12,2)
 1002 FORMAT(2X,'A0=',F10.4,7X,'A1=',F10.4,7X,'A2=',F10.4,7X,'A3=',
     $ F10.4,7X,'A4=',F10.4,7X,'A5=',F10.4)
 1003 FORMAT(2X,'B0=',F10.4,7X,'B1=',F10.4,7X,'B2=',F10.4,7X,'B3=',
     $ F10.4,7X,'B4=',F10.4,7X,'B5=',F10.4,/)
 1004 FORMAT(2X,'C0=',F10.4,7X,'C1=',F10.4,7X,'C2=',F10.4,7X,'C3=',
     $ F10.4,7X,'C4=',F10.4,7X,'C5=',F10.4)
 1005 FORMAT(2X,'D0=',F10.4,7X,'D1=',F10.4,7X,'D2=',F10.4,7X,'D3=',
     $ F10.4,7X,'D4=',F10.4,7X,'D5=',F10.4)
C
C...  START LOOPING OPERATION FOR EACH ROW OF PLOT (CONSTANT Y LINE)
C
      DO 10 J=1,JMAX
      Y=Y0-(J-1)*DY
C
C...  BLANK OUT PRINT FIELD AT EACH LOCATION ALONG ROW.
C
      DO 40 J1=1,120
      LEVEL1(J1)=' '
      LEVEL2(J1)=' '
      LEVEL3(J1)=' '
      LEVEL4(J1)=' '
   40 CONTINUE
C
C...  START LOOPING OPERATION FOR EACH LOCATION ALONG A PARTICULAR ROW.
C
      DO 20 I=1,IMAX
      X=X0+(I-1)*DX
      IF ( ABS(X) .LT. 0.00001) X=0.00001
      X1=X
      X2=X
      Y1=Y*C3
      Y2=Y*C4
C
C...  CALCULATE VELOCITY TRANSFORMED COORDINATES RO1, RO2, FEE1, FEE2
C
      O=SQRT(X1**2+Y1**2)
      P=SQRT(X2**2+Y2**2)
      L=ATAN2(Y1,X1)
      M=ATAN2(Y2,X2)
C
C...  FI(1),FII(1) = SIGMAX; FI(2),FII(2) = SIGMAY; FI(3),FII(3) = TAUXY.
C...  SET THESE TO ZERO INITIALLY, THEN LOOP THROUGH FOR CALCULATION AND
C...  SUMMATION OF EACH TERM OF SERIES EXPRESSIONS FOR THESE QUANTITIES.
C
      DO 21 I1=1,3
      FI(I1)=0.0
      FII(I1)=0.0
      FT(I1)=0.0
   21 CONTINUE
C
      DO 30 K1=1,N2
      XK2=FLOAT(K1-2)/2.0
      AI=C5*A(K1)
      CII=C6*C(K1)
      R1=O**XK2
      R2=P**XK2
      COS1=COS(XK2*L)
      COS2=COS(XK2*M)
      SIN1=SIN(XK2*L)
      SIN2=SIN(XK2*M)
      IF(K1/2*2.EQ.K1)GO TO 31
      FI(1)=FI(1) + AI*(C7*R1*COS1 - C8*R2*COS2)
      FI(2)=FI(2) + AI*(-C9*R1*COS1 + C8*R2*COS2)
      FI(3)=FI(3) + AI*(-2.0*C3*R1*SIN1 + 2.0*C3*R2*SIN2)
C
      FII(1)=FII(1) + CII*(C7*R1*SIN1 - C9*R2*SIN2)
      FII(2)=FII(2) + CII*(-C9*R1*SIN1 + C9*R2*SIN2)
      FII(3)=FII(3) - CII*(-2.0*C3*R1*COS1 + C10*R2*COS2)
      GO TO 30
   31 CONTINUE
      FI(1)=FI(1) + AI*(C7*R1*COS1 - C9*R2*COS2)
      FI(2)=FI(2) + AI*(-C9*R1*COS1 + C9*R2*COS2)
      FI(3)=FI(3) + AI*(-2.0*C3*R1*SIN1 + C10*R2*SIN2)
C
      FII(1)=FII(1) + CII*(C7*R1*SIN1 - C8*R2*SIN2)
      FII(2)=FII(2) + CII*(-C9*R1*SIN1 + C8*R2*SIN2)
      FII(3)=FII(3) - CII*(-2.0*C3*R1*COS1 + 2.0*C3*R2*COS2)
   30 CONTINUE
C
      DO 33 I1=1,3
      FT(I1)=FI(I1) + FII(I1)
   33 CONTINUE
```

```
C
C...  CALCULATE TAUMAX, FRINGE ORDER, N = TAUMAX*2*H/FSIGMA, AND INTENSITY FN.
C
        TAUMAX=SQRT(((FT(2)-FT(1))/2.0)**2 + FT(3)**2)
        XINT1=TAUMAX*2.0*H/FSIGMA
        XINT=(COS(XINT1*3.141592654))**2
        IF (N1.EQ.0) GO TO 880
        XINT=1.0 - XINT
  880   CONTINUE
C
C...  CHECK IF YOU ARE AT CRACK LINE.  IF SO, USE SPECIAL SYMBOL TO DEFINE.
C
        IF (ABS(Y).GT.DY) GO TO 890
        IF(X.GT.0.00001) GO TO 890
        LEVEL1(I)='-'
        GO TO 20
C
C...  CHECK INTENSITY LEVEL TO DECIDE WHICH BAND YOU ARE IN.  THEN PUT TOGETHER
C...  APPROPRIATE PATTERN OF OVERSTRIKES TO OBTAIN DESIRED FRINGE DENSITY AT
C...  THE POINT.
C
  890   IF(XINT.GE.0.90) GO TO 900
        IF(XINT.GE.0.80) GO TO 910
        IF(XINT.GE.0.70) GO TO 920
        IF(XINT.GE.0.60) GO TO 930
        IF(XINT.GE.0.50) GO TO 940
        IF(XINT.GE.0.40) GO TO 950
        GO TO 20
  900   LEVEL1(I)='X'
        LEVEL2(I)='O'
        LEVEL3(I)='A'
        LEVEL4(I)='V'
        GO TO 20
  910   LEVEL1(I)='A'
        LEVEL2(I)='V'
        GO TO 20
  920   LEVEL1(I)='+'
        LEVEL2(I)='O'
        GO TO 20
  930   LEVEL1(I)='X'
        GO TO 20
  940   LEVEL1(I)='+'
        GO TO 20
  950   LEVEL1(I)=':'
  20    CONTINUE
C
C...  END OF LOOP FOR ONE ROW
C...  PRINT OUT RESULTS OF COMPUTATION, AND FRINGE ORDER OF LAST PIXEL.
C
        WRITE(6,400)(LEVEL1(I),I=1,120),XINT1
        WRITE(6,401)(LEVEL2(I),I=1,120)
        WRITE(6,401)(LEVEL3(I),I=1,120)
        WRITE(6,401)(LEVEL4(I),I=1,120)
  400   FORMAT(1X,120A1,F9.4)
  401   FORMAT('+',120A1)
  10    CONTINUE
C
C...  END OF PLOT.  GO BACK AND PICK UP INFORMATION FOR NEXT PLOT.
C
   5    CONTINUE
C
C...  THAT'S ALL FOR NOW, FOLKS !!
C
        STOP
        END
```

C.7 Sample Output from Dynamic Mixed-Mode Fringe Plotting Program

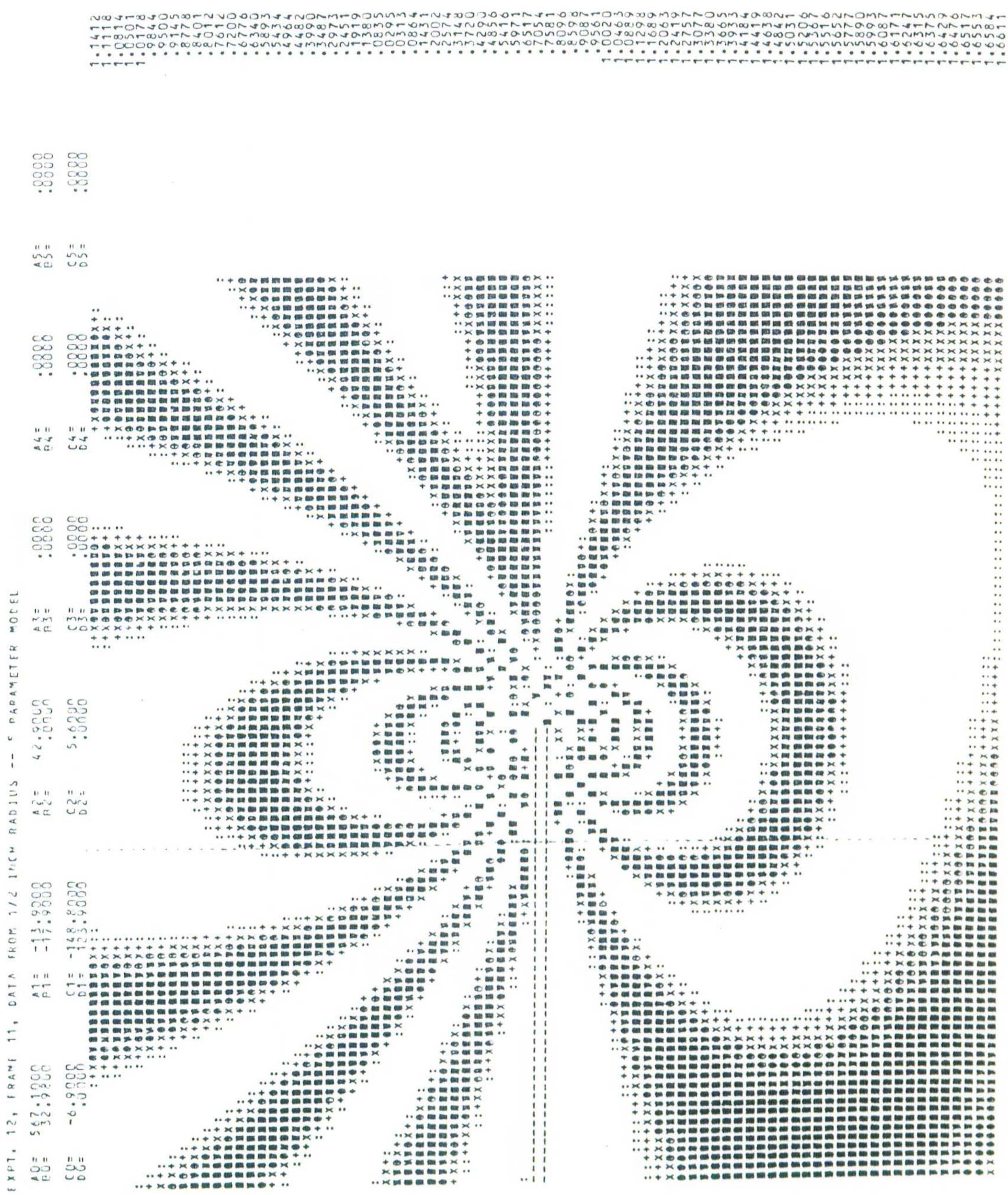

EXPT. 12, FRAME 11, DATA FROM 1/2 INCH RADIUS -- 5 PARAMETER MODEL, K-II=0

A0=	559.4000	A1=	118.1000	A2=	63.8000	A3=	.0000	A4=	.0000	A5=	.0000
B0=	13.3000	B1=	-40.5000	B2=	.0000	B3=	.0000	B4=	.0000	B5=	.0000
C0=	.0000	C1=	-178.6000	C2=	-20.5000	C3=	.0000	C4=	.0000	C5=	.0000
D0=	.0000	D1=	253.5000	D2=	.0000	D3=	.0000	D4=	.0000	D5=	.0000

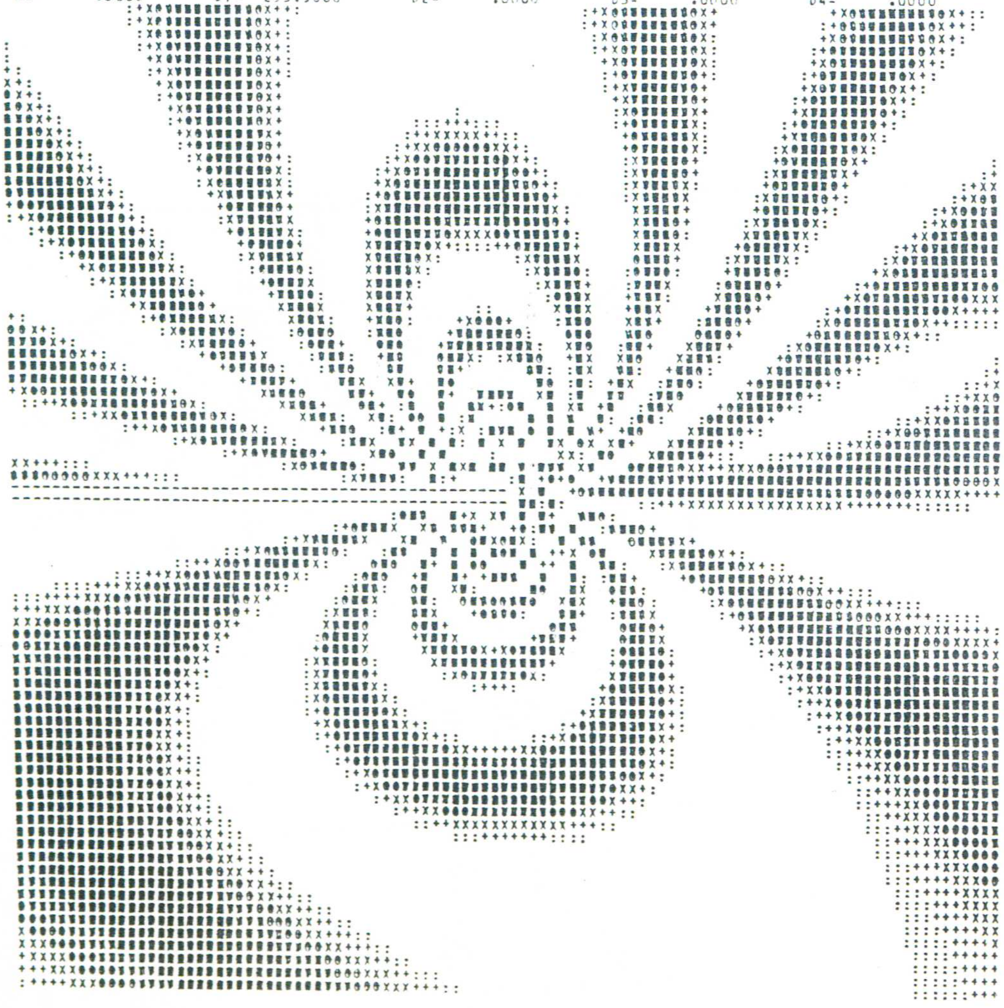

1.1913
1.1617
1.1311
1.0996
1.0671
1.0336
.9990
.9635
.9270
.8894
.8507
.8111
.7704
.7288
.6863
.6429
.5988
.5541
.5090
.4637
.4187
.3744
.3318
.2922
.2575
.2307
.2153
.2143
.2283
.2552
.2914
.3341
.3810
.4307
.4820
.5344
.5873
.6403
.6930
.7454
.7970
.8477
.8974
.9460
.9932
1.0390
1.0834
1.1262
1.1673
1.2068
1.2446
1.2807
1.3151
1.3477
1.3786
1.4079
1.4355
1.4614
1.4858
1.5087
1.5300
1.5500
1.5686
1.5859
1.6019
1.6168
1.6306
1.6433
1.6551
1.6659
1.6758
1.6850
1.6934
1.7011
1.7082
1.7147
1.7207
1.7261
1.7312
1.7358

CURRICULUM VITAE

Name: Ravinder Chona.

Permanent address: 213 Lakeside Drive
Apartment # 201
Greenbelt, Maryland 20770.

Degree and date to be conferred: Doctor of Philosophy, 1987.

Date of birth: January 20, 1955.

Place of birth: New Delhi, India.

Secondary education: Prempeh College, Kumasi, Ghana, 1971.

Collegiate institutions attended	Dates	Degree	Date of Degree
IIT Delhi, New Delhi, India	1971-1976	--	--
University of Maryland College Park, Maryland, USA	1977-1987	BS MS PhD	1984 1985 1987

Major: Mechanical Engineering/Solid Mechanics

Minor: Design & Controls, Mathematics

Professional positions held: Faculty Research Assistant
Instructor, Assistant Instructor
Graduate Research Assistant

Department of Mechanical Engineering
University of Maryland
College Park, Maryland 20742.

Professional Publications:

JOURNAL ARTICLES AND CONFERENCE PROCEEDINGS

1. "The Dynamic Three-Parameter Method for Determining Stress Intensity Factors from Isochromatic Crack-Tip Fringe Patterns," **Mechanics Research Communications**, Vol. 6, No. 5, pp. 275-282 (1979) - with H.P. Rossmanith.

2. "A Comparison of Two and Three Parameter Representations of the Stress Field Around Static and Dynamic Cracks," **Proceedings, Fourth SESA International Congress on Experimental Mechanics**, Boston, Massachusetts, pp. 76-78 (May 1980) - with G.R. Irwin and A. Shukla.

3. "A Survey of Recent Developments in the Evaluation of Stress Intensity Factors from Isochromatic Crack-Tip Fringe Patterns," Advances in Fracture Research (Proceedings of the Fifth International Conference on Fracture, ICF5), Cannes, France, D. Francois, editor, pp. 2507-2516 (1981) - with H.P. Rossmanith.

4. "Analysis of Photoelastic Fracture Patterns with a Sampled Least-Squares Method," Proceedings, 1981 Annual Spring Meeting, Society for Experimental Stress Analysis, Dearborn, Michigan, pp. 273-276 (June 1981) - with R.J. Sanford.

5. "Two and Three Parameter Representations of Crack-Tip Stress Fields," Journal of Strain Analysis, Vol. 17, No. 2, pp. 79-86 (1982) - with G.R. Irwin and A. Shukla.

6. "Characterizing Fracture Mechanics Specimens by Photoelastic Methods," Proceedings, 1982 SESA/JSME Joint Conference on Experimental Mechanics, Oahu-Maui, Hawaii, pp. 263-265 (May 1982) - with R.J. Sanford.

7. "Energy Release Rates for Branched Crack Systems," Proceedings, 1982 SESA/JSME Joint Conference on Experimental Mechanics, Oahu-Maui, Hawaii, pp. 1092-1095 (May 1982) - with W.L. Fourney and A. Shukla.

8. "Influence of Specimen Size and Shape on the Singularity Dominated Zone," Fracture Mechanics: Fourteenth Symposium - Volume I: Theory and Analysis, G.R. Sines and J.C. Lewis, editors, ASTM STP 791, pp. I-3 - I-23 (1983) - with G.R. Irwin and R.J. Sanford.

9. "Dynamic Crack Growth in Polymers," Proceedings, NSF/USARO Workshop on Dynamic Fracture, W.G. Knauss, editor, California Institute of Technology, Pasadena, California, pp. 75-99, (February 1983) - with W.L. Fourney and R.J. Sanford.

10. "Stress-Intensity-Factor Determination from Displacement Fields," Proceedings, 1983 Annual Spring Meeting, Society for Experimental Stress Analysis, Cleveland, Ohio, pp. 445-448 (May 1983) - with D.B. Barker and R.J. Sanford.

11. "Determining Stress Intensity Factors for Running Cracks," Modeling Problems in Crack Tip Mechanics, J.T. Pindera, editor, Martinus Nijhoff Publishers, pp. 207-215 (1984) - with W.L. Fourney, R.J. Sanford and A. Shukla.

12. "Photoelastic Calibration of the Short-Bar Chevron-Notched Specimen," Chevron-Notched Specimens: Testing and Stress Analysis, J. H. Underwood, et al., editors, ASTM STP 855, pp. 81-97 (1984) - with R.J. Sanford.

13. "Simple Techniques for Generating Computer Fringe Patterns," Proceedings, Fifth SESA International Congress on Experimental Mechanics, Montreal, Canada, pp. 502-505 (June 1984) - with R.J. Sanford and D.B. Barker.

14. "Dynamic Crack-Tip Stress Fields in Fracture Test Specimens," Proceedings, Sixth International Conference on Fracture, ICF6, New Delhi, India (December 1984) - with A. Shukla.

15. "The Recoverability of Plastic Zone Energy in Crack Arrest," Proceedings, 1985 SEM Spring Conference on Experimental Mechanics, Las Vegas, Nevada, pp. 13-19 (June 1985) - with W.L. Fourney, R.E. Link and R.J. Sanford.

16. "Analysis of Dynamic Fracture Events," Proceedings, 1985 SEM Spring Conference on Experimental Mechanics, Las Vegas, Nevada, pp. 872-884 (June 1985) - with G.R. Irwin, W.L. Fourney, and C.W. Schwartz.

17. "Computer Generated Fringe Patterns in Speckle Analysis," Proceedings of the SPIE International Conference on Speckle, San Diego, California, pp. 324-331 (August 1985) - with R.J. Sanford and D.B. Barker.

18. "Determining K and Related Stress Field Parameters From Displacement Fields," Experimental Mechanics, Vol. 25, No. 4, pp. 399-407 (1985) - with D.B. Barker and R.J. Sanford.

19. "The Stress Field Surrounding a Rapidly Propagating Curving Crack," Fracture Mechanics: Eighteenth Symposium, D.T. Read and R.P. Reed, editors, ASTM STP 945 (in press - 1987) - with A. Shukla.

20. "Determination of Dynamic Mode I and Mode II Fracture Mechanics Parameters from Photoelastic Data," Proceedings, VIIIth International Conference on Experimental Stress Analysis, Amsterdam, The Netherlands (May 1986) - with A. Shukla.

21. "Determining the Stress Field Parameters Associated with Curving Cracks," Proceedings, 1986 SEM Spring Conference on Experimental Mechanics, New Orleans, Louisiana, pp. 537-545 (June 1986) - with A. Shukla.

22. "A Method for Determining the Crack Arrest Toughness of Ferritic Materials," Fracture Mechanics: Nineteenth Symposium, T.A. Cruse, editor, ASTM STP to appear (1987) - with D.B. Barker, W.R. Corwin, W.L. Fourney, G.R. Irwin, C.W. Marschall, A.R. Rosenfield and E.T. Wessel.

23. "An Examination of the Zero-K_2 Criterion for a Smoothly Curving, Propagating Crack," to appear in Engineering Fracture Mechanics (1987) - with G.R. Irwin and A. Shukla.

24. "Global and Local Energy Release Rates for Branched Crack Systems," to appear in Experimental Mechanics (1987) - with W.L. Fourney and A. Shukla.

CONFERENCE PRESENTATIONS

1. "Examination of a Strip-Zone Model in Fracture Mechanics," 18th Annual Meeting of the Society for Engineering Science, Providence, Rhode Island (September 1981) - with T. Kobayashi.

2. "The Variation of Non-Singular Stress Function Coefficients in Different Fracture Test Specimens," 18th Annual Meeting of the Society for Engineering Science, Providence, Rhode Island (September 1981) - with W.L. Fourney and A. Shukla.

3. "Plastic Zones in Crack Arrest Testing," Presentation to ASTM Committee E-24 on Fracture Testing, Louisville, Kentucky (April 1983) - with W.L. Fourney and R.J. Sanford.

4. "The Recoverability of Plastic Crack Opening Displacements," Presentation to ASTM Committee E-24 on Fracture Testing, Pittsburgh, Pennsylvania (November 1983) - with W.L. Fourney, R.E. Link and R.J. Sanford.

5. "ASTM Round Robin on Crack Arrest Testing -- A Progress Report," Presentation to ASTM Committee E-24 on Fracture Testing, Dallas, Texas (October 1984) - with W.L. Fourney.

6. "Analysis of Dynamic Fracture Propagation Using the SAMCR Code," 21st Annual Meeting of the Society for Engineering Science, Blacksburg, Virginia (October 1984) - with C.W. Schwartz, W.L. Fourney and G.R. Irwin.

7. "ASTM Round Robin on Crack Arrest Testing -- A Progress Report", Presentation to ASTM Committee E-24 on Fracture Testing, Charleston, South Carolina (April 1985) -- with W.L. Fourney.

8. "Proposed Standard Test Method for K_{Ia} Testing", NRC/EPRI Review Meeting on Crack Arrest Concepts in Nuclear Applications, Gaithersburg, Maryland (April 1985) - with W.L. Fourney.

9. "Analysis of Wide Plate Test Results Using the SAMCR Code", NRC/EPRI Review Meeting on Crack Arrest Concepts in Nuclear Applications, Gaithersburg, Maryland (April 1985) - with C.W. Schwartz, W.L. Fourney and G.R. Irwin.

10. "ASTM Round Robin on Crack Arrest Testing -- A Discussion of Results", Presentation to ASTM Committee E-24 on Fracture Testing, Nashville, Tennessee (November 1985) - with W.L. Fourney.

11. "Results from the ASTM Round Robin on K_{Ia} Testing", NRC/EPRI Review Meeting on Crack Arrest Concepts in Nuclear Applications, Gaithersburg, Maryland (April 1986) - with W.L. Fourney.

12. "Determination of Dynamic Mode I and Mode II Fracture Mechanics Parameters from Photoelastic Data," Tenth U.S. National Congress on Applied Mechanics, Austin, Texas (June 1986) - with A. Shukla.

TECHNICAL REPORTS

1. "Photoelastic Studies of Damping, Crack Propagation, and Crack Arrest in Polymers and 4340 Steel," NUREG/CR-1455, University of Maryland (May 1980) - with G.R. Irwin, W.L. Fourney, D.B. Barker, R.J. Sanford, J.T. Metcalf and A. Shukla.

2. "A Photoelastic Study of the Influence of Non-Singular Stresses in Fracture Test Specimens," NUREG/CR-2179 (ORNL/Sub 7778/2), University of Maryland (August 1981) - with R.J. Sanford, W.L. Fourney and G.R. Irwin.

3. "Photoelastic Analysis of Metal-Brittle Material Structures," Progress Report to Sandia National Laboratories for the period June 1, 1982 to September 30, 1983, University of Maryland (September 1983) - with R.J. Sanford and R.E. Link.

4. "SAMCR: A Two-Dimensional Dynamic Finite Element Code for the Stress Analysis of Moving CRacks," NUREG/CR-3891 (ORNL/Sub 7778/3), University of Maryland (November 1984) - with C.W. Schwartz, W.L. Fourney and G.R. Irwin.

5. "A Report on the Round Robin Program Conducted to Evaluate the Proposed ASTM Standard Test Method for Determining the Crack Arrest Fracture Toughness, K_{Ia}, of Ferritic Materials," NUREG/CR-xxxx (ORNL/Sub 7778/4), University of Maryland (July 1986) - with D.B. Barker, W.L. Fourney and G.R. Irwin.

THESES

1. "Non-Singular Stress Effects in Fracture Test Specimens - A Photoelastic Study," M.S. Thesis, University of Maryland (1985).

2. "The Stress Field Surrounding the Tip of a Crack Propagating in a Finite Body," Ph.D. Dissertation, University of Maryland (1987).